Development and Application of Composite Beam Theory on FRP Reinforced Concrete Flexural Members

by

Xin Sha

A dissertation submitted to the Graduate Faculty of
Auburn University
in partial fulfillment of the
requirements for the Degree of
Doctor of Philosophy

Auburn, Alabama
December 12, 2020

Keywords: Fiber reinforced polymer (FRP) tendons, Transfer length, FRP laminates, Interfacial stresses, Bond-slip relationship, Composite beam theory

Approved by

James S. Davidson, Chair, Gottlieb Professor of Civil and Environmental Engineering
Mary Hughes, Lecturer of Civil and Environmental Engineering
Robert W. Barnes, Associate Professor of Civil and Environmental Engineering
Kadir Sener, Assistant Professor of Civil and Environmental Engineering

Abstract

Although there are specifications and approaches for the design of concrete flexural members reinforced with FRP, most of them were derived from empirical data. In order to obtain the rigorous theoretical definition of the fundamental mechanics associated with partial composite action between concrete and the FRP reinforcement, the practical and theoretical issues that must be further addressed. Therefore the overall goals of this research were to develop the needed theory and demonstrate its accuracy and application.

This study firstly developed a new method to establish an analytical solution for determining the transfer length for FRP tendons in prestressed concrete. The governing equations were derived by combining the local bond-slip relationship for FRP tendons in concrete with composite beam theory. Comparisons to test data strain results demonstrated that the predicted results were accurate. Subsequently, based on the developed method, the difference between sequential release and simultaneous release of tendons in the manufacturing process of pretensioned concrete members was further discussed.

The mechanical response analysis of coupling between longitudinal and transverse interactions was also investigated for concrete beams strengthened with externally bonded FRP laminates using composite beam theory. Associating with the bond stress-slip relationship between FRP laminates and concrete, two sets of governing equations were derived to determine the interfacial stresses. Comparisons between the developed model with published finite element

results and existing analytical solutions in the literature confirmed the feasibility and accuracy of this novel approach. A parametric study was also carried out to investigate the effect of various factors on the interfacial behavior of externally bonded FRP for strengthening concrete beams.

Finally, a novel finite element (FE) modeling approach was developed to further verify the developed theoretical method. The present FE model took into account the friction coefficients obtained from pull-out tests on the FRP tendons and prestressed concrete members. Convergence analysis of two numerical simulations with different mesh densities was carried out as well. The consistency between the analytical solution and FE simulation not only further proved the reliability of composite beam theory, but also demonstrated the importance of the bond-slip relationship in fully understanding the mechanical properties of concrete members reinforced by FRP systems.

Acknowledgements

Firstly, I would like to express my sincere gratitude to my supervisor Prof. Davidson for being with me and helping me all the way throughout my Ph.D. study. His trust on me towards my work had me more confident in my research area, even being my true self. These years have been very challenging for me, however without my supervisor, I am unable to have transformed these difficulties into a positive one. I also greatly appreciate China Scholarship Council (CSC) for the financial support.

Besides my supervisor, I am very grateful to my committee members, Dr. Hughes, Dr. Barnes, Dr. Sener, Dr. Stallings and University Reader Dr. Prorok, for their insightful comments pushed me to sharpen my thinking and brought my work to a higher level from various perspectives. I would also like to show my gratitude to my academic advisor Sherry Ray for helping me reach my goal.

I acknowledge my fellow Dr. Bai who provided worthwhile discussions as well as many good memories and times of happiness. In addition, I would also like to thank my friends, Fan Yin, Xiaolong Guo, Liangxi Li, Anqi Zhang, Songtao Du, and Joseph Broderick for all the fun we have had in the past years. In particular, I am obliged to Mr. Scott Roney for motivating me in everything I want to do in life.

Last but not least, I would like to thank my parents and to my twin brother Lei Sha for a great deal of support me spiritually to pursue a doctoral degree.

Table of Contents

List of Figures

List of Tables

Chapter 1 Introduction

1.1 Background

In the last 100 years, global energy consumption has grown rapidly. Sustainable development is becoming more and more significant to protect the planet and ensure that all people, plants, and animals enjoy lasting peace and prosperity. The acceleration of plastic pollution from billions of plastic bottles and countless plastic bags each year is a considerable threat to life on earth. According to calculations from a seminal report released in 2014, there are at least 268,940 tons of plastic waste floating in the world's oceans [1]. As shown in Fig.1.1, plastic pollution has resulted in the death of a staggering number of animals in the marine environment.

Consequently, to address this problem, in addition to reducing plastic use in our daily life, it is urgent to promote the reuse and recycling of thermoplastic matrices. Numerous studies [3-7] over the years have shown that recycled thermoplastics can be used as matrix materials in fiber reinforced polymer (FRP) composites. In this perspective, the use of FRP composite materials for new construction and rehabilitation of existing structures not only has obvious advantages over conventional steel reinforcement, but also can effectively promote recycling plastic with concomitant environmental benefits. For the above reasons, this dissertation is devoted to the study of the application of FRP reinforcements in concrete structures.

Fig. 1.1 The effect of plastic pollution on marine life [2]

The application and development of FRP reinforcements in civil engineering structures as an important topic has attracted much attention at many research institutes around the world over recent decades. FRP composite materials are typically made of a polymer matrix reinforced with strong fibers. There are many types of FRP reinforcements, such as Aramid Fiber Reinforced Polymer (AFRP), Carbon Fiber Reinforced Polymer (CFRP), and Glass Fiber Reinforced Polymer (GFRP), etc. Sometimes other fibers are used, such as paper, wood, and basalt. Differences in the fiber type products result in variable tensile strengths, compressive capacities, durability characteristics, etc. [8]. The longitudinal thermal expansion coefficients for AFRP, CFRP, and GFRP are approximately $-6\times10^{-6}/{}^{o}C$, $0/{}^{o}C$, and $10\times10^{-6}/{}^{o}C$ respectively, which will affect concrete cracking when employed as internal reinforcement [9]. Kobayashi and Fujisaki [10] carried out compressive tests on FRP reinforcement and found that the compressive strength of AFRP, CFRP, and GFRP were approximately 10%, 30% to 50%, and 30% to 40% of the tensile

strength, respectively. GFRP are highly sensitive to alkali attack. In general, GFRP is typically used as non-prestressed reinforcement and CFRP is used for prestressed reinforcement. AFRP can be used as different composite structural parts in various applications due to its high tensile modulus combined with strong resistance to chemicals. Table 1.1 summarizes the basic physical and mechanical properties of different types of FRP reinforcements compared with steel bars.

Table 1.1 Properties of different types of FRP reinforcements compared with steel bars [11]

Properties	**Material types**			
	AFRP	**CFRP**	**GFRP**	**Steel**
Tensile strength (MPa)	1720 – 2540	600 – 3690	483 – 1600	483 – 690
Young's Modulus (GPa)	41 – 125	120 – 580	35 – 51	200
Ultimate elongation %	1.9 – 4.4	0.5 – 1.7	1.2 – 3.1	6.0 – 12.0
Longitudinal coefficient of linear expansion ($10^{-6}/^{o}C$)	-6.0 – 2.0	-9.0 – 0.0	6.0 – 10.0	11.7
Density (g/cm^3)	1.25 – 1.40	1.50 – 1.60	1.25 – 2.10	7.85

The promise of FRP composite materials lies in excellent corrosion resistance, higher ratio of strength to self-weight, high fatigue strengths, electromagnetic neutrality, low coefficient of thermal expansion in the axial direction (especially for CFRP), and outstanding fatigue characteristics of CFRP and AFRP tendons [12]. These advantages make FRP composites suitable for reinforcements in concrete structures, or even superior to conventional steel reinforcements.

In general, FRP reinforcements are available in several forms, including FRP tendons as a substitute for traditional materials, FRP laminates for repair and rehabilitation, concrete-filled circular FRP tubes as efficient structural members, and FRP decks for bridge systems, as illustrated by Fig. 1.2. In this dissertation, the focus is on the use of FRP tendons in prestressed concrete and externally bonded FRP laminates applied to the surface of the concrete for strengthening or repair.

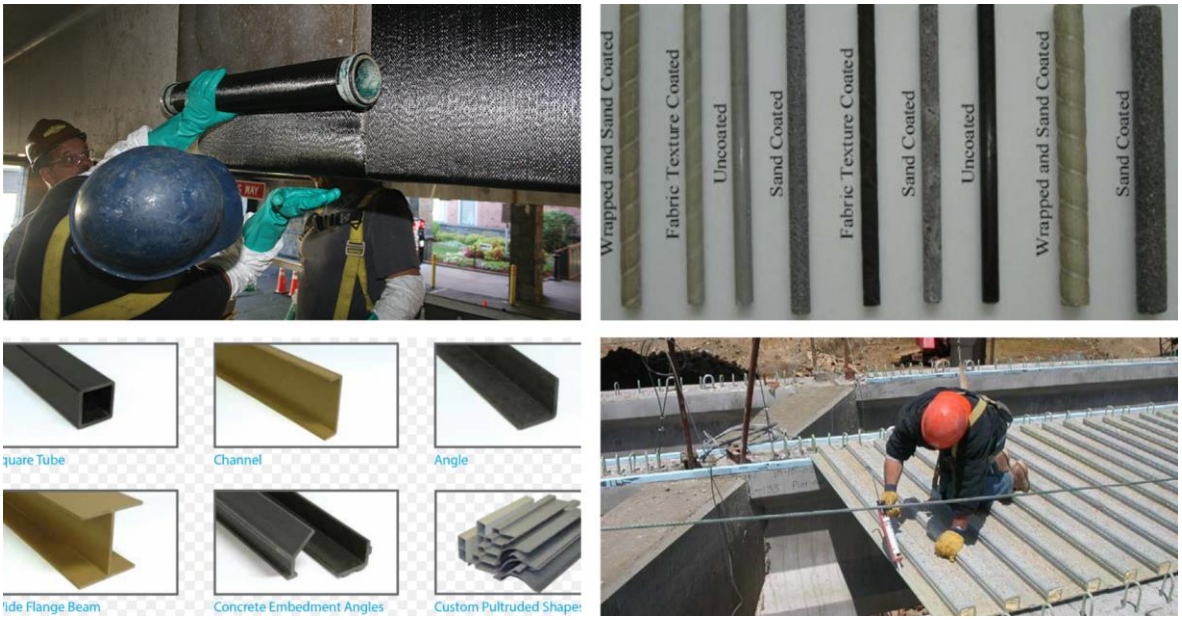

Fig. 1.2 Structural engineering applications of FRP materials [13-16]

Classical Euler-Bernoulli beam theory is generally adopted to calculate the load-carrying and deflection of beams in the field of the practical engineering structures analysis and design. As the simplification of Timoshenko beam theory, it is limited to the case for elastic and small displacement. In other words, Euler-Bernoulli beam theory is applied in situations where shear deformation of the cross section is negligible. The deformation of Timoshenko beam compared with that of Euler-Bernoulli beam is illustrated in detail by Fig. 1.3. The fact is that engineers tend to use simplified analysis methods to solve engineering problems, but those approaches are recognized to have inherent limitations that can result in a false impression of the true behavior of

the structure. Therefore it is very necessary to not only improve the accuracy of current analytical method, but also to understand the nature of the response based upon mechanics theory to meet the requirements of both mathematics and engineering.

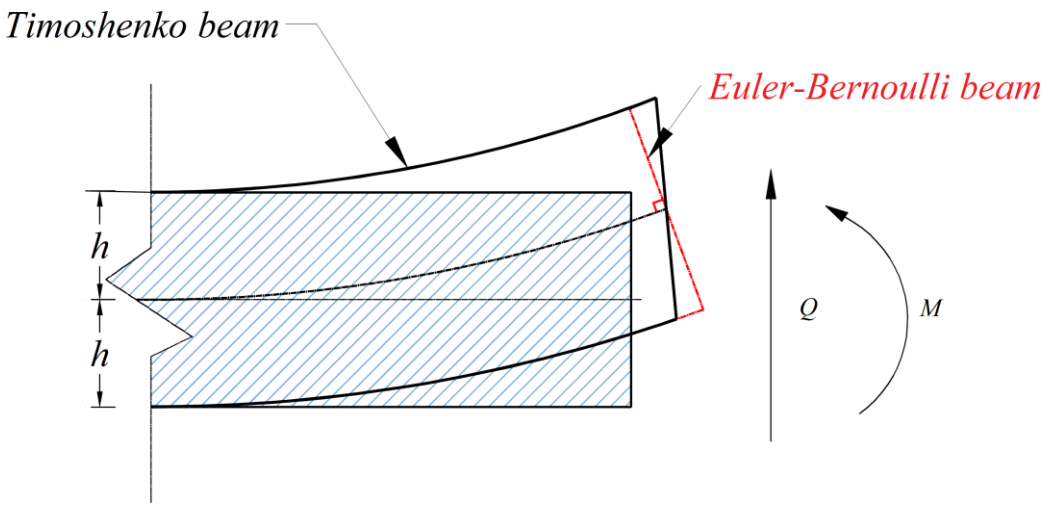

Fig. 1.3 Comparison of the deformation of Timoshenko beam with that of Euler-Bernoulli beam

For partial composite beams, even for full composite beams, a number of studies [17-20] have shown that there are slip effects that must be taken into account. It is worth noting that "slip" is relevant to the relative movement between layers or components within the cross section. Due to the adopted assumptions, shear slip causes many problems that cannot be solved by classical Euler-Bernoulli beam theory.

For example, there is no interface slip in the prestressed concrete reinforced with FRP tendons under ideal conditions. In other words, the analysis of behavior and design of pretensioned prestressed members is always established by assuming that the FRP tendons are perfectly bonded to the concrete. However, this assumption is not completely coincident with the actual situation of engineering practice. In pretensioned prestressed concrete with FRP tendons, the transmission

of prestressing force is not completed at the beginning of the contact between FRP tendons and concrete, but requires a certain distance to reach a constant value at the effective prestress level. This is because shear slip occurs between the interface of FRP tendons and concrete within the transfer length.

As another example, consider the rehabilitation of existing concrete structures using externally bonded FRP laminates. The conventional method for predicting interfacial stresses distributions along the interface is based upon the assumption of fully composite action between the FRP laminate and the concrete substrate. That means that the slip effects were ignored. However, considering interface slip can have a significant effect on the accuracy of analysis results for interfacial stresses. As can be observed from Fig. 1.4, the composite beam composed of different materials has a considerable amount of slip when the bending moment is occurring.

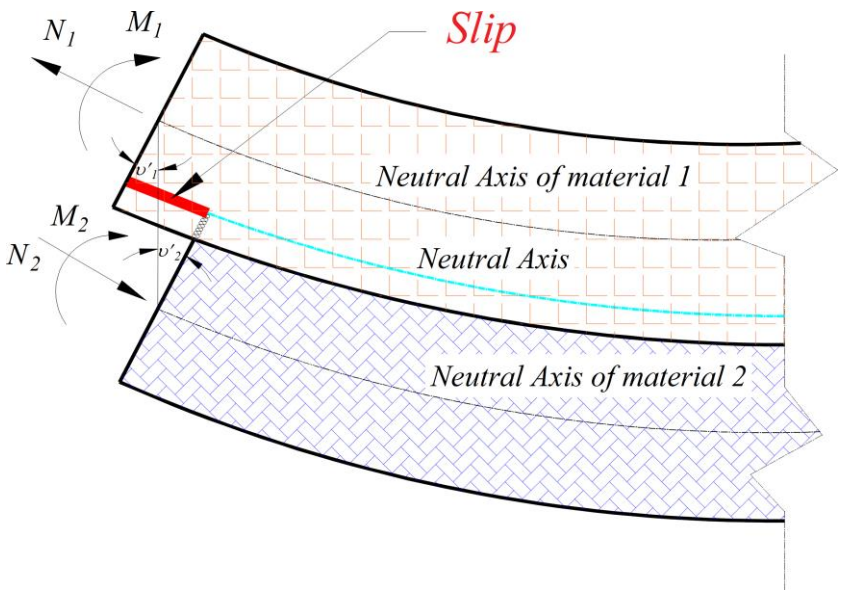

Fig. 1.4 The slip due to bending moment between different material

Although there are specifications and approaches for the design of concrete flexural members reinforced with FRP, most of them were derived from empirical data. In order to obtain the rigorous theoretical definition of the fundamental mechanics associated with partial composite action between concrete and the FRP reinforcements, the practical and theoretical issues must be further addressed. Slip effects on the prediction of transfer length for pretensioned concrete members and FRP end debonding failures must be carefully considered in the analyses. Most importantly, in this dissertation, the proposed method used for dealing with these problems is associated with the local bond stress-slip relationship between concrete and FRP tendons as well as the concrete substrate and FRP laminates.

1.2 Objectives

The overall objective of this research was to develop a novel composite beam theory that is applicable to strengthening of concrete flexural members using FRP reinforcements. Applications include solutions to the transfer length of prestressing FRP tendons and interfacial stresses of reinforced concrete beams strengthened by externally bonded FRP laminates. Through analysis of the mechanics behavior in terms of partially composite action associated with the local bond-slip relationship between FRP systems and concrete, rigorous closed-form solutions of transfer length and interfacial stress for relevant structures were derived, respectively. In addition, the study by Newmark et al. [17] claimed that composite beam theory could be used for any case of structures composed of two interconnected elements based upon some reasonable assumptions. For this reason, another important objective of this research was to confirm Newmark et al.'s conclusion, as well as to expand the scope of application of the composite beam theory.

1.3 Methodology and scope

Governing differential equations are derived in terms of the equilibrium of axial force acting on the cross section of the concrete and FRPs as well as the balance of the overall bending moment. Based on the proposed analytical models, the empirical bond stress-slip relationships between concrete and FRP were fully taken into account. The accuracy of presented analytical solution was verified through the comparison with the existing experiment data and analytical solutions from available literature. In addition, the simulation results from nonlinear finite element analyses are compared with the corresponding results obtained by using composite beam theory, which comprehensively evaluate the accuracy and reliability of the present method. Furthermore, based upon the developed theory, this dissertation also discusses the effect of various key mechanical factors on related problems of different FRP reinforcements. The theoretical development of this dissertation mainly focuses on the following two aspects: (1) determination of transfer length for prestressed FRP tendons in pretensioned concrete; and (2) prediction of interfacial stresses in externally bonded FRP laminates for strengthening concrete structures. In the developed analysis model, it is particularly emphasized that this research was based upon the hypothesis of linear elastic constitutive behavior and small displacement. Moreover, the beam analyzed in this topic is limited to the shallow beam form and the shear deformation through the cross section of the concrete beam and FRP components is neglected.

1.4 Organization

Chapter 1 provides an introduction of the dissertation including background information, research objectives, and a brief description of the methodology.

Chapter 2 reviews the historical development of composite beam theory research and discusses applications related to different types of structures. It also describes factors that are relevant to the transfer length and interfacial stresses for this dissertation topic in more detail and relates the present work to voids in the literature.

Chapter 3 presents an analytical model for pretensioned concrete members with prestressed FRP tendons. The transfer length is determined with closed-form solutions based on composite beam theory as well as the local bond stress-slip relationship between FRP tendons and concrete. This chapter has been published in *Composite Structures*, "Sha, X. and Davidson, J.S., 2019. Analysis of transfer length for prestressed FRP tendons in pretensioned concrete using composite beam theory. Composite Structures, 208, pp.665-677.".

Chapter 4 presents analysis methodology for concrete beams strengthened by externally bonded FRP laminates and presents the interfacial shear and normal stress with closed-form analytical solution using the developed composite beam theory associated with the bond-slip relationship between FRP laminates and concrete. This chapter has been published in *Composite Structures*, "Sha, X. and Davidson, J.S., 2020. Analysis of Interfacial Stresses in Concrete Beams Strengthened by Externally Bonded FRP Laminates Using Composite Beam Theory. Composite Structures, p.112235."

Chapter 5 further verifies the developed analytical method. An innovative three-dimensional finite element model is proposed that takes into account the friction coefficients

obtained from pull-out tests on the FRP tendons and prestressed concrete members. This chapter has been submitted to the *Composite Structures* and is currently under review.

Chapter 6 summarizes the most important conclusions and recommends future work.

References

[1] Yeoman, Barry. “A Plague of Plastics” The National Wildlife Federation, 01 Jun. 2019. Web. 15 Oct. 2020. <https://www.nwf.org/Home/Magazines/National-Wildlife/2019/June-July/Conservation/Ocean-Plastic>

[2] “The Effect of Plastic Pollution on Marine Life” Pegasus Foundation, 10 May. 2019. Web. 15 Oct. 2020. <https://www.pegasusfoundation.org/the-effect-of-plastic-pollution-on-marine-life/>

[3] Cantwell WJ. The fracture behavior of glass fiber/recycled PET composites. Journal of reinforced plastics and composites. 1999 Mar;18(4):373-87.

[4] Castro AC, Carvalho JP, Ribeiro MC, Meixedo JP, Silva FJ, Fiúza A, Dinis ML. An integrated recycling approach for GFRP pultrusion wastes: recycling and reuse assessment into new composite materials using Fuzzy Boolean Nets. Journal of Cleaner Production. 2014 Mar 1;66:420-30.

[5] Dormer A, Finn DP, Ward P, Cullen J. Carbon footprint analysis in plastics manufacturing. Journal of Cleaner Production. 2013 Jul 15;51:133-41.

[6] Eriksson O, Reich MC, Frostell B, Björklund A, Assefa G, Sundqvist JO, Granath J, Baky A, Thyselius L. Municipal solid waste management from a systems perspective. Journal of cleaner production. 2005 Feb 1;13(3):241-52.

[7] Turner RP, Kelly CA, Fox R, Hopkins B. Re-Formative Polymer Composites from Plastic Waste: Novel Infrastructural Product Application. Recycling. 2018 Dec;3(4):54.

[8] Lees JM. Fibre-reinforced polymers in reinforced and prestressed concrete applications: moving forward. Prog Struct Eng Mater 2001;3:122–31.

[9] Uomoto, T. Recommendation for design and construction of concrete structures using continuous fiber reinforcing materials. Ed. Atsuhiko Machida. Japan Soc. of Civil Engineers, 1997.

[10] Kobayashi K, Fujisaki T. 32 Compressive Behavior of Frp Reinforcement in Non-Prestressed Concrete Members. InNon-Metallic (FRP) Reinforcement for Concrete Structures: Proceedings of the Second International RILEM Symposium 1995 Aug 3 (Vol. 29, p. 267). CRC Press.

[11] Ahmed A, Guo S, Zhang Z, Shi C, Zhu D. A review on durability of fiber reinforced polymer (FRP) bars reinforced seawater sea sand concrete. Construction and Building Materials. 2020 Sep 30;256:119484.

[12] Mahmoud ZI. Bond characteristics of fibre reinforced polymers prestressing reinforcement [Ph. D.]. Alexandria University (Egypt). 1997.

[13] Guadagnini, Maurizio. “Fibre Reinforced Polymers” The University of Sheffield, 2010. Web. 22 Oct. 2020. < http://mguadagnini.staff.shef.ac.uk/frp/frp.php>.

[14] Ringelstetter E, Bank LC, Oliva MG, Russell JS, Nanni MA, Ringelstetter TE. Development of a cost-effective structural FRP stay-in-place formwork system for accelerated and durable bridge deck construction.

[15] Alkhrdaji, Tarek. "Strengthening of concrete structures using FRP composites." STRUCTURE magazine 12 (2015): 18-20.

[16] “FRP Structural Shape” 949 Supplies, 2014. Web. 22 Oct. 2020. < http://www.949supplies.com/custom_products/frp-gratings-copy/>

[17] Newmark NM, Siess CP, Viest IM. Test and analysis of composite beams with incomplete interaction. Proceedings of Society for Experimental Stress Analysis. 1951;9(1):75-92.

[18] Grant JA, Fisher JW, Slutter RG. Composite beams with formed steel deck. Engineering Journal. 1977 Mar;14(1).

[19] Nie J, Cai CS. Steel–concrete composite beams considering shear slip effects. Journal of Structural Engineering. 2003 Apr;129(4):495-506.

[20] Bai F, Davidson JS. Analysis of partially composite foam insulated concrete sandwich structures. Engineering Structures. 2015 May 15;91:197-209.

Chapter 2 Literature Review

2.1 Composite beam theory development

Composite structures comprising two or more elements have played an extensive and irreplaceable role in engineering practice for a long time. Consequently, many experimental and theoretical analyses have been conducted on the behavior and design of composite structures. The basic theory by Granholm [1] (1949) initially proposed the concept used for nailed timber structures. The axial force in each layer and the overall bending moment of the entire cross section are analyzed by establishing of static force equilibrium equations. The following assumptions were involved in Granholm's work:

(1) The connector spacing along the beam is constant.

(2) The linear elastic constitutive relationship exists between the force and deformation of the connector.

(3) Each component in the composite beam has the same cross section and material properties.

Based on the simply supported composite beam shown in Fig. 2.1, the governing equations are given by Eq. (1) and Eq. (2).

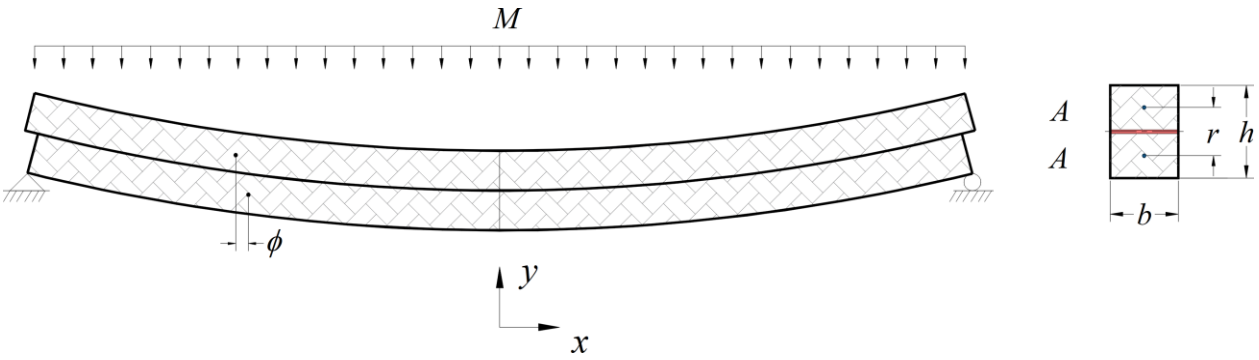

Fig. 2.1 Simple supported composite beam with the slip under external moment [1]

$$\frac{d^2\phi}{dx^2}-\frac{2bk'}{EA}\phi=r\frac{d^3y}{dx^3} \tag{1}$$

$$\frac{d^2y}{dx^2}-\frac{EAr}{2EI_s}\frac{d\phi}{dx}=-\frac{M}{EI_s} \tag{2}$$

where ϕ = the relative longitudinal displacement between two members in the composite beam; b = the width of component; k' = the shear stiffness related to the relationship of slip, $\tau=k'\phi$; τ = shear force per unit length at the interlayer; M = external moment; I_s = the moment of inertia of equivalent rigid connection section; E = the modulus of elasticity of component; A = the cross section area of each component; r = distance between centroids of components; y = the deflection of system. On the basis of Granholm's theory study, Holmberg (1965) [5] took into account additional transverse action, and used this method to analyze concrete structures. From the assumption in the theory, it can be seen that the previous method is limited to composite structures with the same cross section and material properties, as well as uniform distribution of connectors.

Newmark et al. [2] (1951) presented an analytical model with partial interaction for the composite T-beams composed of a steel I-beam and a concrete slab interconnected with channel shear connectors. Experimental investigation and theoretical analysis on the mechanical behavior of T-beams of composite construction were carried out. Newmark et al. derived equilibrium and compatibility equations to study the effect of incomplete interaction based on the load-slip characteristics from the push-out test. Furthermore, the study by Newmark et al. (1951) also puts forward an important conclusion that the proposed theory may be used not only for the composite T-beams, but also for any kind of structures composed of two or more interconnected elements under reasonable assumptions.

In the theoretical development of Newmark et al., the following assumptions and limitations are specifically presented:

(1) The shear connectors between the concrete slab and the I-beam are continuously distributed along the length of the beam.

(2) The slip caused by shear connector is directly proportional to the transmitted force.

(3) It assumed that strains throughout the depth of the concrete slab and the I-beam is in linear distribution.

(4) The concrete slab and the I-beam have the same transverse deflection at all points.

As shown in Fig. 2.2, considering the composite T-beam with partial interaction under the internal forces, the lower fibers of the concrete slab tend to lengthen, and the upper fibers of the I-beam tend to shorten. The governing differential equations for the force F and the deflection y are derived in the following:

$$\frac{d^2F}{dx^2}-\frac{k}{s}\frac{\overline{EI}}{\overline{EA}\sum EI}F=-\frac{k}{s}\frac{z}{\sum EI}M \tag{3}$$

$$\frac{d^2y}{dx^2}=-\frac{M}{\sum EI}+\frac{F\,z}{\sum EI} \tag{4}$$

where F = forces acting on the centroids of the concrete slab and the I-beam; M = the external moment; y = the deflection of the composite I-beam; k = modulus of shear connectors; s = spacing of shear connectors; z = the distance from the concrete slab centroid to that of I-beam; E_s = the elastic modulus of concrete slab; E_b = the elastic modulus of I-beam; I_s = the moment of inertia of concrete slab; I_b = the moment of inertia of I-beam; A_s = cross section area of the concrete slab; A_b = cross section area of I-beam; $\sum EI=E_s I_s+E_b I_b$; $\frac{1}{\overline{EA}}=\frac{1}{E_s A_s}+\frac{1}{E_b A_b}$; $\overline{EI}=\sum EI+\overline{EA}z^2$. Similarly, the relative inconvenience is that the analytical model of Newmark et al. does not consider the effect of the different shear connectors spacings.

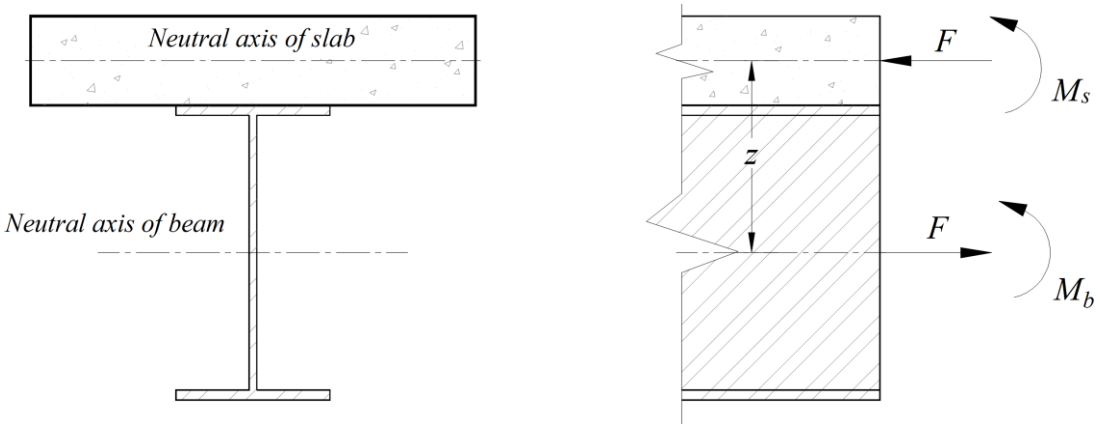

Fig. 2.2 Cross section of the composite T-beam with partial interaction [2]

Therefore, as an attempt to provide a more reliable and effective theoretical basis for practical design, the method for the analysis of concrete structures strengthened by FRPs in this dissertation is developed based on the bond-slip relationship between concrete and FRP reinforcements from the available pullout tests.

In 1968, the research by Goodman and Popov [3] was devoted to establishing a general theory for the analysis of layered beams with interlayer slip, which also proved that Granholm's study (1949) on the composite beam theory is comparable with Newmark et al.'s theory (1951) for incomplete interaction. It clearly shows the influence of interlayer slip on the deflection of the layered beam through experiments by Goodman and Popov (1968), which is contained in the proposed theory. The analytical method is based on the assumption that is same as those from the theory presented by Newmark et al. (1951). In addition, it is also assumed that friction effects between the layers are negligible.

The geometry and notation for a three-layered beam cross-section subjected to internal forces are illustrated in Fig. 2.3, and the governing equation for the deflection y is given as follows:

$$3EI\frac{d^4y}{dx^4}-\frac{Kn}{S}\frac{1}{AE}\left(EI_s\frac{d^2y}{dx^2}+M\right)=-\frac{d^2M}{dx^2} \tag{5}$$

where $F = F_1 = F_3$ = axial forces acting on each layer; h = the thickness of each layer; M_1, M_2, M_3 = the internal moment acting on each layer; $M=M_1+M_2+M_3+F_1h+F_3h$; y = the deflection of the three-layered beam; K = modulus of each shear connector; S = spacing of shear connectors; n = the number of shear connectors per row; E = the elastic modulus; A = cross

section area of each layer; I = the moment of inertia of each layer; I_s = the moment of inertia of equivalent solid beam.

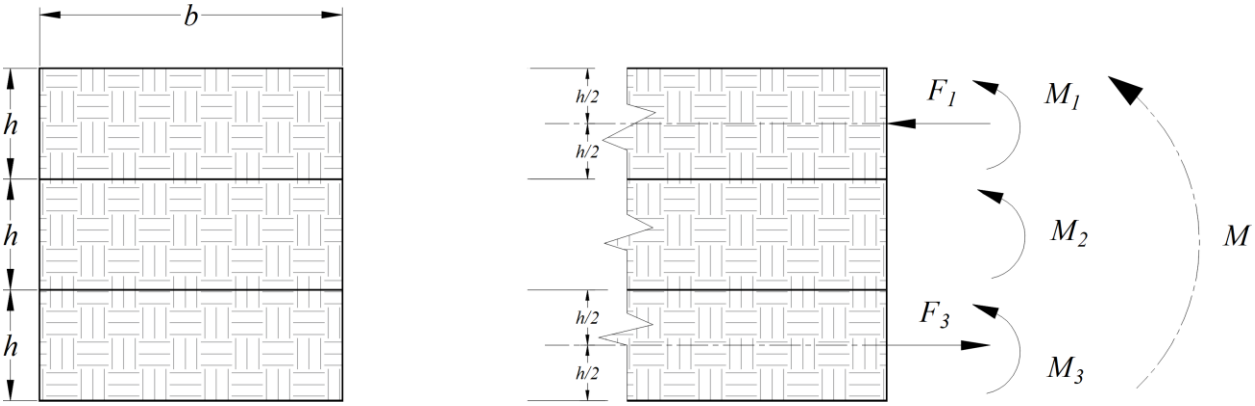

Fig. 2.3 Cross section of three-layer beam under the internal forces [3]

With the rapid application and development of composite structures in the fields of civil engineering and construction, researchers are more and more aware of the importance of interface slip effects on the partial composite sections, even for full composite sections. There have been numerous studies conducted in the different aspects of composite theories since then. In addition to the closed-form solutions mentioned above, the layered wood systems is analyzed with finite element method developed by Thompson et al. [6] (1975). Murakami [7] (1984) developed a Timoshenko beam theory with built-in interlayer slip for the analysis of the simply supported sandwich beam under a concentrated load in which the effect of transverse shear was considered. Based on the analysis method by Newmark et al. [2], theoretical study of concrete beams strengthened by epoxy-bonded steel plate was carried out by Vilnay [8] (1988). During the same period, Roberts and Haji-Kazemi [9,10] (1989) developed a staged analysis approach that predicted interfacial stress distributions for the case of the uniformly distributed load acting on the reinforced concrete beam with externally bonded steel plate. It should be noted that the previous

solutions [8,9,10] assume fully composite action between concrete and externally bonded plates, which means that the slip effects were ignored. The conventional method used to predict interfacial stresses in these existing studies have a common feature, which is beginning with the compatibility expression as follows:

$$\tau(x)=\frac{G_a}{t_a}\left(u_2-u_1\right) \tag{6}$$

where $\tau(x)$ = interfacial shear stress, G_a = shear modulus of the adhesive layer, t_a = thickness of the adhesive layer, u_1 = displacements along the x axis of the bottom fiber of concrete, u_2 = displacements along the x axis of the top fiber of the bonded plate. Accordingly, mechanical constitutive equations were established acting on the adhesive layer, which provides a starting point for deriving the governing differential equations for interfacial shear and normal stresses. However, a large number of experimental and analytical studies [11-17] have indicated that the bond behavior between concrete and FRP laminates is not only affected by G_a/t_a from adhesive, but also affected by some other factors, such as the bond width of FRP laminates, FRP material types, the roughness of concrete surface, concrete strength. Therefore, the analysis of the behavior of concrete beams strengthened by externally bonded FRP laminates should be conducted based on the partial composite action rather than full composite action. For the partial composite beam, even for full composite beams, there are the slip effect which have to be taken account. The present study (presented in Chapter 4) however relies upon a novel and theoretically partial composite beam theory developed specifically for determining the interfacial stresses of reinforced concrete beams strengthened by externally bonded FRP laminates. Most importantly, the proposed method for the analysis of interfacial stresses in which the local bond stress-slip relationship between concrete and FRP laminates is considered.

The closed-form solutions of beam-column subjected to transverse and axial loading is presented in the study of Girhammar and Gopu [18] (1993) with consideration of first-order and second-order cases. Compared with the first-order, in the case of second-order, the deformed geometry of the component is considered. Buckling loads for composite beam-column is analyzed with the developed approximate formula, which considers the pure column in the second-order case. Adam et al. [19] (1997) extend the study involving partial composite action to analyze the simply supported composite beam subjected to dynamic loads. Foraboschi [20] (2009) dealt with the two-layer beam based on bilinear cohesive zone model in which the analytical model of composite beams considering transverse shear deformation was carried out. It was also proved that nonlinear interface slip is very important to accurately study the behavior of composite beam.

Similarly, there are also a large number of papers [4,21-23] focused on the studies of finite element formulations of composite beam model with partial shear interaction based on Newmark model [2]. Dall'Asta and Zona [21] (2002) present EB-EB model of finite elements with 16DOF, which couples two Euler-Bernoulli beams through distributed deformable shear connectors between the interfaces. Only the flexural deformability and bending failure mode of each beam component are considered. EB-T model proposed by Ranzi and Zona [22] (2007) is composed of Euler-Bernoulli beam and Timoshenko beam representing the concrete slab and the steel component, respectively. Zona and Ranzi [23] (2010) extended the nonlinear analysis of composite beam with partial interaction by means of finite element models, developed 16DOF displacement-based finite element of T-T model formulated by coupling two Timoshenko beams. In addition, Zona and Ranzi also compared three different composite beam models, namely EB-EB model, EB-T model, and T-T model. Moreover, as an alternative to the analytical solution, some approximated analysis procedures can be found in the literature [4,24,25], which devote

much attention to the performance of composite beam with partial interaction using finite element simulation. For example, based on a three-dimensional FE model implemented using an explicit formulation in the Abaqus software packages, Tahmasebinia et al. [24] (2012) conduct a probabilistic study on effect of material parameter uncertainties on the structural behavior of steel-concrete beams. Turmo et al. [4] (2015) propose a 2-dimensional FE model with six different types of elements to simulate the behavior of composite beams. Nevertheless, the solution accuracy of numerical simulations depends on convergence rate, target scale, element type, computational time, as well as computer memory, which discourages their application for complex structures in the analysis of practical engineering problems. Therefore, this research explores a novel and advanced composite beam theory, in particular, which is a simplified analysis method that is suitable for engineers to use.

For composite structures, such as composite steel-concrete beam bridges, nailed timber systems, and sandwich panels, an in-depth and comprehensiveness understanding of the interlayer slip is important for mechanical response analysis. The relative interlayer movement called slip that occur as a result of deformation of shear connectors at the interface between all the components of composite systems. In other words, this interlayer slip is caused either by the flexibility of adhesive and subsequent delamination in the case of continuous contact surfaces, or by the deformation of mechanical connectors, such as shear connectors in the T-beam of composite steel-concrete as well as the sandwich structures illustrated in Fig. 2.4. More importantly, numerous studies [4,7,27] in the literature have indicated that not only longitudinal interaction should be taken into account for the interlayer slip, but also the effect of transverse composite action should be included. For example, as demonstrated in Fig. 2.4, the distortion near the end

support is due to the transverse interaction between the interface of concrete wythes in the composite sandwich panel under bending moment.

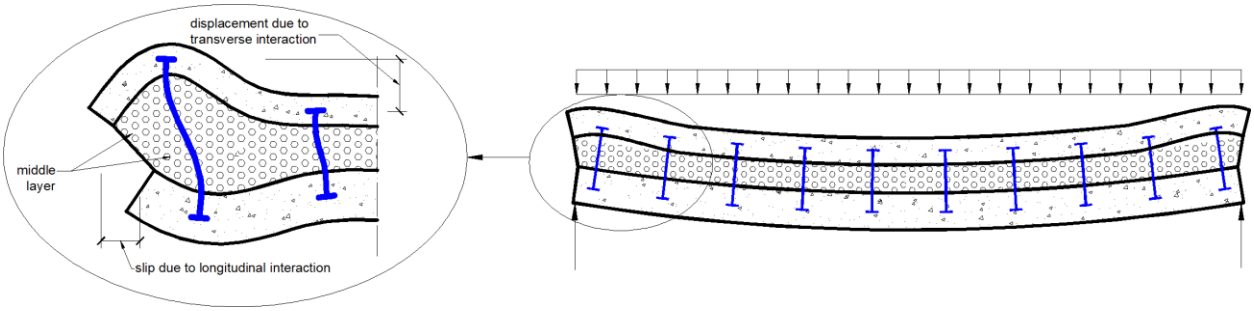

Fig. 2.4 Slip due to longitudinal and transverse interactions in the sandwich panel [27]

Accordingly, Bai and Davidson [26,27] extended composite beam theory for insulated concrete sandwich panels, and proposed closed-form solutions that are available for both symmetrical and unsymmetrical wythes. It is worth noting that the longitudinal and transverse interactions are coupled to have an impact on the deflection and stress of each component in the sandwich panel. Subsequently, Bai and Davidson [28] developed composite beam theory to analyze pretensioned concrete structures, and established the force equilibrium between prestressing strands and concrete by means of a linear relationship assumption between slip and interface shear force.

Considering the influence of bond behavior between concrete and reinforcing FRP tendons on the accurate assessment of structural performance, this dissertation (presented in Chapter 3) provides an innovative method employed to determine the transfer length for FRP tendons in prestressed concrete. Through associating the developed composite beam theory with the nonlinear local bond stress-slip relationship between FRP tendons and concrete, a closed-form solution is established.

2.2 Pretensioned concrete members reinforced with FRP tendons

In the current application of practical engineering, FRP materials can be divided into internal reinforcements and externally bonded reinforcements [29]. Internal FRP reinforcements could be used both as FRP tendons or multidimensional shapes such as grid reinforcements, whereas externally bonded reinforcements such as FRP laminates are applied to the surface of existing concrete structures for strengthening or retrofitting. FRP tendons as an alternative to steel reinforcement bars for strengthening concrete buildings have attracted much attention in recent decades, mainly because of their superior performance over conventional steel materials, such as light weight, noncorrosive, and nonmagnetic [30]. Among the structural application of FRP composite materials, prestressed concrete members with FRP tendons have become a promising research priority. For the prestressed concrete, it is very important to transfer the prestress force to concrete through end anchors or direct bonding. In pretensioned prestressed concrete members, the transmission of prestress depends on direct bonding, which means the investigation on bond behavior between concrete and FRP tendons is essential for understanding the nature of structure [31]. The part of post-tensioned prestressed concrete members is beyond the scope of this dissertation, and related study will be discussed in future work.

2.2.1 Bond-slip relationship for FRP tendons in concrete

According to a large number of experimental studies by Eligehausen et al. [32] (1983), the bond stress-slip behavior was investigated in which the deformed bars embedded in concrete as specimens are installed in a testing frame illustrated in Fig. 2.5 and subjected to monotonic and

cyclic loading, respectively. The expression of bond stress-bond relationship called Bertero-Eligehausen-Popov (BEP) model is given as follows:

$$\tau(s)=\tau_0\,(s/s_0)^{\alpha} \tag{7}$$

where $\tau(s)$ = bond stress acting on the contact surface as a function of slip s, s = the slip, the unknown parameters τ_0, s_0, α can be determined from test data.

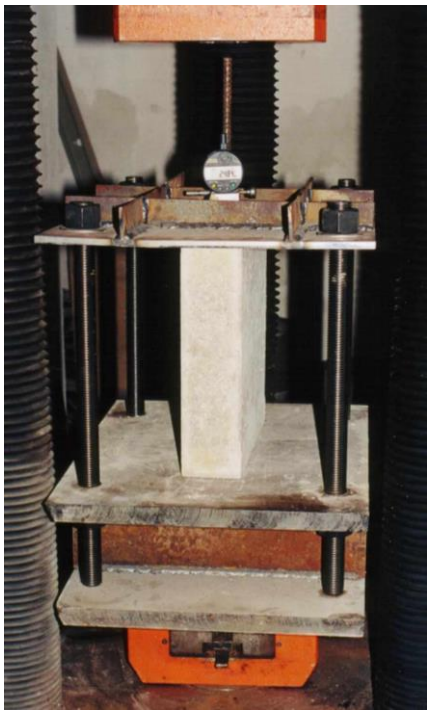

Fig. 2.5 Local bond-slip relationship test setup [33]

An analytical model presented in Filippou's study [34] (1986) is describing the hysteretic response of a single reinforcing bar anchored in the interior beam-column joint under random cyclic excitation. Based on the equilibrium and compatibility equations, it is assumed that the function of bond stress along the bar anchorage length is approximately piecewise linear, and the effect of concrete strains on slip is ignored. In 1990, Russo et al. [35] presented the analytical

solution for the system of reinforcing bar anchorage using the bond stress-slip relation expressed by the exponential functions from Eligehausen et al. [32].

$$\frac{d^2 s}{dx^2} = \frac{\pi d_b}{E_{lb} A_b} \tau(s) \tag{8}$$

where A_b = cross section area of reinforcing bars, d_b = diameter of reinforcing bar, E_{lb} = elastic modulus of reinforcing bars. For FRP materials, the characteristic of anisotropic results in different mechanical bond behavior compared to that of steel reinforcements. Therefore, Malvar [36] (1994) initially evaluated bond-slip performance between FRP rebars and surrounding concrete through experimental investigation on four types of GFRP rebars characterized by different surface deformations. Subsequently, the modified BEP model as an alternative to BEP model by Eligehausen et al. [32] is developed by Cosenza et al. [37] (1997) and is defined by the following expression:

$$\tau(s) = C s^{\alpha} \left(1 - \frac{s}{\bar{s}}\right) \tag{9}$$

In the case of modified BEP model, three unknown parameters C, α, and $\bar{s}$ can be calibrated by pullout tests. Since most of the work is focused on the structure within the serviceability state level, previous study by Cosenze et al. [37] (1997) has shown that it is sufficient to build a refined Cosenza-Manfredi-Realfonzo (CMR) model for the ascending branch. The expression of CMR model is as follows:

$$\tau(s) = \tau_m \left[1 - \exp\left(-\frac{s}{s_r}\right)\right]^{\beta} \tag{10}$$

where t_m = peak bond stress, unknown parameters β and s_r are also based on the curve-fitting of experimental data.

Based on experimental results of FRP tendons pullout tests, Focacci et al. [38] (2000) calibrated the set of parameters of previously given local bond stress-slip relationships, namely the BEP model, modified BEP model, and CMR model. In this dissertation (presented in Chapter 3), the expression of BEP model with parameters from Focacci et al.'s [38] study is assumed for the bond stress-slip relationship between FRP tendons and concrete.

2.2.2 Transfer length of prestressed FRP tendons

In a pretensioned concrete beam, the distance from the end of member over which the effective prestressed force is reached is defined as the transfer length. As an important parameter for the analysis of the flexural and shear strength, the knowledge of transfer length is essential for the design guidelines and performance evaluation of prestressed concrete members. Due to the lack of a thorough understanding of the mechanical behavior at the interface between concrete and FRP tendons, various empirical formulas have been presented to define the transfer length of prestressed FRP tendons in the literature [31,39-43].

Nanni et al. [31] (1992) investigated the transfer length of AFRP tendons (diameter of 8 mm to 16 mm) by measuring strain changes in concrete. The results showed that transfer lengths of AFRP tendons ranged from 300 mm to 400 mm and 250 mm to 450 mm, respectively, corresponding to the low and high level pretension. In the experimental study of Ehsani et al. [39] (1997), five commercially available FRP tendons, including three AFRP tendons and two CFRP

tendons, were measured to analyze the bonding behavior. It is concluded that the prestress level affects the transfer length significantly, which is also proved through theoretical analysis in this dissertation (presented in Chapter 3). Lu et al. [40] (2000) investigated three types of nominally 5/16-inch diameter FRP tendons made of Carbon Leadline^{TM}, Aramid Technora, and a carbon fiber reference material. The result of the study suggest that the ACI equation should be modified based on the fact that nominal bond stress of FRP materials is higher than that of steel tendons. It was also recommended that 50 bar diameters should be used for FRP tendon transfer length. A comparative study by Issa et al. [43] (1993) was carried out to determine the instantaneous and long-term transfer length of identical fiberglass and steel pretensioned members. The experimental results show that the transfer length of fiberglass and steel tendon is 10 to 11 inches. and 28 times the nominal diameter, respectively. A more detailed review on FRP tendons transfer length will be extended in Chapter 3.

Experimental methods vary among researchers, and inconsistency will inevitably exist in the process of defining the strain plateau. However, the proposed model (presented in Chapter 3) attempts to develop an appropriate and rigorous theory, specifically for prestressed concrete reinforced with FRP tendons in which a simple mechanics-based explanation is given to the nature of the transfer length. Perhaps just as important, the methodology explains how various mechanical variables and parameters influence the transfer length, which has not been mathematically defined before.

2.3 Externally bonded FRP laminates strengthening concrete

The importance of using FRP laminates for retrofitting or strengthening of existing concrete members is rapidly increasing in the field of structural design and engineering recent years for their prominent advantages, such as corrosion resistant, low installation costs, and readily available in several forms. Detailed information about material properties, design, installation, and maintenance of FRP systems for externally strengthening concrete structures is provided by ACI [44]. In addition, a large number of theoretical analysis and experimental investigations have been adopted to assess the mechanical performance of concrete beams strengthened with externally bonded FRP laminates. It is important to predict the FRP debonding failure with the aim of improving the flexural and shear strength of this type of beam. Research has shown that premature failures are primarily attributed to the distribution of interfacial shear stress and normal stress.

2.3.1 Interfacial stresses

There are many research efforts of available literature [8-10,45,46] focused on the debonding failure, and it was confirmed that the existence of a combination of interfacial stresses concentration near the cutoff end of plate caused the debonding failure. Based on the elastic analysis, Vilnay [8] (1988) conducted the early analysis of concrete beams strengthened by epoxy-bonded steel plate. For the case of applying a concentrated load in the midspan of a simple support beam, the shear and peeling distributed forces were studied, and it was concluded that the maximum stress value appeared at the end of the bonded plate. Compared to Vilnay's method [8], Täljsten [47] (1997) considered the curvature of the beam and different boundary conditions to

provide an analytical solution for the interfacial stresses in plated beams. The analytical solution of Malek et al. [45] (1998) was developed for predicting interfacial shear and normal stresses at the plate ends in strengthening RC beams with FRP plates, which was validated by comparison with the results of finite element analysis. However, the bending deformation was neglected in Malek et al.'s [45] solution, resulting in a lack of information on the influence of various parameters on interfacial stresses at failure. Based on the deformation compatibility approach, Smith and Teng [46] (2001) made predictions for interfacial stresses in plated beams in terms of three load cases.

Instead of the above approaches, Robert and Hajikazemi [9] (1989) developed a two-stage model used to analyze interfacial shear and normal stress distributions for the case of the uniformly distributed load acting on the RC beam with externally bonded steel plate. Robert [10] (1989) established an analytical method consisted of three stages to estimate the interfacial stress, in which full composite action was assumed between the bonded plate and concrete. However, the analysis of the behavior of concrete beams strengthened by externally bonded FRP laminates that should be performed based on the partial composite action rather than full composite action. Consequently, the prediction of interfacial stress from this dissertation is based on an innovative partial composite action, taking into account the shear stiffness from experimental results reported in the literature [17,48]. For this reason, the proposed model (presented in Chapter 4) leads to an improved understanding of the nature of the response in terms of mechanics.

2.3.2 Bond behavior between FRP laminates and concrete

As mentioned above, an accurate knowledge of the bond behavior between FRP laminates and concrete plays a substantial role in developing a reliable solution for the evaluation of interfacial stresses, thereby helping understand the debonding failure. Some existing studies [48-51] have found out that the bond performance of FRP laminates to the concrete substrate mainly depends on surface preparation, concrete strength, bond length, FRP laminates to concrete width ratio, FRP laminates axial stiffness, and adhesive strength. There are three basic methods commonly adopted to explore the bond-slip relationship between concrete and FRP laminates, pull test [11-13,16,17,48], theoretical analysis [49], and meso-scale finite element simulation [14,52,53]. Lorenzis et al. [48] (2001) evaluated the slip modulus based upon flexural tests, which was performed on a plain concrete beam externally bonded with an inverted-T shape CFRP laminate, and a linear-elastic analysis was carried out by the shear lag approach. As an alternative to the conventional method for recording the strain distribution, Dai et al. [13] (2005) accurately measured pullout forces and end slips in pullout tests for FRP laminates to concrete through experimental study and theorical analysis. According to fib Model Code for concrete structures 2010 [54], Ko et al. [17] (2014) calibrated three primary parameters of the given bilinear local bond-slip model by means of experimental results of 18 double-shear bond tests. Compared with the other two nonlinear bond stress-slip models, Ko et al.'s model is proved effectively. Therefore, the elastic ascending branch in the bilinear model by Ko et al. [17] is used as the constitutive bond-slip definition between the FRP laminates and concrete in this dissertation (presented in Chapter 4), associating with developed composite beam theory, to further evaluate the influence of various mechanical variables and parameters to the interfacial stresses.

References

[1] Granholm, H. “Om sammansatta balkar och pelare med särskild hänsyn till spikade träkonstruktioner.” (On composite beams and columns with particular regard to nailed timber structures). Transaction of Chalmer University of Technical, No. 88. Gothenburg 1949.

[2] Newmark NM, Siess CP, Viest IM. Test and analysis of composite beams with incomplete interaction. Proceedings of Society for Experimental Stress Analysis. 1951;9(1):75-92.

[3] Goodman JR, Popov EP. Layered beam systems with interlayer slip. J Struct Div 1968;94:2535-48.

[4] Turmo J, Lozano-Galant JA, Mirambell E, Xu D. Modeling composite beams with partial interaction. Journal of Constructional Steel Research. 2015 Nov 1;114:380-93.

[5] Holmberg, Ake, and Erik Plem. Behaviour of load-bearing sandwich-type structures. Handlingar nr 49 Transactions, Statens institut för byggnadsforskning, 1965.

[6] Thompson EG, Vanderbilt MD, Goodman JR. Finite element analysis of layered wood systems. Journal of the structural Division. 1975 Dec;101(12):2659-72.

[7] Murakami H. A laminated beam theory with interlayer slip. Journal of Applied Mechanics 1984; 51:551-559.

[8] Vilnay O. The analysis of reinforced concrete beams strengthened by epoxy bonded steel plates. International Journal of Cement Composites and Lightweight Concrete. 1988 May 1;10(2):73-8.

[9] Roberts TM, Hajikazemi H. Theoretical study of the behaviour of reinforced concrete beams streng-thened by externally bonded steel plates. Proceedings of the Institution of Civil Engineers. 1989 Mar;87(1):39-55.

[10] Roberts TM. Approximate analysis of shear and normal stress concentrations in the adhesive layer of plated RC beams. The Structural Engineer. Part A: the journal of the Institution of Structural Engineers-monthly. 1989;67(12):229-33.

[11] Lee YJ, Boothby TE, Bakis CE, Nanni A. Slip modulus of FRP sheets bonded to concrete. Journal of Composites for Construction. 1999 Nov;3(4):161-7.

[12] Nakaba K, Kanakubo T, Furuta T, Yoshizawa H. Bond behavior between fiber-reinforced polymer laminates and concrete. ACI Structural Journal. 2001 May 1;98(3):359-67.

[13] Dai J, Ueda T, Sato Y. Development of the nonlinear bond stress–slip model of fiber reinforced plastics sheet–concrete interfaces with a simple method. Journal of Composites for Construction. 2005 Feb;9(1):52-62.

[14] Lu XZ, Teng JG, Ye LP, Jiang JJ. Bond–slip models for FRP sheets/plates bonded to concrete. Engineering Structures. 2005 May 1;27(6):920-37.

[15] Pellegrino C, Tinazzi D, Modena C. Experimental study on bond behavior between concrete and FRP reinforcement. Journal of Composites for Construction. 2008 Apr;12(2):180-9.

[16] Guo ZG, Cao SY, Sun WM, Lin XY. Experimental study on bond stress-slip behaviour between FRP sheets and concrete. In: FRP in Construction, Proceedings of the International Symposium on Bond Behaviour of FRP in Structures; 2005 Dec; 77-84.

[17] Ko H, Matthys S, Palmieri A, Sato Y. Development of a simplified bond stress–slip model for bonded FRP–concrete interfaces. Construction and Building Materials. 2014 Oct 15;68:142-57.

[18] Girhammar UA, Gopu VK. Composite beam-columns with interlayer slip—exact analysis. Journal of Structural Engineering. 1993 Apr;119(4):1265-82.

[19] Adam C, Heuer R, Jeschko A. Flexural vibrations of elastic composite beams with interlayer slip. Acta Mechanica. 1997 Mar 1;125(1-4):17-30.

[20] Foraboschi P. Analytical solution of two-layer beam taking into account nonlinear interlayer slip. Journal of engineering mechanics. 2009 Oct;135(10):1129-46.

[21] Dall'Asta A, Zona A. Non-linear analysis of composite beams by a displacement approach. Computers & structures. 2002 Nov 1;80(27-30):2217-28.

[22] Ranzi G, Zona A. A steel–concrete composite beam model with partial interaction including the shear deformability of the steel component. Engineering Structures. 2007 Nov 1;29(11):3026-41.

[23] Zona A, Ranzi G. Finite element models for nonlinear analysis of steel–concrete composite beams with partial interaction in combined bending and shear. Finite Elements in Analysis and Design. 2011 Feb 1;47(2):98-118.

[24] Tahmasebinia F, Ranzi G, Zona A. Probabilistic three-dimensional finite element study on composite beams with steel trapezoidal decking. Journal of Constructional Steel Research. 2013 Jan 1;80:394-411.

[25] Titoum M, Tehami M, Achour B, Jaspart JP. Analysis of semi-continuous composite beams with partial shear connection using 2-D finite element approach. Asian Journal of Applied Sciences. 2008;1(3):185-205.

[26] Bai F, Davidson JS. Analysis of partially composite foam insulated concrete sandwich structures. Engineering Structures. 2015 May 15;91:197-209.

[27] Bai F, Davidson JS. Theory for composite sandwich structures with unsymmetrical wythes and transverse interaction. Engineering Structures. 2016 Jun 1;116:178-91.

[28] Bai F, Davidson JS. Composite beam theory for pretensioned concrete structures with solutions to transfer length and immediate prestress losses. Engineering Structures. 2016 Nov 1;126:739-58.

[29] Sha X, Davidson JS. Analysis of transfer length for prestressed FRP tendons in pretensioned concrete using composite beam theory. Composite Structures. 2019 Jan 15;208:665-77.

[30] ACI 440.4R-04, Prestressing Concrete with FRP Tendons, American Concrete Institute, 2004.

[31] Nanni A, Utsunomiya T, Yonekura H, Tanigaki M. Transmission of prestressing force to concrete by bonded fiber reinforced plastic tendons. ACI Structural Journal. 1992 May 1;89(3):335-44.

[32] Eligehausen R. Local bond stress-slip relationships of deformed bars under generalized excitations, Earthquake Engineering Research Center. Report No. UCB/EERC-83/23, University of California. 1983.

[33] Campione, Giuseppe, et al. Experimental investigation on local bond-slip behaviour in lightweight fiber reinforced concrete under cyclic actions. 13th World Conference on Earthquake Engineering Vancouver, BC, Canada, Paper. No. 2087. 2004.

[34] Filippou FC. A simple model for reinforcing bar anchorages under cyclic excitations. Journal of Structural Engineering. 1986 Jul;112(7):1639-59.

[35] Russo G, Zingone G, Romano F. Analytical solution for bond-slip of reinforcing bars in RC joints. Journal of Structural Engineering. 1990 Feb;116(2):336-55.

[36] Malvar LJ. Bond stress-slip characteristics of FRP rebars. Naval Facilities Engineering Service Center Port Hueneme CA; 1994 Feb.

[37] Cosenza E, Manfredi G, Realfonzo R. Behavior and modeling of bond of FRP rebars to concrete. Journal of composites for construction. 1997 May;1(2):40-51.

[38] Focacci F, Nanni A, Bakis CE. Local bond-slip relationship for FRP reinforcement in concrete. Journal of composites for construction. 2000 Feb;4(1):24-31.

[39] Ehsani MR, Saadatmanesh H, Nelson CT. Transfer and flexural bond performance of aramid and carbon FRP tendons. PCI Journal. 1997 Jan 1;42(1):76-86.

[40] Lu Z, Boothby TE, Bakis CE, Nanni A. Transfer and development lengths of FRP prestressing tendons. PCI J 2000;45:84-95.

[41] Mahmoud ZI, Rizkalla SH, Zaghloul EE. Transfer and development lengths of carbon fiber reinforced polymers prestressing reinforcement. ACI Structural Journal. 1999 Jul 1;96:594-602.

[42] Soudki KA, Green MF, Clapp FD. Transfer length of carbon fiber rods in precast pretensioned concrete beams. PCI Journal. 1997 Sep 1;42(5):78-87.

[43] Issa MA, Sen R, Amer A. Comparative study of transfer length in fiberglass and steel pretensioned concrete members. PCI Journal. 1993 Dec;38(6).

[44] American Concrete Institute. Committee 440. Guide for the Design and Construction of Externally Bonded FRP Systems for Strengthening Concrete Structures: ACI 440.2 R-08. American Concrete Institute.

[45] Malek AM, Saadatmanesh H, Ehsani MR. Prediction of failure load of R/C beams strengthened with FRP plate due to stress concentration at the plate end. ACI Structural Journal. 1998 Mar 1;95:142-52.

[46] Smith ST, Teng JG. Interfacial stresses in plated beams. Engineering Structures. 2001 Jul 1;23(7):857-71.

[47] Täljsten B. Strengthening of beams by plate bonding. Journal of Materials in Civil Engineering. 1997 Nov;9(4):206-12.

[48] De Lorenzis L, Miller B, Nanni A. Bond of FRP laminates to concrete. ACI Materials Journal. 2001 May;98(3):256-64.

[49] Chen JF, Teng JG. Anchorage strength models for FRP and steel plates bonded to concrete. Journal of structural engineering. 2001 Jul;127(7):784-91.

[50] Ueda T, Dai JG, Sato Y. A nonlinear bond stress-slip relationship for FRP sheet-concrete interface. InProc. of international symposium on latest achievement of technology and research on retrofitting concrete structures 2003 Jul 14 (Vol. 113).

[51] Yuan H, Teng JG, Seracino R, Wu ZS, Yao J. Full-range behavior of FRP-to-concrete bonded joints. Engineering structures. 2004 Apr 1;26(5):553-65.

[52] Lu XZ, Ye LP, Teng JG, Jiang JJ. Meso-scale finite element model for FRP sheets/plates bonded to concrete. Engineering Structures. 2005 Mar 1;27(4):564-75.

[53] Baky HA, Ebead UA, Neale KW. Nonlinear micromechanics-based bond–slip model for FRP/concrete interfaces. Engineering Structures. 2012 Jun 1;39:11-23.

[54] Taerwe L, Matthys S. Fib Model Code for Concrete Structures 2010.

Chapter 3 Analysis of Transfer Length for Prestressed FRP Tendons in Pretensioned Concrete using Composite Beam Theory

3.1 Introduction

The use of fiber reinforced polymer (FRP) for concrete construction as important research has attracted much attention at many research institutes around the world over recent decades. FRP materials offer significant advantages over conventional steel reinforcement: excellent corrosion resistance, high strength-to-weight ratio, linear-elastic behavior to a failure of the former and non-magnetism [1]. In general, FRP reinforcement can be categorized based on the types of fiber use to form the reinforcement: organic fibers, such as Aramid Fiber Reinforced Polymer (AFRP), and inorganic fibers, such as Carbon Fiber Reinforced Polymer (CFRP) and Glass Fiber Reinforced Polymer (GFRP). The applications of FRPs can be divided into internal reinforcements and externally bonded reinforcements. Internal FRP reinforcements have been used both as one-dimensional FRP tendons or multidimensional shapes such as grid reinforcements whereas externally bonded reinforcements such as FRP sheets are applied to the surface of the concrete for strengthening or repair.

As early as the 1960s, the U.S. Army Corps of Engineers Waterways Experiment Station stated that pioneering developments were being established for FRP in polymer concrete reinforcement applications [2]. In the 1970s, the University of Stuttgart in Germany studied GFRP as prestressing tendons [3]; experimental FRP studies were also carried out in Japan in the 1970s

[4]. In 1995, the Canadian Network of Centres of Excellence on Intelligent Sensing for Innovative Structures (ISIS Canada) was established to investigate the development of the FRP used in bridges as a replacement for steel reinforcement [5].

One significant challenge with pretensioned concrete members is in understanding how the prestressing force is transferred from the prestressing tendon to the concrete. The distance along the tendon over which the effective prestressing force is gradually reached is referred to as the transfer length [6]. The sum of the transfer length and the flexural bond length is referred to as the development length, which significantly influences the bending and shear strength of prestressed concrete members. As an important parameter for checking the flexural and shear strength, the determination of transfer length is absolutely necessary for the development of design guidelines and performance evaluation of prestressed concrete members. Prestressing force transferred to the concrete depends primarily on the bond behavior in the end-region of the pretensioned concrete structures. It should be noted that the material properties and the mechanical behavior differences between FRP tendons and steel strands are very significant, as demonstrated by a large number of experimental studies presented in the literature [7,13,33,34]. Therefore, it is believed that the bond characteristics used for steel strands in concrete members cannot be assumed for FRP tendons, and therefore standardization and guidelines for the design of FRP reinforced concrete members should be based on knowledge specifically dedicated to FRP materials.

Several equations intended to define the transfer length of prestressed FRP tendons in pretensioned concrete members have been presented in the literature [8,11,14,17]. These equations were primarily developed by measuring strain change in tests, and accordingly, pure mechanics-based definitions of these important relationships is lacking. Therefore the overall objective of this study is to develop a new method of determining the transfer length for FRP

tendons in pretensioned prestressed concrete members by means of combining the local bond-slip nonlinear relationship for FRP tendons in concrete with composite beam theory. The transfer length is solved with closed-form solutions based on composite beam theory as well as the knowledge of the local bond stress-slip relationship between FRP tendons and concrete. The transfer length model is solved through an exact solution of piecewise functions. This novel approach is offered as a potentially more accurate method than the conventional numerical methods that involve excessively complicated formulas. Furthermore, the result of comparisons between the model-predicted data and the existing experimental data demonstrates that the closed-form solutions of the piecewise functions are effective and accurate. The proposed model improves convenience and accuracy compared to the conventional use of empirical formulations.

3.2 Background

3.2.1 Transfer length for FRP tendons

As illustrated by Fig. 3.1, to obtain the effective prestress f_c in a pretensioned concrete member, the stress in the concrete at the free end is zero, which increases over the transfer length. The transfer length of prestressed FRP tendons in concrete flexural members is affected by many factors, including the diameter of tendons, concrete compression strength, initial prestress force, bond characteristics between FRP tendons and concrete, release method, etc. However, these factors have not been completely agreed on in specifications and literatures used for the design of prestressed concrete beams. The conventional method for determining transfer length during testing is by measuring the strain change in concrete or in the tendons using strain gauges before and after prestressing force release.

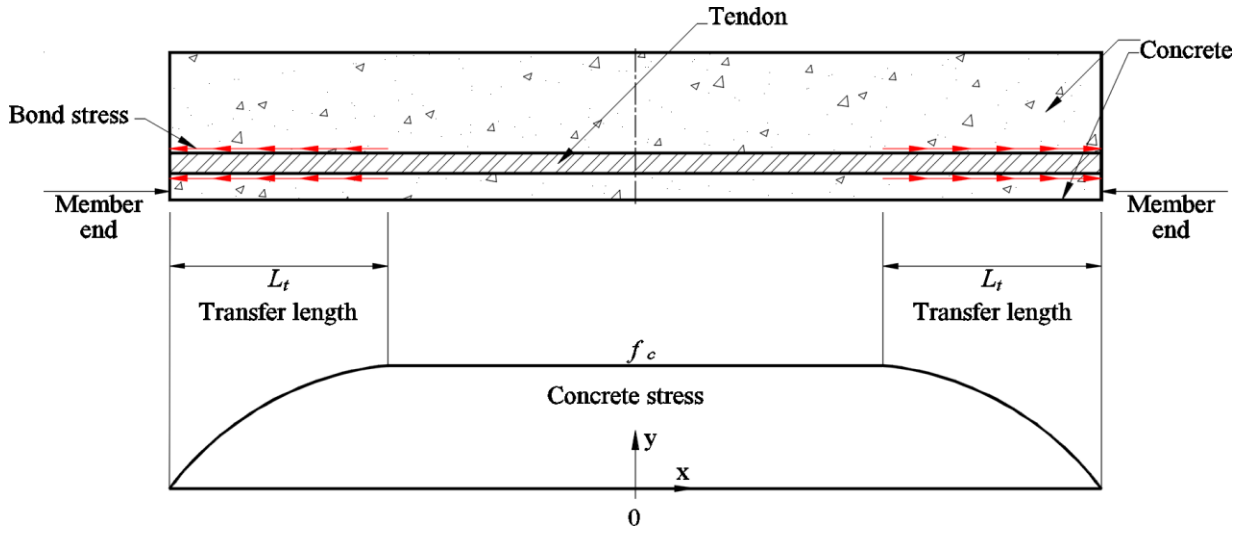

Fig. 3.1 Stress transfer from tendon to concrete

In ACI 440.4R-04 [9], "Prestressing Concrete Structures with FRP Tendons," which is used for the design of structural concrete members reinforced with FRP bars, the transfer length of carbon FRP is recommended as Eq. (1), which is based on test data by Mahmoud et al. [10].

$$L_t = \frac{f_{pe}\, d_b}{\alpha_t\, f_c'^{0.67}} \tag{1}$$

where f_{pe} is the effective stress in tendon, b_d is the diameter of the reinforcing tendon, f_c' is the specified concrete compressive strength, and α_t is 1.9 and 4.8 for N-mm units (10.0 and 25.3 for inch-pound units) for Leadline™ and Carbon Fiber Composite Cables (CFCC), respectively. Cousins et al. [11] conducted an experimental investigation for determining the transfer length of epoxy-coated and bare (uncoated) prestressing strands, and also studied the effects of time on transfer length. Based on experiments using both uncoated and epoxy coated strands, Cousins et al. [12] developed analytical equations that assumed a plastic zone and an elastic zone within the transfer length. Nanni et al. [13] examined the transfer length for the AFRP tendons using

nondestructive measurement of the strain variation in the tendons and in concrete. The results proved that adhesion of sand to the tendon surface, tendon size and concrete strength could affect the transfer length of AFRP tendons. In addition, the study showed differences of the transmission mechanism between AFRP tendons and steel strands due to the lower rigidity and higher Poisson's ratio of the AFRP tendons. From the measurement made by Soudki et al. [14], the transfer length of CFRP rods was estimated as 80 and 90 bar diameters for a prestress level of 50 and 70 percent, respectively. It was also found that the equations for steel strands in the provision of the ACI Code (318-08) [15] was not applicable to CFRP Leadline™ rods. Grace [16] carried out the empirical study on double-T girders prestressed with CFRP Leadline™ tendons and CFCC strands. On the basis of modification in an available model, the transfer length of CFRP Leadline™ tendons and CFCC strands was predicted. The test from Rambo-Roddenberry et al. [18] focused on CFCC in prestressed concrete piles for bridge foundations. Strain measurements indicated that the transfer length of CFCC tendons was 16.7% less than that recommended by ACI 440.4R–04, 30.6% less than AASHTO [19] provisions of 50 d_b (30 in.) and 60 d_b (36 in.), and 35.9% less than predicted by the equation from ACI Code (318-08) [15]. The transfer length for prestressed FRP tendons recommended by the equation from different sources is summarized in Table 3.1.

Table 3.1 Transfer length for FRP tendons from literature

ACI 440.4R-04 [9]	$L_t = \dfrac{f_{pe}\, d_b}{\alpha_t\, f_c'^{0.67}}$
Cousins et al. [11]	$L_t = 0.5\left(\dfrac{U_t' \sqrt{f_{ci}'}}{B}\right) + \dfrac{f_{se}\, A_s}{\pi\, d\, U_t' \sqrt{f_{ci}'}}$
Soudki et al. [14]	$L_t = 80\, d_b \ or\ 90\, d_b$
ACI Code (318-08) [15]	$L_t = \left(\dfrac{f_{se}}{3}\right) d_b$, inch
AASHTO [19]	$L_t = 50\, d_b \ or\ 60\, d_b$

3.2.2 Composite beam theory

The earliest composite beam theory was presented in 1949 by Granholm [20] for nailed timber structures. In short, this theory was developed for beams composed of two separate elements in which the horizontal shear is transmitted from one element of the member to the other through the shear connectors, as illustrated in Fig. 3.2. The set of governing equations for this situation is derived and is solved for the composite beam under external load.

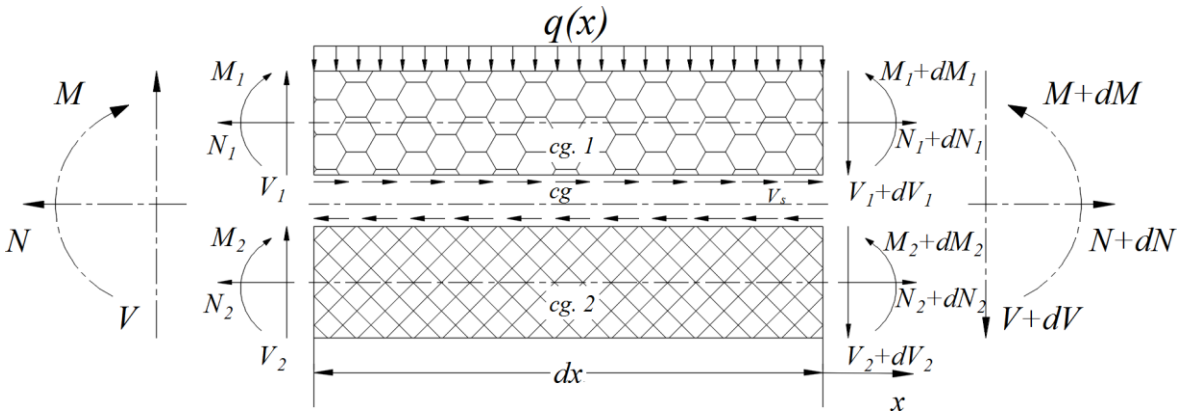

Fig. 3.2 Differential element in composite beam member subjected to axial load (N), moment (M), shear force (V), and distributed load (q(x))

In the study by Newmark et al. [21], the theoretical analysis of composite beams with incomplete interaction was compared with results from the tests of T-beams consisting of a rolled steel I-beam and a concrete slab. The good agreement between the test and analytical results indicated the feasibility and effectiveness of composite beam theory. The research presented in Goodman and Popov's [22] paper shows excellent agreement with experimental results of layered wood beams, and also confirms the feasibility of the theories previously developed. Girhammar and Gopu [23] dealt with the composite beam-columns with partial interaction and presented closed-form solutions for first- and second-order cases. Based on Girhammar and Pan's [24] dynamic analysis of composite members, flexural vibration of elastic composite beams with interlayer slip was analyzed by the different dynamic responses in Adam et al. [25]. Foraboschi [26] presented the analytical solution of composite beams with nonlinear interlayer slip and proved that nonlinearity cannot be ignored. Bai and Davidson [27] provided closed form solutions for the analysis of foam insulated concrete sandwich panels considering both the longitudinal and transverse interactions using composite beam theory. Subsequently, Bai and Davidson [28] applied this theoretical development to pretensioned concrete structures and established the force

equilibrium between prestressing strands and concrete by means of a linear relationship assumption between slip and interface shear force. The composite beam theory may be used for any kind of structures composed of two interconnected elements as long as the underlying assumptions are satisfied.

3.2.3 Bond stress-slip of FRP tendons to concrete

An accurate formulation of the local bond-slip relationship between the tendon and surrounding concrete is critical to any analytical model intended to describe the behavior of pretensioned concrete with prestressing tendons. The local bond stress-slip relationships expressed by an exponential monomial function were proposed from extensive experiments in the study of Eligehausen et al. [29]. The same model was used in CEB-FIP Model Code 90 [30]; the function of the bond stresses τ and slip s is defined in Eq. (2) and illustrated in Fig. 3.3:

$$\tau = \begin{cases} \tau_{\max}\left(s/s_1\right)^{\alpha}, & 0 \le s \le s_1 \\ \tau_{\max}, & s_1 \le s \le s_2 \\ \tau_{\max} - \left(\tau_{\max} - \tau_f\right)\left(\dfrac{s - s_2}{s_3 - s_2}\right), & s_2 \le s \le s_3 \\ \tau_f, & s_3 \le s \end{cases} \tag{2}$$

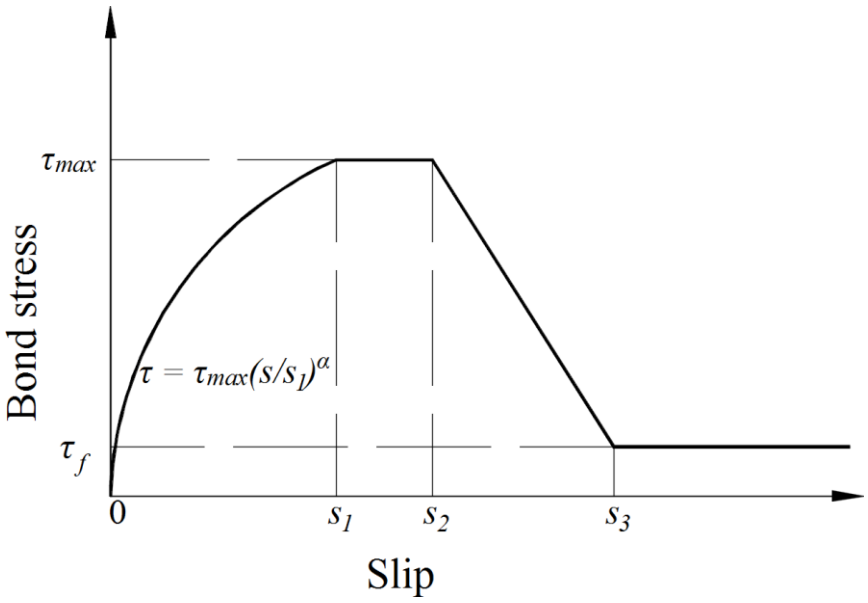

Fig. 3.3 Analytical bond stress-slip relationship

where the analytically obtained coefficient $\alpha = 0.4$ agreed with bond stress-slip test data [30]. Other parameters depended on factors such as confinement, bond condition and concrete strength. In Russo et al. [31], the analytical solution for the system of reinforcing bar anchorage was made by using the bond stress-slip relation expressed by the exponential functions from Eligehausen et al. [29]. Eligehausen et al. established that experimental bond stress-slip relationship data from research using conventional steel strands is not accurate for the case of FRP tendons in pretensioned prestressed concrete members. Because FRP tendons may be composed of aramid, carbon, or glass fiber embedded in a resin matrix, the differences arise both from the Poisson's ratio and from the axial strain ratio with respect to that of the steel materials. As the first FRP bond-slip analytical model, the Malvar model [32] was obtained by conducting experiments on four types of GFRP rebars characterized by different surface deformations. Nanni et al. [33] provided experimental results obtained with a braided AFRP tendon having a nominal diameter of 16-mm and initial prestress force of 156.6 KN and used Finite Element Method (FEM) analysis to

predict the performance of AFRP tendon during prestress force transfer. Cosenza et al. [34] proposed a modified Bertero-Eligehausen-Popov (mBEP) model as an alternative to Bertero-Eligehausen-Popov (BEP) model by Eligehausen et al. [29] and the Cosenza-Manfredi-Realfonzo (CMR) model, which represented the entire $\tau - s$ curve shown in Fig. 3.3 and the ascending branch of the curve, respectively. In the experimental investigation focused on the pull-in behavior of FRP tendons by Lees et al. [35], the comparison of the transfer behavior of two types of AFRP tendons with steel strands was addressed by assuming both a constant and a nonlinear relationship between the bond stress and slip through the transfer zone. Focacci et al. [36] calibrated the set of unknown parameters of two given local $\tau = \tau(s)$ relationships using energy approach based upon experimental results of FRP tendons pullout tests. The proposed model and parameters characterize the local bond stressslip relationship resulting from the average behavior of FRP tendons with diameter of 6.4 mm, 9.5 mm, 12.7 mm, and 15.9 mm. In the present study, the BEP expression with parameters from Focacci et al.'s [36] study was assumed for the bond stress-slip relationship between FRP tendons and concrete, as given by Eq. (3). In metric (SI) units:

$$\tau(s) = 8.847\, s^{0.337} \tag{3}$$

3.3 Methodology

The development of theory and analysis approach presented herein for pretensioned concrete members with prestressed FRP tendons is based on the following assumptions and limitations:

(1) Since this development focuses on transfer length that will involve small strains under typical conditions, linear elastic constitutive law behavior and small displacement of structures are assumed.

(2) The application of interest is towards relatively slender concrete members and therefore Euler-Bernoulli beam theory is applied in which shear deformation of the cross section is negligible.

(3) FRP tendons provide no bending resistance.

(4) The tendons are straight and occupy the same position at each cross section; the eccentricity of the prestressing strands is constant along the length.

3.3.1 Axial force equilibrium

The geometry and notation for a pretensioned concrete member cross-section with prestressed FRP tendons is illustrated in Fig. 3.4.

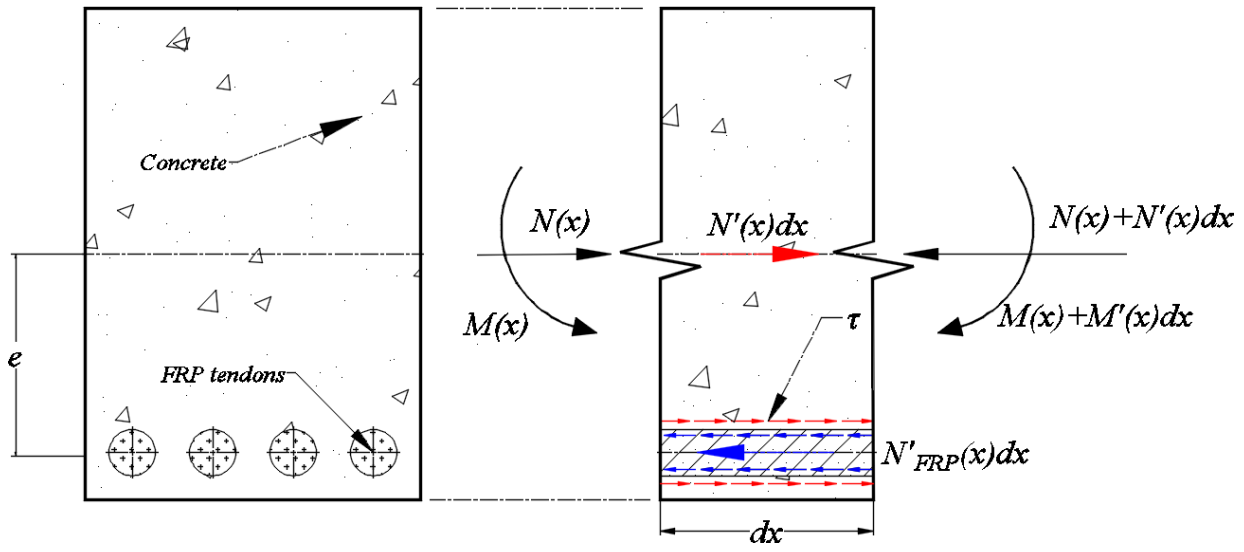

Fig. 3.4 Cross-section of prestressed FRP reinforced concrete member under internal forces

The prestress force $N(x)$ in the concrete is transferred by the bond stress τ at the interface between the concrete and FRP tendons. The bond stress τ is composed of three parts: adhesion, friction, and shearing resistance [37]. The axial direction equilibrium condition of the force acting on the infinitesimal element shown in Fig. 3.4 is given by Eq. (4):

$$\tau C\,dx = \left[N(x) + N'(x)\,dx\right] - N(x) = N'(x)\,dx \tag{4}$$

where τ = bond stress generated in the concrete surrounding the FRP tendons, C = total circumferences of FRP tendons and $N(x)$ = resultant axial force acting on the cross section of the member as well as $N(x)+N'(x)$ = the first degree Taylor polynomial for a given function of resultant axial force acting on the cross section.

It can be noted that the bond stress τ at the interface exists not only in the concrete but also in the FRP tendons. The resultant axial force $N'_{FRP}(x)\,dx$ in the FRP tendons results, which

is the same magnitude and the opposite direction relative to the resultant axial force $N'(x)\,dx$ in the concrete shown in Fig. 3.4. This is defined by Eq. (5) without considering the sign:

$$\tau\, C\, dx = N'(x)\, dx = N'_{FRP}(x)\, dx \tag{5}$$

Substituting $N(x) = A_c\, \sigma_c$ and $N_{FRP}(x) = A_{FRP}\, \sigma_{FRP}$ into the Eq. (5), where σ_c = the concrete stress due to axial direction deformation, σ_{FRP} = the FRP tendons stress due to axial direction deformation, A_c = the cross section area of the concrete and A_{FRP} = the total cross section area of the FRP tendons:

$$\tau\, C = \left(A_c\, \sigma_c\right)' = \left(A_{FRP}\, \sigma_{FRP}\right)' \tag{6}$$

Substituting the concrete stress $\sigma_c = E_c\, \varepsilon_c$ into Eq. (6), yields Eq. (7), where E_c = the elastic modulus of the concrete and ε_c = the concrete axial strain:

$$\tau\, C = A_c\, E_c\, \varepsilon_c' \tag{7}$$

Eq. (8) is obtained by substituting the expression of $\varepsilon_c = s_{2c}'$ into Eq. (7), where s_{2c} = the concrete displacement due to the axial force. Correspondingly, s_{2FRP} = the FRP tendon displacement due to the axial force.

$$\tau\, C = A_c\, E_c\, s_{2c}'' \tag{8}$$

The relative movement between the FRP tendons and concrete is defined as the slip s. To illustrate this further, the slip s is broken into three parts: s_1, s_2 and s_3. The slip s_1 associated with bending is illustrated in Fig. 3.5, where e = eccentricity, υ = the deflection of the elastic curve

and θ = the slope angle. Using $\theta \approx \tan\theta = \upsilon'$, the relationship is established as Eq. (10). The slip s_2 is the displacement difference between the concrete and FRP tendons under the axial force, and the slip $s_3 = \int \varepsilon_{is}\, dx$ is the result of prestressing tendon retraction, where ε_{is} is the strain associated with the prestress force before transfer.

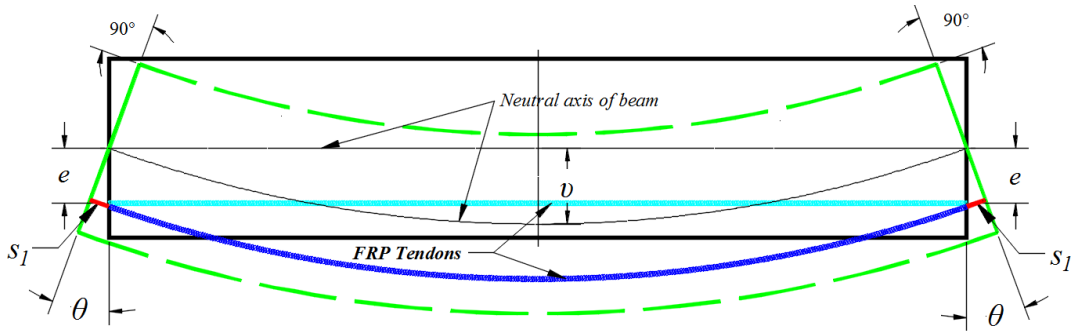

Fig. 3.5 The slip s_1 resulting from curvature

$$s = s_1 + s_2 + s_3 \tag{9}$$

$$s_1 = e\theta = e\upsilon' \tag{10}$$

$$s_2 = s_{2FRP} + s_{2c} \tag{11}$$

$$s_3 = \int \varepsilon_{is}\, dx \tag{12}$$

Taking the second derivative of Eq. (11) with respect to the independent variable x:

$$s_2'' = s_{2FRP}'' + s_{2c}'' \tag{13}$$

Accordingly,

$$N(x) = N_{FRP}(x) \tag{14}$$

Establishing the equilibrium condition given by Eq. (15):

$$A_c \, \sigma_c = A_{FRP} \, \sigma_{FRP} \tag{15}$$

Substituting $\sigma_c = E_c \, \varepsilon_c$ and $\sigma_{FRP} = E_{FRP} \, \varepsilon_{FRP}$ into Eq. (15), where E_{FRP} = the elastic modulus of the FRP tendons and ε_{FRP} = the axial strain of the FRP tendons:

$$A_c \, E_c \, \varepsilon_c = A_{FRP} \, E_{FRP} \, \varepsilon_{FRP} \tag{16}$$

Substituting the expressions of $\varepsilon_c = s'_{2c}$ and $\varepsilon_{FRP} = s'_{2FRP}$ into Eq. (16) yields Eq. (17):

$$A_c \, E_c \, s'_{2c} = A_{FRP} \, E_{FRP} \, s'_{2FRP} \tag{17}$$

Taking the first derivative of Eq. (17):

$$A_c \, E_c \, s''_{2c} = A_{FRP} \, E_{FRP} \, s''_{2FRP} \tag{18}$$

Eq. (19) is obtained by combining Eq. (13) with Eq. (18):

$$s''_2 = \left(1 + \frac{A_c \, E_c}{A_{FRP} \, E_{FRP}} \right) s''_{2c} = \left(1 + \frac{A_{FRP} \, E_{FRP}}{A_c \, E_c} \right) s''_{2FRP} \tag{19}$$

Substituting Eq. (8) into Eq. (19), results in Eq. (20):

$$\tau \, C = A_c \, E_c \, \frac{s''_2}{\left(1 + \dfrac{A_c \, E_c}{A_{FRP} \, E_{FRP}} \right)} \tag{20}$$

In terms of average $\tau = \tau(s)$ relationships proposed by Focacci et al. [36], the curve reported in Fig. 3.6 assumes a relationship between the bond stress and slip for FRP tendons in concrete corresponding to Eq. (3). The empirical models based directly on regression analysis of test data is only for a general indication of the average bond-slip behavior of the FRP tendons with diameters of 6.4 mm, 9.5 mm, 12.7 mm and 15.9 mm.

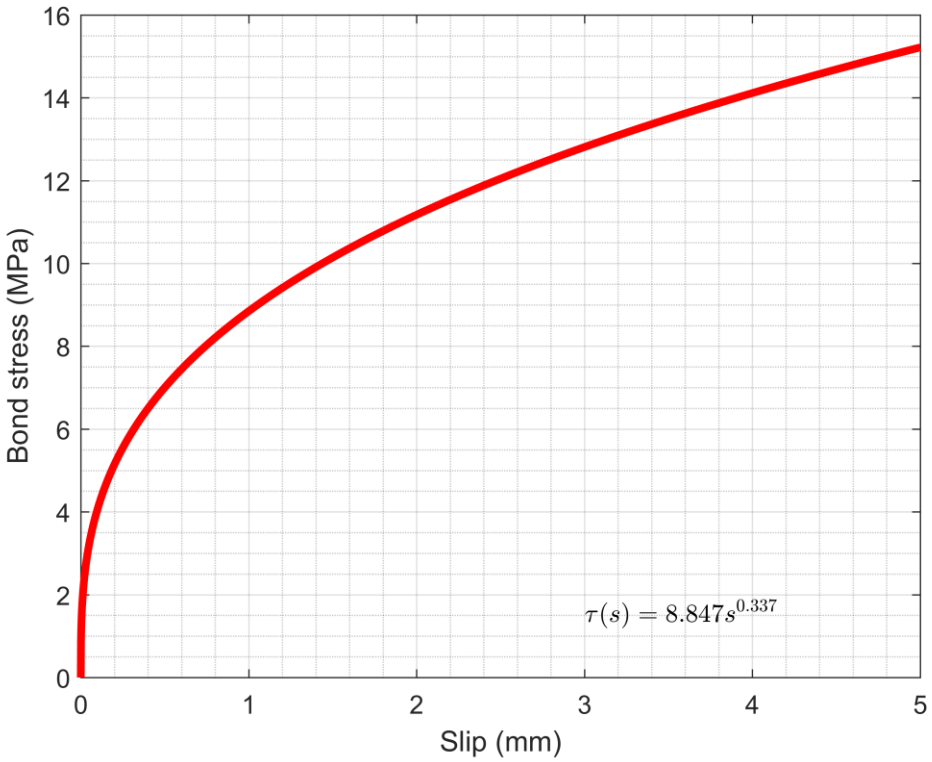

Fig. 3.6 BPE Model for $\tau = \tau(s)$ relationship with calibrated parameters

In certain situations, such as when the serviceability criteria is dealt with in structural analyses, the ascending branch of the curve is applied as a refined modeling of the bond stress and slip, and the horizontal branch and descending branch of the bond stress-slip curve presented in CEB-FIP Model Code can be considered negligible. Focacci et al. [36] has verified the reliability

and accuracy of the BPE model using the parameters presented in their paper. For these reasons, Eq. (3) is substituted into Eq. (20). In metric (SI) units:

$$8.847\, s^{0.337}\, C = A_c\, E_c \frac{s_2''}{\left(1+\dfrac{A_c\, E_c}{A_{FRP}\, E_{FRP}}\right)} \tag{21}$$

Substituting Eq. (10), Eq. (11), and Eq. (12) into Eq. (9), then taking the second derivative of the result, Eq. (22) can be written as:

$$s_2'' = s'' - e\upsilon''' \tag{22}$$

Substituting Eq. (22) into Eq. (21), yields Eq. (23):

$$8.847\, s^{0.337}\, C = A_c\, E_c \frac{s'' - e\upsilon'''}{\left(1+\dfrac{A_c\, E_c}{A_{FRP}\, E_{FRP}}\right)} \tag{23}$$

To simplify the expression by setting the new symbol ζ, Eq. (24) is obtained:

$$\zeta = \frac{A_c\, E_c}{\left(1+\dfrac{A_c\, E_c}{A_{FRP}\, E_{FRP}}\right) C} = \frac{E_{FRP}\, A_c\, E_c\, r}{2A_{FRP}\left(A_{FRP}\, E_{FRP} + A_c\, E_c\right)} \tag{24}$$

where r = the radius of the single FRP tendon. By merging the same terms, Eq. (25), which is relevant to axial force, is as follows:

$$s'' - \frac{8.847}{\zeta} s^{0.337} = e\upsilon''' \tag{25}$$

3.3.2 Bending moment equilibrium

As illustrated in Fig. 3.4 and Fig. 3.5, the internal bending moment consists of two parts: (1) the component of internal moment due to concrete bending, and (2) the component of internal moment due to force couple resulting from prestressing forces in the strands. The bending resistance provided by the FRP tendons is assumed to be negligible relative to these two moment components. The bond forces at the interface between the concrete and FRP tendons can be replaced by a couple $M(x)$ and a force $N(x)$ acting at the centroid of the concrete beam. These two moments can be written in terms of the known external moment as follows:

$$M_{ex} = M_c + M(x) \tag{26}$$

where M_{ex} = the external moment, M_c = concrete moment due to bending and $M(x)$ = pure moment due to equivalent force couple systems. Algebraically, they are defined as the following:

$$M_c = -E_c I_c \upsilon'' \tag{27}$$

$$M(x) = e N(x) \tag{28}$$

$$M_{ex} = -E_c I_c \upsilon'' + e N(x) \tag{29}$$

where I_c = the concrete member moment of inertia. From Eq. (14) and Eq. (17):

$$N(x) = A_{FRP} E_{FRP} s'_{2FRP} \tag{30}$$

Eq. (31) is obtained by taking the first derivative of Eq. (11):

$$s'_2 = s'_{2c} + s'_{2FRP} \tag{31}$$

Eq. (32) is obtained by combining Eq. (31) with Eq. (17), and becomes:

$$s_2' = \left(1 + \frac{A_c E_c}{A_{FRP} E_{FRP}}\right) s_{2c}' = \left(1 + \frac{A_{FRP} E_{FRP}}{A_c E_c}\right) s_{2FRP}' \tag{32}$$

Substituting Eq. (24) into Eq. (32), yields Eq. (33):

$$s_{2FRP}' = \frac{\zeta C s_2'}{A_{FRP} E_{FRP}} \tag{33}$$

Eq. (34) evolves from substituting Eq. (33) into Eq. (30), and Eq. (29) becomes Eq. (35).

$$N(x) = \zeta C s_2' \tag{34}$$

$$M_{ex} = -E_c I_c \upsilon'' + e \zeta C s_2' \tag{35}$$

Taking the first derivative of Eq. (9) with respect to *x*, then substituting Eq. (10) and Eq. (12) into it, Eq. (36) can be written as:

$$s_2' = s' - e\upsilon'' - \varepsilon_{is} \tag{36}$$

Substituting Eq. (36) into Eq. (35) results in:

$$M_{ex} = -E_c I_c \upsilon'' + e \zeta C \left(s' - e\upsilon'' - \varepsilon_{is}\right) \tag{37}$$

Simplifying by establishing two new symbols K_s and T_s:

$$K_s = E_c I_c + e^2 \zeta C \tag{38}$$

$$T_s^2 = \frac{e^2 \zeta C}{K_s} \tag{39}$$

As a result of rearranging Eq. (37), the expression with regard to bending moment is generated as following:

$$\upsilon'' - \frac{T_s^2}{e} s' = -\frac{M_{ex}}{K_s} - \frac{T_s^2}{e} \varepsilon_{is} \tag{40}$$

The governing equations can now be defined by combining Eq. (25) and Eq. (40):

$$\begin{cases} s'' - \dfrac{8.847}{\zeta} s^{0.337} = e\upsilon''' \\ \upsilon'' - \dfrac{T_s^2}{e} s' = -\dfrac{M_{ex}}{K_s} - \dfrac{T_s^2}{e} \varepsilon_{is} \end{cases} \tag{41}$$

3.3.3 Exact solution of piecewise functions

Generally speaking, specimens from experimental investigations were placed on the ground without any external loading before prestress release and only subjected to their own weight after release. On the other hand, according to Bai and Davidson's [28] study bending moment due to dead weight of the pretensioned concrete members has little influence on the transfer length. Therefore it is reasonable to assume that the external moment is equal to zero, $M_{ex} = 0$. To illustrate this, the center of the simply supported beam with the span of L is located at the origin of the coordiate system as shown in Fig. 3.7.

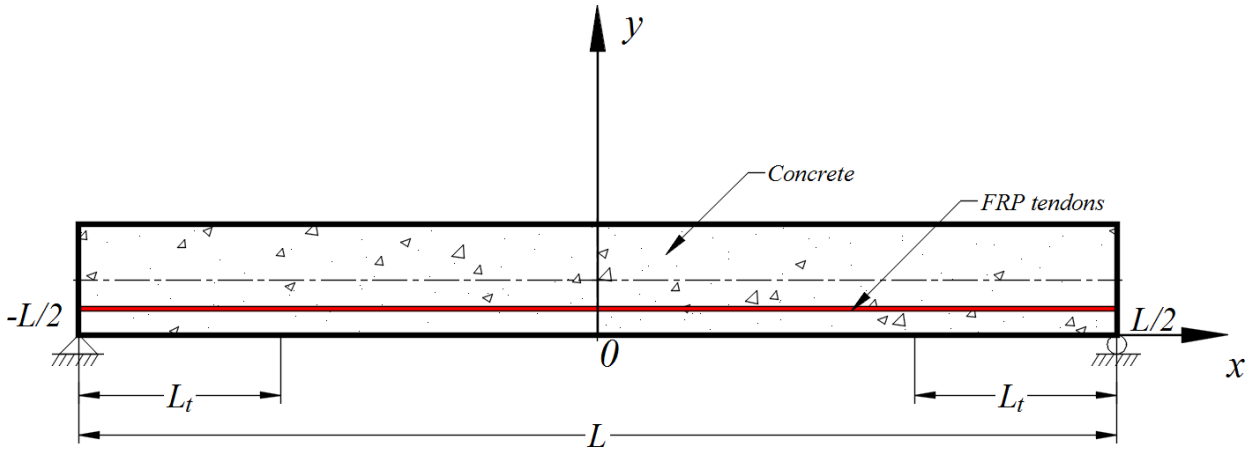

Fig. 3.7 The coordinate system of the simply supported beam

The boundary conditions for the governing equations, Eq. (41), with respect to the coordinate system can be defined as:

At $x = 0$, the slip $s(0) = 0$;

At $x = L/2$ or $x = -L/2$, the deflection $\upsilon(L/2) = \upsilon(-L/2) = 0$ and the bending moment $\upsilon''(L/2) = \upsilon''(-L/2) = 0$.

Eq. (42), which is a nonlinear second order ordinary differential equation with rational exponent that defines the prestressed FRP tendons slip along the *x*-axis, is generated by differentiating Eq. (40) after substituting the result into Eq. (25).

$$\left(1 - T_s^{\,2}\right) s'' - \frac{8.847}{\zeta} s^{0.337} = 0 \tag{42}$$

Due to the bending moment being zero at both ends of beam as illustrated in Fig. 3.7, $\upsilon''(L/2) = \upsilon''(-L/2) = 0$ is substituted into Eq. (40). The result, known as Dirichlet and Neumann boundary conditions, are given by the following expression:

$$\begin{cases} s(0)=0 \\ s'(L/2)=s'(-L/2)=\varepsilon_{is} \end{cases} \tag{43}$$

It is extremely difficult to derive a closed form expression to solve the nonlinear differential equation Eq. (42). However, a piecewise function solution approach provides a feasible and reasonable approach to solving the GDEs. For $x \geq 0$, the solution is:

$$s(x)=\begin{cases} 0, & 0 \leq x \leq L/2-L_t \\ A\left(x-L/2+L_t\right)^B, & otherwise \end{cases} \tag{44}$$

Eq. (45) is obtained by introducing the symbol ψ:

$$\psi=\frac{8.847}{\zeta\left(1-T_s^{\,2}\right)} \tag{45}$$

In order to make the solution process clear, α = 0.337 is used, and Eq. (42) can be rewritten as:

$$s''(x)=\psi\, s(x)^{\alpha} \tag{46}$$

and the transfer length L_t can be expressed as following, in metric (SI) units:

$$L_t=\left[\frac{\varepsilon_{is}(1+\alpha)\left(0.5\varepsilon_{is}\right)^{-\alpha}}{\psi(1-\alpha)^{1+\alpha}}\right]^{\frac{1}{1+\alpha}} \tag{47}$$

$$A=e^{\frac{\ln\frac{2(1+\alpha)}{\psi(\alpha-1)^2}}{\alpha-1}} \tag{48}$$

$$B=\frac{2}{1-\alpha} \tag{49}$$

It can be observed that Eq. (42) has a solution of the form $s(x)=Ax^B$. By substituting this function into Eq. (42) and equating the exponents of x on both sides, A and B can be determined, which results in Eq. (49). Equating the coefficients of x on both sides, the expression of A is shown in Eq. (48).

The boundary conditions as shown in Eq. (43) are associated with the property of pretensioned concrete members as described in Fig. 3.1. The transfer length is referred to as the distance from which the prestress force transferred by the bond stress increases from zero to the effective prestressing force, which ends with the location of slip $s=0$. This accounts for the bond stress $\tau=0$. In the mathematical model, the transfer length must be shorter than or equal to half of the beam span. However, recall the boundary condition $s'\left(L/2\right)=\varepsilon_{is}$, which conflicts with the hypothetical solution $s(x)=Ax^B$ for $0\le x\le L/2$. $s'(x)=\varepsilon_{is}$ is reached by setting the symbol $K=L/2-L_t$. Consequently, $s(x)=Ax^B$ turns into $s(x)=A\left(x-K\right)^B$. It should be noted that the transfer length L_t must be shorter than $L/2$. The expression of L_t is shown in Eq. (47) by solving the equation $(AB)L_t^{B-1}=\varepsilon_{is}$ in terms of $s'(L_t)=\varepsilon_{is}$. Finally, the solution of the slip can be proposed as Eq. (44), which also satisfies the boundary conditions. The advantage of using this type of piecewise function (Eq. (44)) is that it allows avoidance of a complicated numerical solution and simplifies the computation of the empirical formula.

3.4 Comparison with experimental results

To confirm the accuracy of the proposed method, the results from three different experimental studies on FRP tendon transfer length by other investigators were compared with those of this study. The details of the experimental programs can be found in Soudki et al. [14], Nanni et al. [13], and Grace [16]. The characteristics of the parameters for all specimens are reported in Table 3.2.

Table 3.2 Specimen characteristics

Specimen	Diameter of FRP tendon, d_{FRP} (mm)	Total area of FRP tendons, A_{FRP} (mm^2)	Elastic modulus of FRP tendon, E_{FRP} (MPa)	Prestressing for each tendon, f_{pe} (MPa)	Eccentricity, e (mm)	Area of concrete cross-section, A_c (mm^2)	Elastic modulus of concrete, E_c (MPa)	Inertia moment of cross-section, I (mm^4)	Span length, L (mm)
R1 to R4	1 ϕ8mm	46.1	150000	25% release ε_{is} =2.274e-03	100	45000	38000 ~44000	3.375e8	3000
				50% release ε_{is} =4.549e-03					
				75% release ε_{is} =6.823e-03					
				100% release ε_{is} =9.098e-03					
B1-S8	1 ϕ12mm	90	67600	50% release ε_{is} =0.052e-01	35	25200	23000 ~25000	9.261e7	4000
				100% release ε_{is} =0.103e-01					
CDT1-4 (two top draped, bottom straight)	2 ϕ8mm	92.2	147000	33% release ε_{is} =0.010	19.05	100645	41000	1.131e9	5890
	4 ϕ8mm	184.4		67% release ε_{is} =0.010	57.15				
	4 ϕ8mm 2 ϕ10mm	328		100% release ε_{is} =0.010	124.0				

In the test program of Soudki et al. [14], four rectangular beams R1, R2, R3, and R4 were tested with 3.0 m in length, depth of 0.3 m and width of 0.15 m, as shown in Fig. 8. Each beam adopted a single 8 mm nominal diameter CFRP Leadline^{TM} rod with strength of 2300 MPa, which provided 60% of strength as the prestress level of specimen in the measurements. Strain gauges were attached to the concrete surface at the level of the FRP tendons to determine the strain profile. The results were recorded at 25%, 50%, 75%, and 100% of prestress force release, which made the initial strain ε_{is} = 2.274e-03, 4.549e-03, 6.823e-03, and 9.098e-03, respectively. The concrete modulus of elasticity was calculated by specimen strength reported in the paper according to ACI Code (318-14). The transfer length results were compared to the predictions from Eq. (47) and are summarized in Table 3.3.

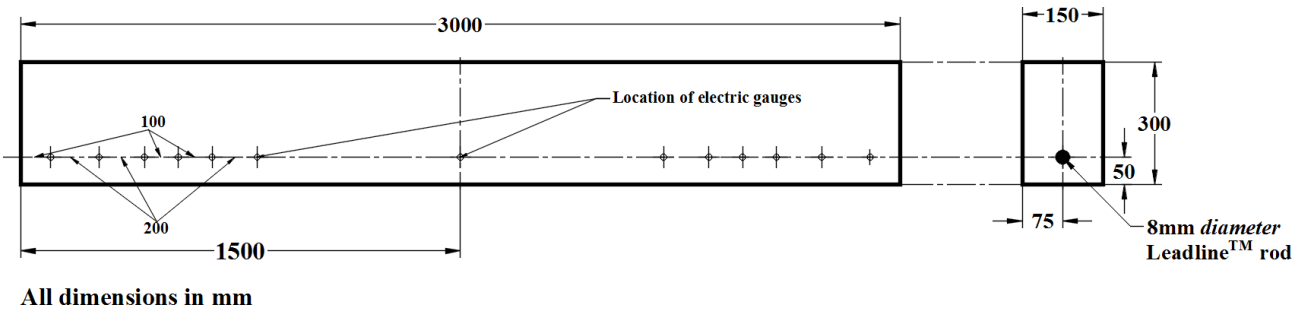

Fig. 3.8 Rectangular beam R1 to R4 with a single 8 mm CFRP Leadline^{TM} rod [14]

Table 3.3 Comparison of transfer length for FRP tendons

Description		Measured (mm)	Predicted (mm)	ACI 440.4R-04 (mm)	AASHTO (mm)
Soudki et al. [14]	**R1** (25% release)	545 to 695	265	168	400 to 480
	R2 (50% release)	545 to 695	374	336	400 to 480
	R3 (75% release)	545 to 695	457	504	400 to 480
	R4 (100% release)	545 to 695	527	672	400 to 480
Nanni et al. [13]	**B1-S8** (50% release)	400	296	230	600 to 720
	B1-S8 (100% release)	450	417	461	600 to 720

The comparison between the measured strain profiles using strain gauges and predicted strain profiles using the approach in the present study is illustrated in Fig. 3.9, which demonstrates reasonable agreement; for example the error between effective prestress strain analysis results and test values at the midspan is less than 7%. From the different prestress strain profile levels, as summarized in Table 3.3, the transfer length value is actually increasing with increasing levels of prestress. As expected according to Eq. (47), this is the result of the different initial strain caused by a different value of prestress force. Note that the predicted transfer length is a little shorter than the experimental data; one possible explanation for this behavior is that the bond strength for the 8 mm CFRP Leadline^{TM} rods used in the experiment is lower than the one used in the currently proposed model. Therefore, the more transfer length is needed along the CFRP Leadline^{TM} rod over which the effective prestressing force is reached.

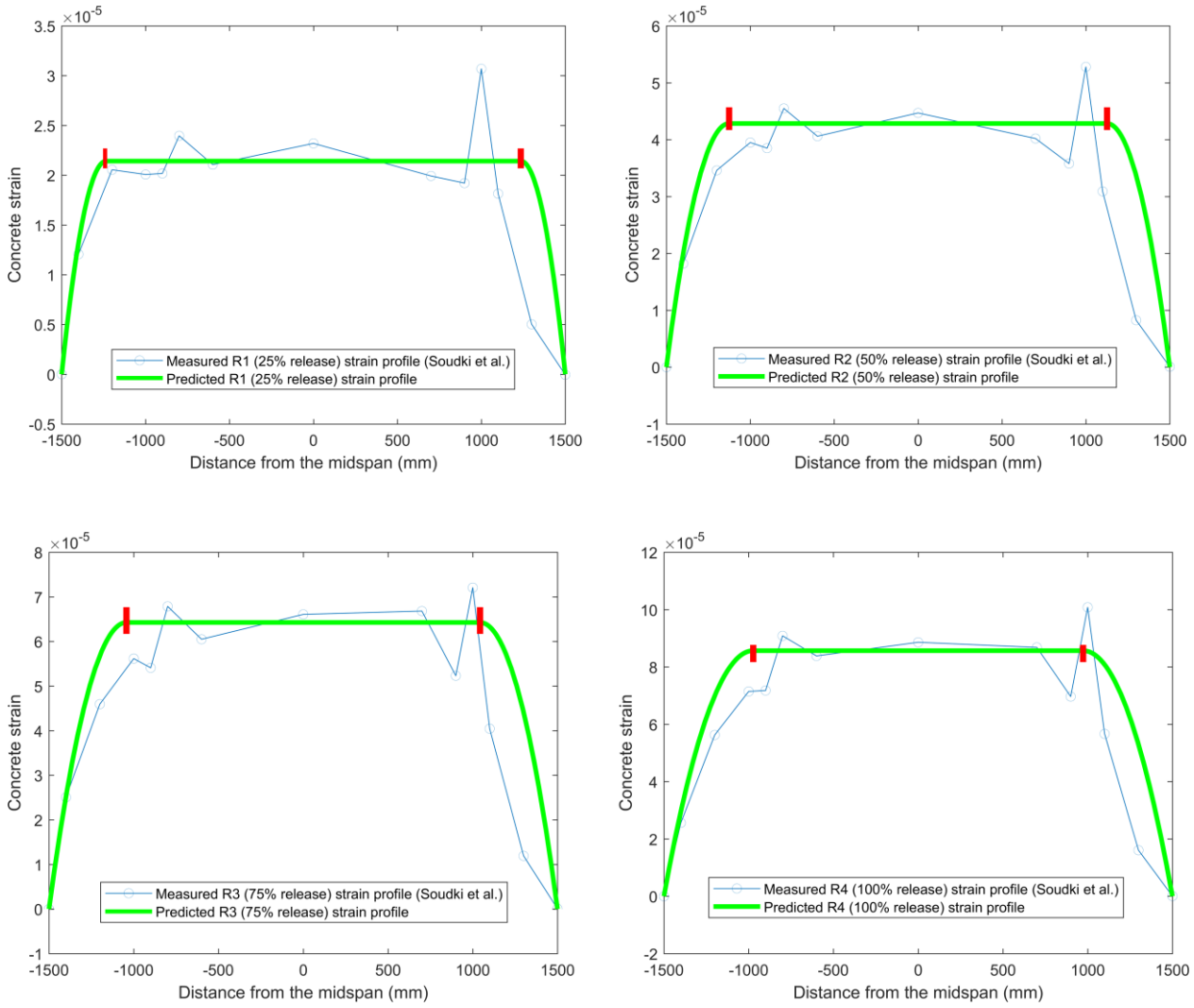

Fig. 3.9 Predicted strain profiles for rectangular beam R1 to R4 [14] at 25%, 50%, 75%, 100% release

Comparisons to the test data by Nanni et al. [13] were also performed. The specimens had span length of 4000 mm and a 120 mm by 210 mm rectangular cross-section. The pretensioned concrete beam was prestressed with a single braided epoxy-impregnated AFRP tendon. Two levels of 50% and 100% initial prestress force were used in the test, which made the initial strain ε_{is} = 0.0052, and 0.0103, respectively. The concrete elastic modulus ranged from 22660 to 25070 MPa; other specimen characteristics are defined in Table 3.2. The transfer length was examined

by means of measurement of the strain variation, gluing the contact points close to both ends of the beam at the depth of the AFRP tendons with 5 cm spacing. Fig. 3.10 shows the predicted strain profiles for specimens B1-S8 on 50% and 100% level released prestress force.

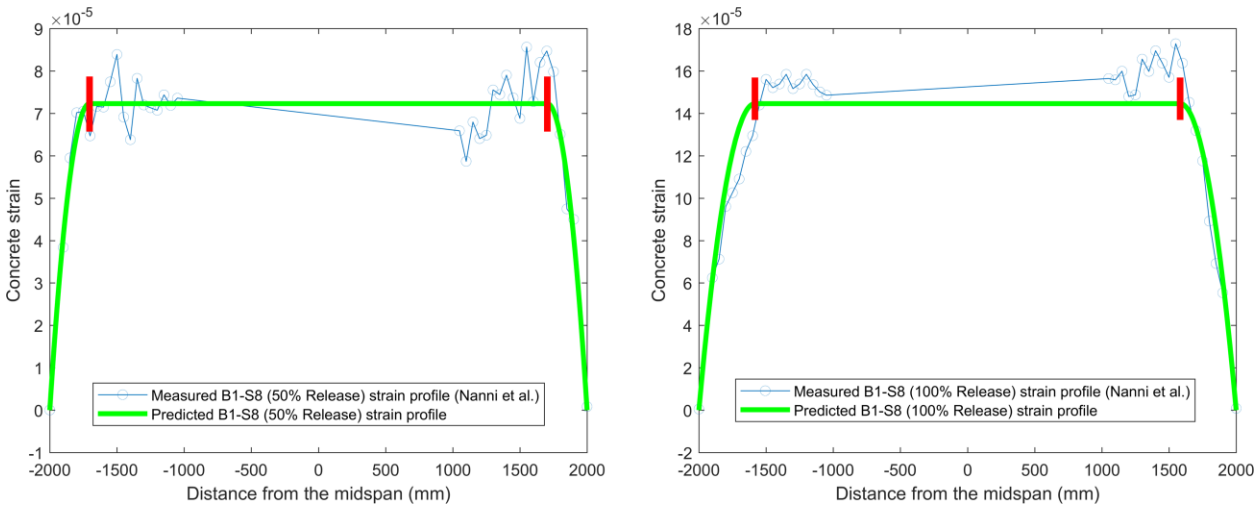

Fig. 3.10 Predicted strain profiles for B1-S8 [13] at 50% and 100% release

As can be seen from Fig. 3.10, the predicted results for 50% and 100% release levels are in good agreement with the strain measurements presented in Nanni et al. [13]; the differences between the modeling values and experimental values are less than 15%. It is worth noting that the slope of both curves within the transfer zone experienced the greatest rate of strain change, which is accurately calculated using Eq. (44). These results demonstrate the reliability of bond stress-slip relationship defined as Eq. (3), which further supports the feasibility of the present method. On the other hand, the predicted transfer lengths are also slightly shorter than the test results, which may be due to the variable behavior of the concrete properties examined in the test since they are influenced by external factors such as temperature, relative humidity, etc. Another reason may be associated with the methods used to measure the transfer length. Only minor

discrepancies occurred to the strain plateau of both curves, which may be caused by prestress loss as a consequence of using anchors during the process of FRP tendons released at different levels.

Fig. 3.11 and Fig. 3.12 represent bar chart comparisons of transfer length predicted by the present study with measured results and those in the specifications, respectively. In Soudki et al.'s tests, the method of measuring the transfer length is not clear, and all of the predicted values are lower than the results from the measurement. However, the agreement between the predicted strain profiles and the measures is good enough to demonstrate the accuracy of the present method. By comparing the obtained values from Nanni et al.'s test, the predicted results are very close to the test results. As demonstrated in the comparisons, regardless of which specifications are used to calculate the transfer length, it is almost impossible to be completely consistent with the measured values from testing. Determining the transfer length during testing is based on the 95% Average Maximum Strain (AMS) method. In defining the strain plateau, inconsistency and preference may exist between different researchers. Again, the theoretical equation proposed by Guyon [38] for determining transfer length was as following:

$$L_t = \alpha' \frac{\delta}{\varepsilon_{pi}} \tag{50}$$

Where δ = the end slip, ε_{pi} = the initial strand strain, α' = a factor depending the bond stress distribution, which was varied from 2 to 3. In addition, Bai and Davidson's [28] study confirmed that the lower bound corresponds with an α' coefficient of 2.0, and upper bound represents an α' coefficient of 3.0. Furthermore the determination of transfer length using 95% AMS method is relevant to the transfer length calculated by using equation (50) with α' coefficient of 3.0. Since the proposed transfer length definition, which is in the average level, is approximately equivalent

to that with α' coefficient of 2.5. That is the reason why the proposed model underestimates the values measured in the tests.

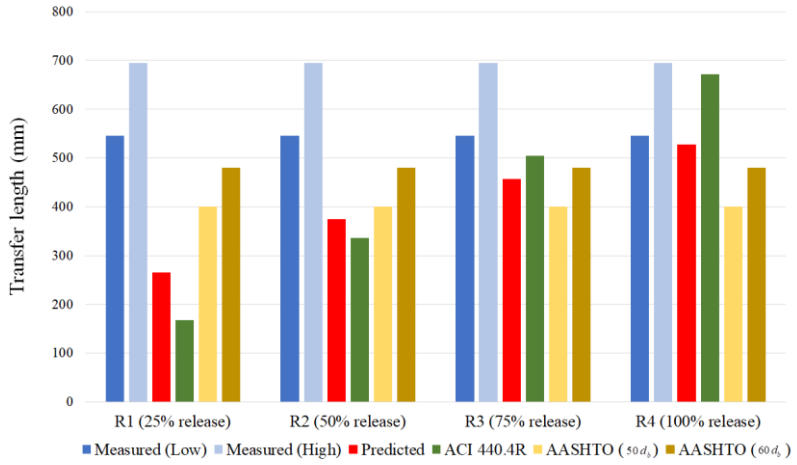

Fig. 3.11 Comparison of transfer length in Soudki et al. [14]

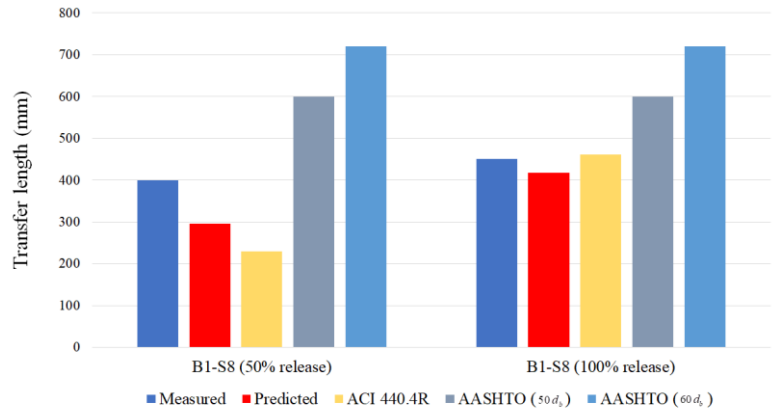

Fig. 3.12 Comparison of transfer length in Nanni et al. [13]

The difference between sequential release and simultaneous release of the tendons during manufacture of prestressed concrete members is now demonstrated using Grace's [16] experimental investigation on double-T girders prestressed with CFRP Leadline^{TM} tendons. The specimen was designated as CDT1-4, which is a simply supported beam. It had a total length of

5890 mm with a cross-section of 1016 mm flange by 343 mm depth. The details of the geometry and reinforcement are shown in Fig. 3.13.

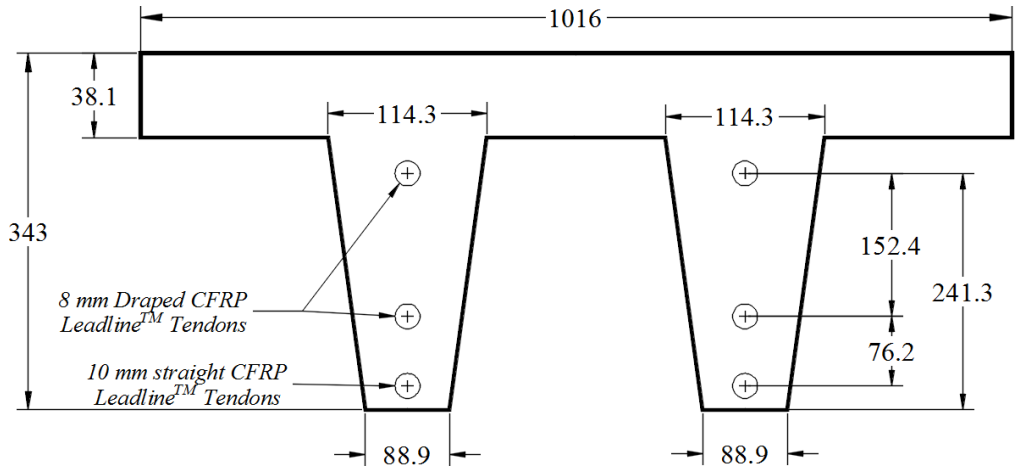

Fig. 3.13 Cross-section for Double-T Girder CDT1-4 [16]

The transfer length calculation method presented in this paper cannot be compared to the the results from Grace's tests since those tests involved draped tendons. Importantly however, the Grace tests involved three levels of prestressing force release that depended on which group (position) of tendons were released, i.e., 33%, 67%, and 100% release refer to the prestress force acting on tendons being sequentially released from top to bottom, respectively. Assuming all of the FRP tendons are straight, it will be interesting to see how the performance of strain profiles allows simultaneous releasing of prestress force, which means 67% release represents that the top four prestressed tendons are being released at the same time. The model for 100% release indicates that all prestressed FRP tendons were released at the same time. The details of two levels of releases are respectively summarized in Table 3.4.

Table 3.4 Details of 67% release and 100% release sequentially compared with simultaneously

Description	67%		100%	
	Sequentially	**Simultaneously**	**Sequentially**	**Simultaneously**
ε_{is}	0.01	0.01	0.01	0.01
The number of times for elastic shortening	2	1	3	1
ε_{eff}	$9.006 * 10^{-5}$	$8.361 * 10^{-5}$	$2.838 * 10^{-4}$	$2.678 * 10^{-4}$
Δf_p *(MPa)*	13.24	12.29	41.72	39.37

Where ε_{is} refers to the initial strain in each FRP tendon due to prestress force. ε_{eff} is the strain in the concrete after undergoing immediate loss, namely the value shown in the strain plateau. The drop in prestress Δf_p in the FRP tendons refers to the immediate prestress losses.

As Fig. 3.14 demonstrates, strain plateaus differ from that computed previously. In another words, the concrete strain at the level of the FRP tendons due to prestress force being released simultaneously decreased compared with that of being released sequentially. The concrete strain is equivalent to the change in strain in the FRP tendons on the basis of strain compatibility, which means that prestress loss was reduced by using the simultaneous release method. In this case, the prestress loss due to being released simultaneously decreased by 7.2% and 5.6% more than that of being released sequentially for 67% and 100% release, respectively. Thus, releasing prestressing tendons simultaneously helps to improve the strength of pretensioned concrete members.

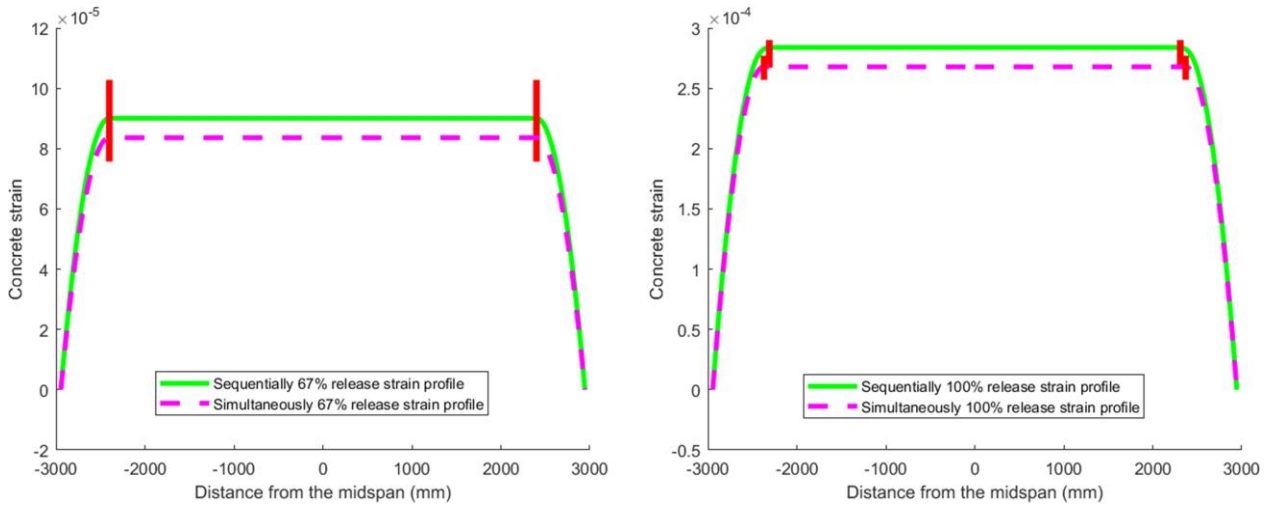

Fig. 3.14 Comparison of 67% release and 100% release sequentially and simultaneously

On the contrary, using the proposed approach illustrates how that various factors influence the FRP tendon transfer length. As illustrated by Fig. 3.15, by normalizing the parameters the influential factors on the transfer length of FRP tendons that takes into account the relationship given by Eq. (47) has been clearly quantified through the study of experimental data [13,14,16]. Considering FRP tendons show higher bond strength than steel strands as well as there is little tendon slippage proved in experiments [13], which is the reason why 1 mm is chosen as the maximum value of the slip shown in Fig. 3.16. It is noted that the bond strength decreases with an increasing coefficient α within the range of slip less than 1 mm in Fig. 3.15. Meanwhile, the solid line from Fig. 3.15 demonstrates that the transfer length is increasing with an increasing bond stress coefficient α ($\alpha = 0 \sim 0.6$), which means that the stronger bond will shorten the distance of transmission force within the range of slip less than 1 mm.

Fig. 3.15 also shows that the transfer length is related to the initial strain ($\varepsilon_{is} = 0.005 \sim 0.01$) and the radii of FRP tendons ($r = 6 \sim 16\,mm$). This is because the larger amount of initial strain is equivalent to the larger slip as illustrated by Eqs. (9) to (12), which further affects the bond stress.

The larger radius of FRP tendons results in increasing the interface area between the tendons and concrete, increasing the bond strength. Furthermore, it can be seen that the effect of the concrete elastic modulus ($E_c = 20000 \sim 41230\,MPa$) and the eccentricity ($e = 0 \sim 120\,mm$) on transfer length are not as evident. Due to the dependence of bond strength of FRP tendons on fiber and resin properties rather than on concrete strength, which has been proved in Cosenza et al.'s [34] study. Therefore the accuracy of the transfer length of prestressed FRP tendons in pretensioned concrete members primarily depends on the bond stress distribution.

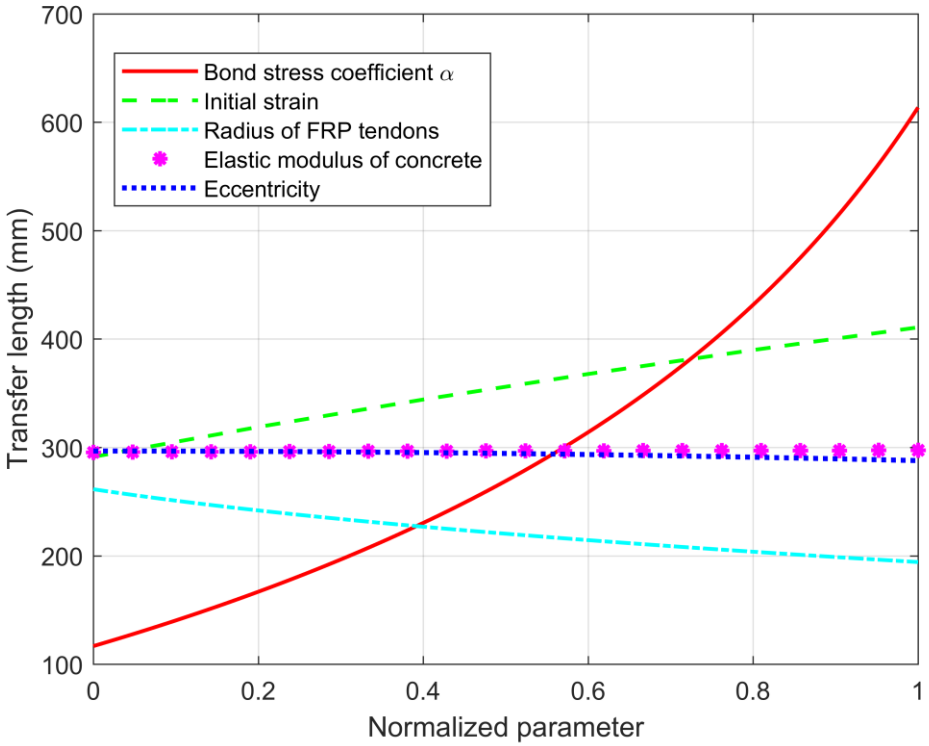

Fig. 3.15 Influence of parameters on FRP tendon transfer length

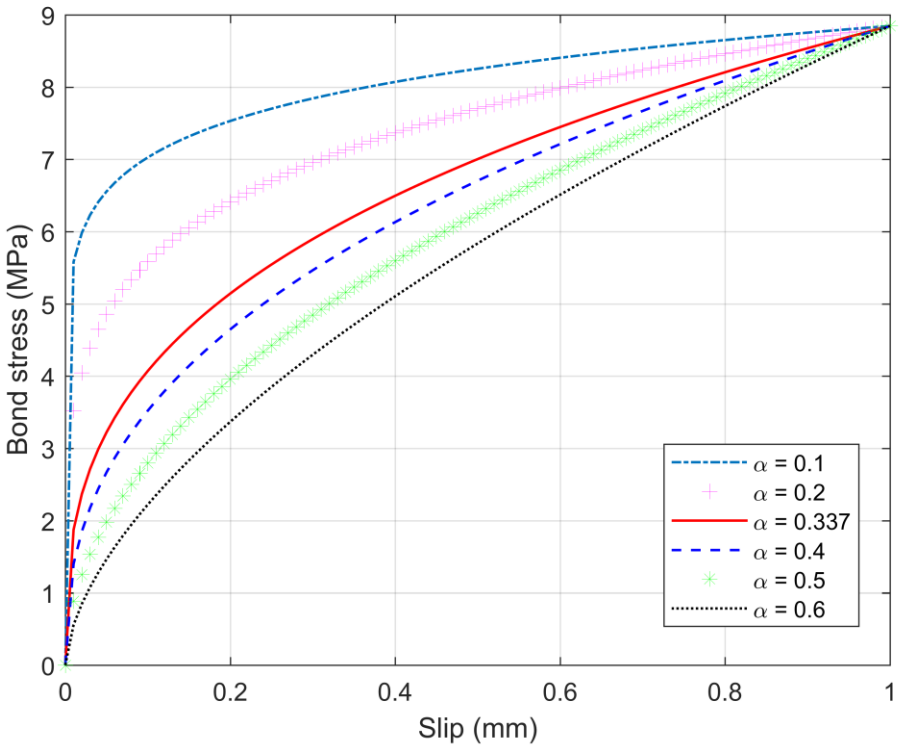

Fig. 3.16 Influence of coefficient α on bond stress

3.5 Conclusions

A set of governing equations that define the flexural behavior of FRP tendon reinforced prestressed concrete beams in which the nonlinear relationship between FRP tendons and concrete is taken into account was derived using composite beam theory. To establish a closed-form solution, a piecewise function was applied to determine the transfer length of prestressed FRP tendons in pretensioned concrete members. Through comparing the strain profiles predicted by this method with experimental results from literature, as well as formulas provided in design specifications, the following conclusions were drawn:

1. The feasibility and effectiveness of the proposed method are demonstrated in terms of comparison with variable materials (i.e. AFRP, CFRP) and experimental studies by other investigators.

2. Using the developed formulation it is demonstrated that different release methods result in prestress loss variations. The prestress loss due to FRP tendons being released simultaneously is slightly less than that of being released sequentially for multi-level pretensioned concrete member prestressed by FRP tendons.

3. An accurate definition of the bond strength between the FRP tendons and concrete is critical to accurately determining the transfer length.

4. Although other predictors based upon empirical data exist and are being used, and importance of the developed formulation is that it defines the primary parameters that affect the transfer length based upon mechanics theory, namely the bond stress coefficient, initial strain, and the FRP tendon radii.

5. The development presented herein represents an advancement in theory associated with the flexural behavior of FRP tendon reinforced prestressed concrete beams. However, there are practical and theoretical issues that must be further addressed. For example, additional calibration of local bond stress-slip relationship parameters through pullout tests on AFRP, CFRP, and GFRP tendons is needed. Also, the development of analytical equations and solutions for prestressed concrete members with draped FRP tendons is needed.

References

[1] Bakis CE, Bank LC, Brown V, Cosenza E, Davalos JF, Lesko JJ, Machida A, Rizkalla SH, Triantafillou TC. Fiber-reinforced polymer composites for construction—State-of-the-art review. Journal of composites for construction. 2002 May;6(2):73-87.

[2] Dolan CW. FRP prestressing in the USA. Concr Int 1999;21:21–4.

[3] Taerwe L, Matthys S. FRP for concrete construction: activities in Europe. Concr Int 1999;21:33–6.

[4] Fukuyama H. FRP composites in Japan. Concr Int 1999;21:29–32.

[5] Rizkalla S, Labossiere P. Structural engineering with FRP-in Canada. Concr Int 1999;21:25–8.

[6] Zia P, Mostafa T. Development length of prestressing strands. Precast Concr Inst J 1977;22.

[7] Dolan CW, Nanni A. Status of fiber-reinforced plastic reinforcement development and cement based research needs. Adv Cem Based Mater 1994;1:185–91.

[8] Ehsani MR, Saadatmanesh H, Nelson CT. Transfer and flexural bond performance of aramid and carbon FRP tendons. PCI J 1997;42:76–86.

[9] El-Hacha R. Prestressing Concrete Structures with FRP Tendons (ACI 440.4 R-04). Struct Congr 2005: Metropolis and Beyond; 2005.

[10] Mahmoud ZI, Rizkalla SH, Zaghloul E-ER. Transfer and development lengths of carbon fiber reinforced polymers prestressing reinforcement. ACI Struct J 1999;96:594–602.

[11] Cousins Thomas E, Johnsone David W, Zia Paul. Transfer length of epoxy-coated prestressing strand. ACI Mater J 1990;87:193–203.

[12] Cousins TE, Johnston DW, Zia P. Transfer and development length of epoxy coated and uncoated prestressing strand. PCI J 1990;35:92–103.

[13] Nanni A, Utsonomiya T, Yonekura H, Tanigaki M. Transmission of prestressing force to concrete by bonded fiber reinforced plastic tendons. Struct J 1992;89:335–44.

[14] Soudki KA, Green MF, Clapp FD. Transfer length of carbon fiber rods in precast pretensioned concrete beams. PCI J 1997;42:78–87.

[15] Committee ACI, Institute AC. Standardization IO for Building code requirements for structural concrete (ACI 318-08) and commentary. American Concrete Institute; 2008.

[16] Grace NF. Transfer length of CFRP/CFCC strands for double-T girders. PCI J 2000;45.

[17] Lu Z, Boothby TE, Bakis CE, Nanni A. Transfer and development lengths of FRP prestressing tendons. PCI J 2000;45:84–95.

[18] Rambo-Roddenberry M, Joshi K, Fallaha S, Herrera R, Kampmann R, Chipperfield J, et al. Construction, strength, and driving performance of carbon-fiber-reinforced polymer prestressed concrete piles. PCI J 2016.

[19] AASHTO M. 320. Stand specif perform-graded Asph Bind Am Assoc State Highw Transp Off; 2010.

[20] Granholm H. On composite beams and columns with particular regard to nailed timber structures. Chalmer Tech Univ; 1949.

[21] Newmark NM. Test and analysis of composite beams with incomplete interaction. Proc Soc Exp Stress Anal 1951;9:75–92.

[22] Goodman JR, Popov EP. Layered beam systems with interlayer slip. J Struct Div 1968;94:2535–48.

[23] Girhammar UA, Gopu VK. Composite beam-columns with interlayer slip—exact analysis. J Struct Eng 1993;119:1265–82.

[24] Girhammar UA, Pan D. Dynamic analysis of composite members with interlayer slip. Int J Solids Struct 1993;30:797–823.

[25] Adam C, Heuer R, Jeschko A. Flexural vibrations of elastic composite beams with interlayer slip. Acta Mech 1997;125:17–30.

[26] Foraboschi P. Analytical solution of two-layer beam taking into account nonlinear interlayer slip. J Eng Mech 2009;135:1129–46.

[27] Bai F, Davidson JS. Analysis of partially composite foam insulated concrete sandwich structures. Eng Struct 2015;91:197–209.

[28] Bai F, Davidson JS. Composite beam theory for pretensioned concrete structures with solutions to transfer length and immediate prestress losses. Eng Struct 2016;126:739–58.

[29] Eligehausen, Rolf, Egor P. Popov, Vitelmo V. Bertero. Local bond stress-slip relationships of deformed bars under generalized excitations; 1982.

[30] CEB-FIP M.90. Design of concrete structures. CEB-FIP-Model-Code 1990. Lond Br Stand Inst; 1993.

[31] Russo G, Zingone G, Romano F. Analytical solution for bond-slip of reinforcing bars in RC joints. J Struct Eng 1990;116:336–55.

[32] Malvar LJ. Bond stress-slip characteristics of FRP rebars. Port Hueneme CA: Naval Facilities Engineering Service Center; 1994.

[33] Nanni A, Tanigaki M, Hasuo K. Bond anchorage of pretensioned FRP tendon at force release. J Struct Eng 1992;118:2837–54.

[34] Cosenza E, Manfredi G, Realfonzo R. Behavior and modeling of bond of FRP rebars to concrete. J Compos Constr 1997;1:40–51.

[35] Lees JM, Burgoyne CJ. Transfer bond stresses generated between FRP tendons and concrete. Mag Concrete Res 1999;51(4):229–39.

[36] Focacci F, Nanni A, Bakis CE. Local bond-slip relationship for FRP reinforcement in concrete. J Compos Constr 2000;4:24–31.

[37] Leonhardt F. Prestressed concrete: design and construction. W. Ernst.; 1964.

[38] Guyon, Yves Félix. Prestressed concrete; 1953.

Chapter 4 Analysis of Interfacial Stresses in Concrete Beams Strengthened by Externally Bonded FRP Laminates Using Composite Beam Theory

4.1 Introduction

Externally bonded fiber reinforced polymer (FRP) laminates are a valuable technique for the repair and retrofit of existing concrete structures due to the superior properties of FRP composites, such as high strength to weight ratio, excellent corrosion resistance, non-magnetism, and low axial coefficient of thermal expansion. Another benefit of using externally bonded FRP laminates with epoxy resins for strengthening concrete structures is that it does not require changes of member dimensions; even if the structure is still in use, the repair or retrofit work can be conducted quickly and easily.

Over the last three decades, many studies have been carried out on strengthening concrete structures by externally bonded FRP laminates. The results of extensive investigations have indicated that premature failures due to loss of bond between the FRP laminates and concrete structures are one of the key factors that reduce the level of safety of the strengthened structures [1-8]. Such loss of bond refers to debonding failures that occur at or near the FRP laminates end, either by separation of the concrete cover beneath the bottom layer of reinforcement or interfacial debonding of FRP laminates from the concrete substrate. Furthermore, those that initiate at any

flexural crack then propagate to the end of the FRP laminates. This paper focuses on analytical modeling of the first type, referred to herein as FRP end debonding failures.

For reinforced concrete (RC) beams strengthened by externally bonded FRP laminates, FRP end debonding failures depend largely on interfacial stresses, including shear and normal stresses in the adhesive layer [2,9-14]. Numerous studies have shown that such brittle failure mechanisms induced by FRP end debonding failures begin early in the loading phase of the beam, which results from interfacial stress concentration at the end of the FRP laminate [1,2,4,10-15]. As a result, it is critical to develop a sound understanding of interfacial stresses between the FRP laminate and the concrete substrate. Therefore, many interfacial stress-based models intended to predict FRP end debonding failures for concrete beams bonded by FRP laminates have been presented in the literature [1,2,10,13,15]. These models were primarily developed based on linear elastic behavior of the concrete, resulting in relatively simple approximate closed-form solutions to predict interfacial stresses. Nevertheless, the constitutive mechanism of bond-slip between FRP laminates and concrete was not taken into consideration.

In this study, two sets of governing equations that define the mechanics behavior of concrete beams strengthened by externally bonded FRP laminates in which bond-slip relationship between FRP laminates and concrete is taken into account are derived using composite beam theory. The interfacial shear and normal stresses between FRP laminates and concrete are solved with closed-form solutions. Validation is performed to compare the analytical solution with the published finite element (FE) model and existing analytical solutions in the literature to ensure the accuracy and feasibility of the present method. This novel approach is offered as a more rigorous and accurate model than existing models that involve incomprehensible formulas. Furthermore,

the effect of various parameters on the interfacial behavior of externally bonded FRP for strengthening concrete beams is evaluated based upon the developed model.

4.2 Literature review

4.2.1 Interfacial stresses

For a simply supported beam strengthened by externally bonded FRP laminates, as illustrated by Fig. 4.1, it is very significant to provide a rigorous analytical solution for predicting the interfacial normal σ and shear τ stresses between the bonded FRP laminates and concrete. All existing prediction models were based on the assumption of linear elastic material behavior and that the interfacial stresses are constant along the thickness of the adhesive.

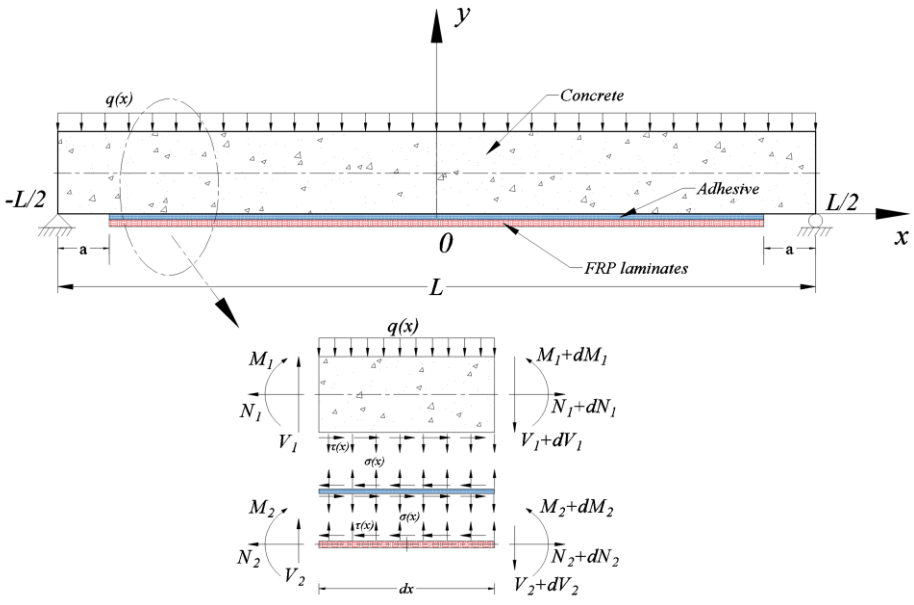

Fig. 4.1 Differential element in a simply supported beam strengthened by externally bonded FRP laminates

Early development work on an analytical method for concrete beams strengthened by epoxy-bonded steel plate was carried out by Vilnay [9]. Based on the elastic analysis, both the shear and the peeling distributed forces were investigated for the case where a concentrated load was applied at the center of a simply supported beam, indicating that maximum stress values occurred at the ends of the bonded plate. Robert and Hajikazemi [12] developed a two-stage model that predicted interfacial shear and normal stress distributions for the case of the uniformly distributed load acting on the RC beam with externally bonded steel plate. Täljsten [13] also carried out the derivation of an analytical solution to the interfacial stresses in plated beams with a point load using linear elastic theory. The difference with the method by Vilnay [9] was that the curvature of the beam was taken into account, as well as different boundary conditions. The analytical models of Malek et al. [1] show good agreement with results of FE analysis, providing closed-form solutions for calculating shear and normal stresses at the plate ends in strengthening RC beams with FRP plates. However, it should be noted that the bending deformation was neglected in the analytical procedure in Malek et al.'s [1] solution, resulting in the lack of information about how various parameters affect interfacial stresses at failure. Based on the deformation compatibility approach, the solution of Smith and Teng [2] focused on predicting interfacial stresses in plated beams for three load cases, namely, a uniformly distributed load (UDL), a single point load, and two-point loads. From the solution by Zhang and Teng [10], interfacial stresses were estimated for curved plated beams, plated beams with uniformly varying load and tapered beams. Similar to the study of Robert [11], an analytical procedure was conducted with the three-stage analysis that assumes full composite action between the concrete and the bonded plate. However, a large number of experimental and analytical studies [23,25-30,40] have indicated that the bond behavior between concrete and FRP laminates is not only affected by

adhesive lay, but also affected by other factors, such as the bond width of FRP laminates, FRP material types, the roughness of concrete surface, and concrete strength. Therefore, the analysis of the behavior of concrete beams strengthened by externally bonded FRP laminates should be conducted based on the partial composite action rather than full composite action. For the partial composite beam, even for full composite beams, slip effects must be considered [21,41,42]. For this reason, the aim of the current work is to take into account the slip effect between the interface of concrete and the externally bonded FRP laminates, so as to develop rigorous closed form solutions for interfacial stress in which the mechanics behavior of concrete beams strengthened by externally bonded FRP laminates is analyzed in terms of partially composite action.

4.2.2 Composite beam theory

Composite beam theory, as the name suggests, is applicable to a composite beam composed of two or more elements. As illustrated by Fig. 4.2, two separate elements of the member are connected by means of discrete connectors, and in this case, the transverse force p_s and horizontal shear q_s are transmitted from one element to the other through the connector. Simultaneously, the effect of relative movements between each other, referred to as the interlayer slip, will be taken into account.

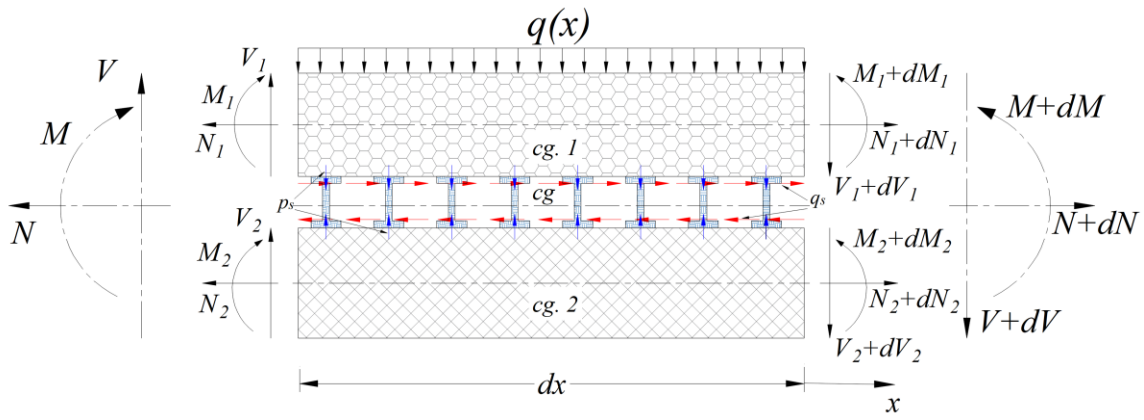

Fig. 4.2 Differential element in composite beam member with axial load (*N*), moment (*M*), shear force (*V*) and distributed load (*q(x)*)

Granholm [17] originally developed the fundamental governing differential equations (GDE) for nailed timber structures in 1949. During the same period, the theoretical analysis of composite beams with incomplete interaction was studied by Newmark et al. [18] in 1951. The results from tests of T-beams composed of rolled steel I-beam and concrete slab were consistent with the theory, which validated the feasibility and effectiveness of Newmark et al. 's work. Furthermore, it also proved that composite beam theory may be used for any kind of structures composed of two or more interconnected elements as long as the underlying assumptions were satisfied. Girhammar and Gopu [19] conducted first- and second-order analyses for composite beam-columns under transverse and axial loading through the consideration of partial composite action, and also determined the critical buckling loads for a pure column in the second-order analysis. The study proposed by Foraboschi [20] addressed the exact analytical solution of the two-layer beam based on the bilinear model of the relationship between the interfacial shear stress and the slip. Bai and Davidson's [21,22] research that focused on the analysis of foam insulated concrete sandwich panels provided a closed-form solution to symmetrical and unsymmetrical wythe structures that included both longitudinal and transverse interactions. Subsequently, Sha

and Davidson [16] developed a new approach to estimate the transfer length in pretensioned concrete with FRP prestressed tendons using composite beam theory. The set of governing equations was derived by combining with the nonlinear bond-slip relationship for FRP tendons in concrete.

4.2.3 Bond-slip (τ - s) relationship

As mentioned above, accurately defining the bond-slip (τ - s) relationship is a key challenge in developing an analytical model for the evaluation of concrete beams strengthened by externally bonded FRP laminates. A number of existing models can be found in the literature that are based on theoretical analysis and experiments, and that range from linear and bilinear to nonlinear mechanics. Lee et al. [23] obtained the slip modulus (E_b) at FRP laminate-concrete interfaces through experimental measurements of three different types of FRP laminates, which is based on a linear model assumption between bond stress and slip. Lorenzis et al. [24] conducted flexural tests on a plain concrete beam externally bonded with an inverted-T shape CFRP laminate and carried out linear-elastic analysis by means of the shear lag approach; the value of the slip modulus was evaluated. Double-face shear type tests were carried out by Nakaba et al. [25], who proposed the local bond stress-slip relationship defined in Eq. (1), which was based on the Popovics' [31] nonlinear stress-strain relationship for concrete. Moreover, the effective bond length in terms of the proposed model was determined.

$$\frac{\tau}{\tau_m} = \frac{s}{s_m} \frac{n}{(n-1)+(s/s_m)^n} \tag{1}$$

$$\tau_m = 3.5 f_c^{0.19} \tag{2}$$

where τ_m is the maximum local bond stress, f_c is concrete compressive strength for the limited range of 24 to 58 MPa, s_m is the slip corresponding to τ_m with a value of 0.065 mm, n is a constant that is calculated using the least square method and in most cases, $n=3$. Three bond-slip models were proposed in Guo et al. 's [29] experimental study on the bond behavior of GFRP laminate-concrete interfaces that can be used to define the nonlinear bond stress-slip relationship: logarithmic model, modified Popovics model and hyperbola model. Dai et al. [26] provided experimental and analytical results obtained using a method for accurately measuring pullout forces and loaded end slips in pullout tests for FRP laminate-concrete interfaces, instead of the conventional method for recording the strain distribution of FRP laminates to define the local bond stress-slip relationship. The resulting interfacial τ - s model is defined in Eq. (3):

$$\tau = 2 B_D G_f \left[exp(-B_D s) - exp(-2 B_D s) \right] \tag{3}$$

where G_f is the interfacial fracture energy and B_D is the interfacial material parameter, both of which are obtained from the regression analysis of test data. The expression for G_f and B_D by Dai et al. [26] are defined as the following:

$$G_f = 0.446 (G_a / t_a)^{-0.352} f_c^{0.236} (E_p t_p)^{0.023} \tag{4}$$

$$B_D = 6.846 (E_p t_p)^{0.108} (G_a / t_a)^{0.833} \tag{5}$$

where G_a is the shear modulus of the adhesive, t_a is the thickness of the adhesive layer, E_p is the elastic modulus of the FRP laminates, and t_p is the thickness of the FRP laminates. As defined in

the fib Model Code for concrete structures 2010 [32], Ko et al. [30] calibrated three primary parameters of the given bilinear local bond-slip model based upon experimental results of 18 double-shear bond tests: the maximum local bond stress (τ_m), the slip (s_m) corresponding to τ_m , and the ultimate slip (s_{ult}). The proposed model is as follows:

$$\tau = \begin{cases} \tau_m \left(\dfrac{s}{s_m} \right), & 0 \le s \le s_m \\ \tau_m - \dfrac{\tau_m \left(s - s_m \right)}{s_{ult} - s_m}, & s_m \le s \le s_{ult} \end{cases} \tag{6}$$

where the parameters τ_m , s_m , and s_{ult} were defined as the following, and concrete compressive strength is limited to the range of 16 to 76 MPa; in metric (SI) units:

$$\tau_m = 0.165 f_c \tag{7}$$

$$s_m = -0.001 f_c + 0.122 \tag{8}$$

$$s_{ult} = -0.002 f_c + 0.302 \tag{9}$$

Fig. 4.3 compares the bond stress-slip models for externally bonded FRP laminate-concrete interfaces by different researchers using a concrete compression strength of 50 MPa.

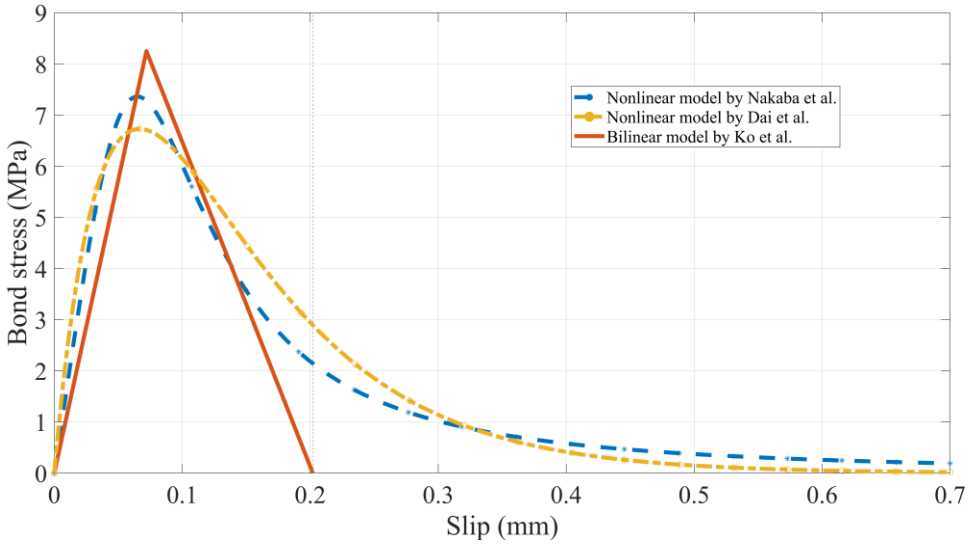

Fig. 4.3 The bond stress-slip models with $f_c = 50\,MPa$

It can be seen that the bilinear model by Ko et al. [30] is in reasonable agreement with the other two nonlinear models [25,26]. The fracture energy of these three bond-slip models is approximately same, especially the elastic ascending branch of Ko et al. [30] is consistent with that of the others. However, the advantage of the bilinear model by Ko et al. [30] is in its simplicity without significant loss of accuracy compared to other models. Consequently, the ascending branch in the bilinear model by Ko et al. [30] was used as the constitutive bond-slip definition between the FRP laminates and concrete in this study.

4.3 Methodology

As shown in Fig. 4.4 (a), the simply supported beam strengthened by externally bonded FRP laminates is subjected to a UDL that can be decomposed into the three cases illustrated in Fig. 4.4 (b), Fig. 4.4 (c), and Fig. 4.4 (d), considers the concrete and FRP laminates as separate parts

connected by adhesive. In the case of Fig. 4.4 (b), the load that the concrete and FRP laminates have at the same the deflection is set, whereas Fig. 4.4 (c) describes the concrete and FRP laminates at the same deflection magnitude but different signs. For the remaining loads shown in the case of Fig. 4.4 (d), the concrete and FRP laminates have different deflections. In the present study, q is the uniformly distributed load on the beam, P is the support reaction equal to $0.5qL$ at both ends, a is the distance between the FRP cutoff point and the support of the span of L, the coordinate origin $x=0$ is located at the left FRP cutoff point defined in Fig. 4.4, E_c is the modulus of elasticity of concrete, E_p is the modulus of elasticity of the FRP laminates, I_c is the moment of inertia of concrete, and I_p is the moment of inertia of FRP laminates, $Q_1 = qE_c I_c / \left(E_c I_c + E_p I_p\right)$, $Q_2 = qE_p I_p / \left(E_c I_c + E_p I_p\right)$, $P_1 = 0.5Q_1\left(L-2a\right)$, $P_2 = 0.5Q_2\left(L-2a\right)$.

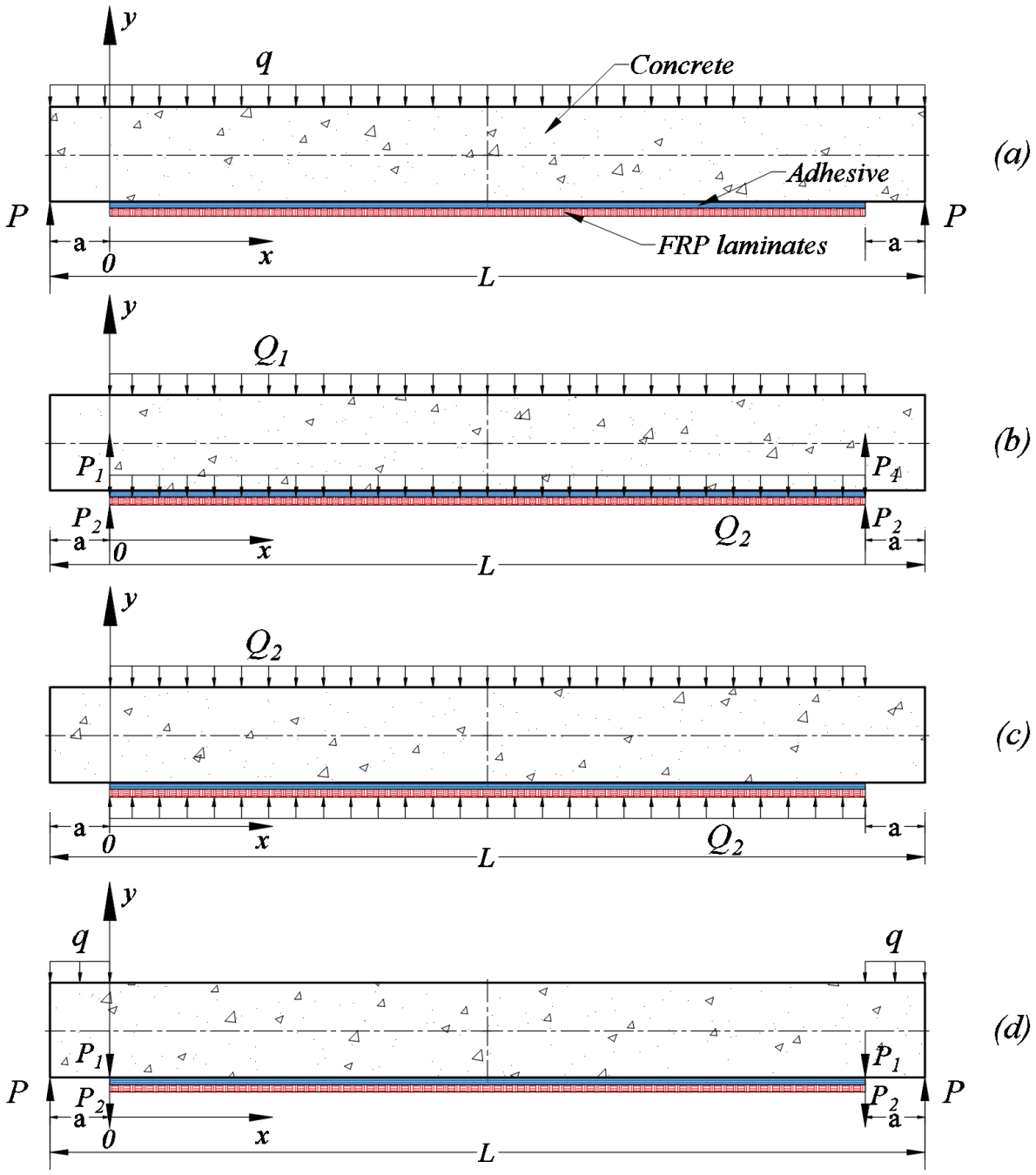

Fig. 4.4 The decoupling process for the simply supported beam strengthened by externally bonded FRP laminates and subjected to UDL

4.3.1 Assumptions

The following assumptions and limitations were involved in the theoretical development presented herein:

(1) Linear elastic constitutive behavior and small displacement.

(2) Shear deformation through the concrete beam cross section is negligible and shear deformation through the laminate cross section is negligible.

(3) FRP laminates provides no bending resistance.

(4) Interfacial stresses are constant through the adhesive thickness.

4.3.2 Interfacial shear stress

4.3.2.1 Axial force equilibrium

The equilibrium of forces in the axial direction of the concrete member cross-section strengthened with FRP laminates illustrated in Fig. 4.5 is given by Eq. (10):

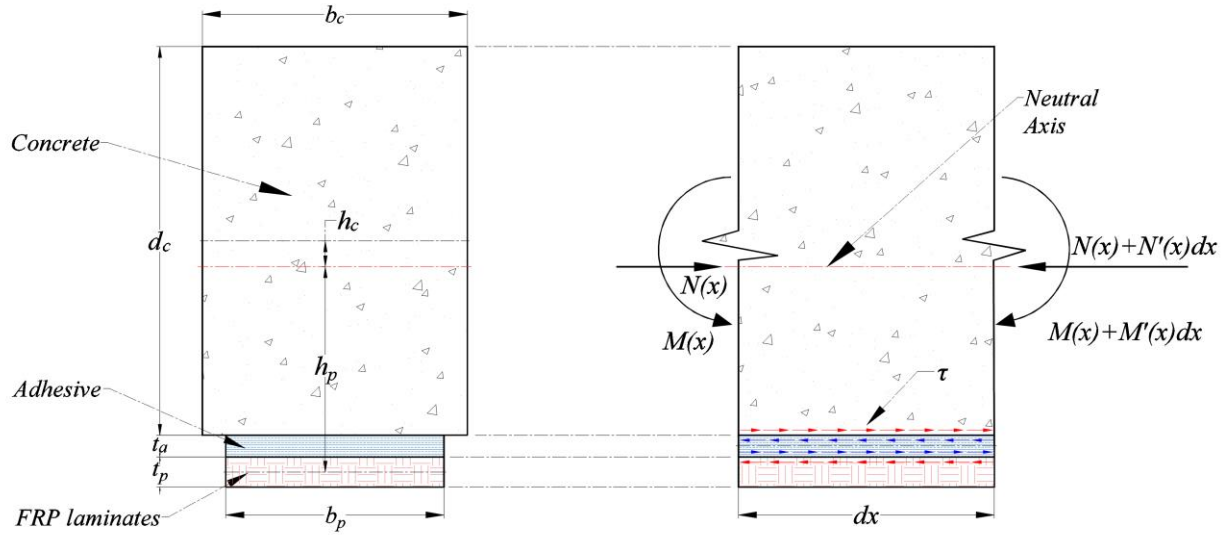

Fig. 4.5 Cross-section and differential length section of concrete member strengthened by externally bonded FRP laminates under internal forces

$$\tau\, b_p\, dx = N'(x)\, dx \tag{10}$$

where τ = interfacial shear stress between concrete and FRP laminates, b_p = the width of FRP laminates, and $N'(x)$ = the first derivative for a given function of resultant axial force acting on the cross section. Substituting $N(x) = A_c\, \sigma_{ac} = A_p\, \sigma_{ap}$ into Eq. (10), where A_c = the cross section area

of the concrete, σ_{ac} = the concrete stress due to the axial force, A_p = the cross section area of FRP laminates, and σ_{ap} = FRP laminates stress due to the axial force.

$$\tau b_p = \left(A_c \sigma_{ac}\right)' = \left(A_p \sigma_{ap}\right)' \tag{11}$$

Eq. (12) is given by substituting $\sigma_{ac} = E_c \varepsilon_c$, $\sigma_{ap} = E_p \varepsilon_p$, and $\varepsilon_c = s'_{1c}$, $\varepsilon_p = s'_{1p}$ into the Eq. (11), where ε_c = the concrete axial strain, ε_p = FRP laminates axial strain, s'_{1c} = the first derivative of concrete displacement due to the axial force, and s'_{1p} = the first derivative of FRP laminates displacement due to the axial force.

$$\tau b_p = A_c E_c s''_{1c} = A_p E_p s''_{1p} \tag{12}$$

It should be noted that the total slip s can be divided into two parts, one is relative movement s_1 due to axial force and the other is relative slip s_2 due to bending. In order to better understand the slip s_2 associated with bending, it is demonstrated in Fig. 4.6, where h_c = the distance from the concrete beam centroid to the neutral axis, v_c = the deflection of the concrete beam, v'_c = the first derivative of the deflection of concrete, which is approximated as the slope angle of concrete. Correspondingly, h_p = the distance from the centroid of FRP laminates to the neutral axis, v_p = the deflection of FRP laminates, and v'_p = the slope angle of FRP laminates.

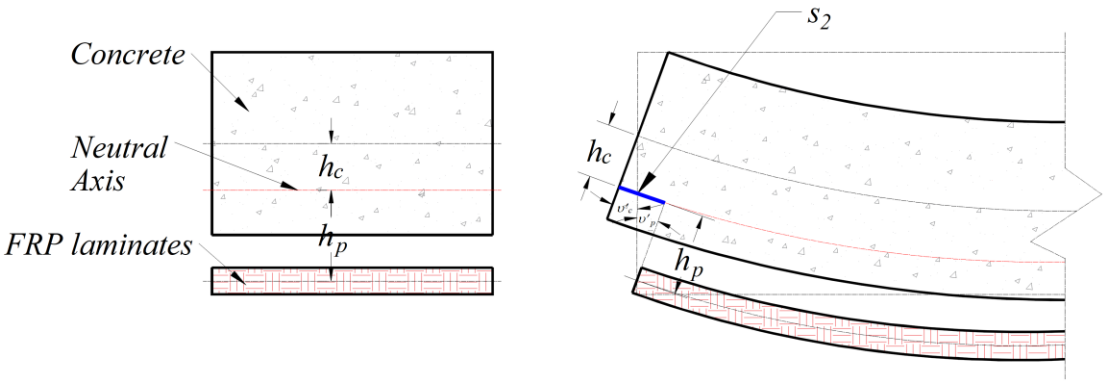

Fig. 4.6 The slip s_2 due to bending

$$s = s_1 + s_2 \tag{13}$$

where

$$s_1 = s_{1c} + s_{1p} \tag{14}$$

$$s_2 = h_c\, v_c' + h_p\, v_p' \tag{15}$$

The second derivative of Eq. (14) with respect to the independent variable x:

$$s_1'' = s_{1c}'' + s_{1p}'' \tag{16}$$

Combining Eq. (12) with Eq. (16), Eq. (17) is given by:

$$s_1'' = \left(1 + \frac{A_c\, E_c}{A_p\, E_p}\right) s_{1c}'' = \left(1 + \frac{A_p\, E_p}{A_c\, E_c}\right) s_{1p}'' \tag{17}$$

Substituting Eq. (12) into Eq. (17), results in Eq. (18):

$$\tau b_p = A_c E_c \frac{s_1''}{\left(1+\frac{A_c E_c}{A_p E_p}\right)} = A_p E_p \frac{s_1''}{\left(1+\frac{A_p E_p}{A_c E_c}\right)} \tag{18}$$

Taking into account the relationship between the slip and the bond stress, namely, that of the total slip s and interfacial shear stress τ:

$$\tau = K s \tag{19}$$

where K = the shear stiffness, which is based on regression analysis of pullout tests for FRP laminate-concrete interfaces. Substituting Eq. (19) into Eq. (18):

$$K s b_p = A_c E_c \frac{s_1''}{\left(1+\frac{A_c E_c}{A_p E_p}\right)} = A_p E_p \frac{s_1''}{\left(1+\frac{A_p E_p}{A_c E_c}\right)} \tag{20}$$

Then substituting the second derivative of Eq. (13) into the Eq. (20) yields:

$$K s = \xi\left(s'' - s_2''\right) \tag{21}$$

where

$$\xi = \frac{A_c E_c}{b_p\left(1+\frac{A_c E_c}{A_p E_p}\right)} = \frac{A_p E_p}{b_p\left(1+\frac{A_p E_p}{A_c E_c}\right)} \tag{22}$$

Rearranging Eq. (21) and substituting the second derivative of Eq. (15) into Eq. (21), Eq. (23) can be written in the form:

$$s'' - \frac{K}{\xi} s = h_c v_c''' + h_p v_p''' \tag{23}$$

4.3.2.2 Bending moment equilibrium

By means of the equilibrium between the internal bending moment and the known external moment M_{ex}, Eq. (24) is given by:

$$M_{ex} = M_c + M_p + h_c N_c + h_p N_p \tag{24}$$

where M_c = concrete moment due to bending, M_p = FRP laminates moment due to bending, N_c = axial force acting at the centroid of concrete, and N_p = axial force acting at the centroid of FRP laminates. It should be noted that the bending resistance provided by FRP laminates is negligible, i.e. M_p = 0, since it is much lower than that provided by concrete. Accordingly,

$$N_c = A_c \sigma_{ac} = A_c E_c \frac{s_1'}{\left(1 + \frac{A_c E_c}{A_p E_p}\right)} = \xi b_p s_1' \tag{25}$$

$$N_p = A_p \sigma_{ap} = A_p E_p \frac{s_1'}{\left(1 + \frac{A_p E_p}{A_c E_c}\right)} = \xi b_p s_1' \tag{26}$$

$$M_c = -E_c I_c v_c'' \tag{27}$$

Consequently, Eq. (24) can be written as:

$$M_{ex} = -E_c I_c v_c'' + \left(h_c + h_p\right) \xi b_p s_1' \tag{28}$$

The first derivative of Eq. (13) after combining with Eq. (14) and Eq. (15) is as follows:

$$s_1' = s' - h_c v_c'' - h_p v_p'' \tag{29}$$

Substituting Eq. (29) into Eq. (28), Eq. (30) with regard to bending moment is expressed as:

$$M_{ex} = -E_c I_c \upsilon_c'' + \left(h_c + h_p\right)\xi b_p \left[s' - \left(h_c \upsilon_c'' + h_p \upsilon_p''\right)\right] \tag{30}$$

The governing equations can be given by combining Eq. (23) and Eq. (30):

$$\begin{cases} s'' - \dfrac{K}{\xi} s = h_c \upsilon_c''' + h_p \upsilon_p''' \\ M_{ex} = -E_c I_c \upsilon_c'' + \left(h_c + h_p\right)\xi b_p \left[s' - \left(h_c \upsilon_c'' + h_p \upsilon_p''\right)\right] \end{cases} \tag{31}$$

4.3.2.3 Solutions of the governing equations

The superposition technique illustrated in Fig. 4.4 (b)-(d) facilitates a rigorous analysis of longitudinal and transverse interactions in an accessible and systematic way. The cases shown in Fig. 4.4 (b) and Fig. 4.4 (d) are applied to determine the interfacial shear stress, whereas the case of Fig. 4.4 (c) has no slip between concrete and FRP laminates that result in the interfacial shear stress is zero. The solutions for estimating the interfacial normal stress based on Fig. 4.4 (c) and Fig. 4.4 (d) will be discussed in a later section. In the case shown in Fig. 4.4 (b), the concrete and FRP laminates have the same the deflection υ_b and therefore Eq. (31) can be rewritten as:

$$\begin{cases} s'' - \dfrac{K}{\xi} s = e \upsilon_b''' \\ \upsilon_b'' - \dfrac{N_s^2}{e} s' = -\dfrac{M_{ex}}{Z_s} \end{cases} \tag{32}$$

where

$$e = h_p + h_c \tag{33}$$

$$Z_s = e^2\,\xi\, b_p + E_c\, I_c \tag{34}$$

$$N_s^2 = \frac{e^2\,\xi\, b_p}{Z_s} \tag{35}$$

Accordingly, with the boundary conditions, the slip is zero at mid-span $s\left(\frac{L}{2}\right)=0$ due to symmetry, and as a result of zero moment at the end of the FRP laminates $v_b''(0)=0$, combining with external moment for the case (b), $M_{ex} = -0.5q\,x^2 + 0.5q(L-2a)\,x$, the general solution for a slip s_b from the case (b) is given by the following expression:

$$s_b = C_1\,cosh(\lambda\,x) + C_2\,sinh(\lambda\,x) + A\,x + B \tag{36}$$

where

$$A = -\frac{e\,\xi\,q}{Z_s\,K} \tag{37}$$

$$B = \frac{e\,\xi}{Z_s\,K}\left[0.5\,q(L-2a)\right] \tag{38}$$

$$\lambda = \sqrt{\frac{K}{\xi\left(1-N_s^2\right)}} \tag{39}$$

$$C_1 = \frac{A}{\lambda}\,tanh\left(\frac{\lambda\,L}{2}\right) + \frac{e\,\xi\,q\,a}{Z_s\,K}\,\frac{1}{cosh\left(\frac{\lambda\,L}{2}\right)} \tag{40}$$

$$C_2 = -\frac{A}{\lambda} \tag{41}$$

Consequently, the shear stress τ_b from the case (b) is expressed as:

$$\tau_b = K s_b \tag{42}$$

In the case shown in Fig. 4.4 (d), the concrete and FRP laminates have different deflections. Recall that the slip due to bending $s_2 = h_c v_c' + h_p v_p'$ can be rearranged as follows:

$$s_2 = e v_c' - h_p \left(v_c' - v_p' \right) \tag{43}$$

It should be noted that, $h_p \left(v_c' - v_p' \right)$ can be negligible compared with the value of $e v_c'$. Therefore, Eq. (43) then becomes:

$$s_2 = e v_c' \tag{44}$$

Similarly, considering that $h_p \left(v_c'' - v_p'' \right)$ can be negligible compared with the value of $e v_c''$, will result in $h_c v_c'' + h_p v_p'' = e v_c'' - h_p \left(v_c'' - v_p'' \right) \approx e v_c''$. Substituting Eq. (44) into Eq. (21), the set of governing equations for case (d) is given by:

$$\begin{cases} s'' - \dfrac{K}{\xi} s = e v_c''' \\ v_c'' - \dfrac{N_s^2}{e} s' = -\dfrac{\bar{M}_{ex}}{Z_s} \end{cases} \tag{45}$$

In accordance with the boundary conditions from case (d), the slip is zero at mid-span $s\left(\frac{L}{2}\right) = 0$ due to symmetry, and as a result of zero moment at the end of the FRP laminates $v_c''(0) = -\frac{1}{2 E_c I_c} q a (L - a)$, combining with external moment for the case (d),

$\bar{M}_{ex} = 0.5\, q\, a\left(L - a\right)$, the general solution for slip s_d from case (d) is given by the following expression:

$$s_d = \bar{C}_1 \cosh\left(\lambda x\right) + \bar{C}_2 \sinh\left(\lambda x\right) \tag{46}$$

where

$$\bar{C}_1 = -\frac{e}{2 N_s^2 \lambda} \tanh\left(\frac{\lambda L}{2}\right) q\, a\left(L - a\right)\left(\frac{1}{Z_s} - \frac{1}{E_c I_c}\right) \tag{47}$$

$$\bar{C}_2 = \frac{e}{2 N_s^2 \lambda} q\, a\left(L - a\right)\left(\frac{1}{Z_s} - \frac{1}{E_c I_c}\right) \tag{48}$$

Consequently, the shear stress τ_d from the case (d) is expressed as:

$$\tau_d = K\, s_d \tag{49}$$

Therefore, in terms of the principle of superposition, the shear stress τ is the sum of the shear stress τ_b from case (b) and the shear stress τ_d from case (d) can be expressed as follows:

$$\tau = K\left[\left(C_1 + \bar{C}_1\right)\cosh\left(\lambda x\right) + \left(C_2 + \bar{C}_2\right)\sinh\left(\lambda x\right) + A x + B\right] \tag{50}$$

4.3.3 Interfacial normal stress

4.3.3.1 Governing equations of interfacial normal stress

Considering that the concrete and FRP laminates parts are connected by the adhesive for interfacial transverse and longitudinal stresses transfer, the equilibrium can be established as illustrated by Fig. 4.7:

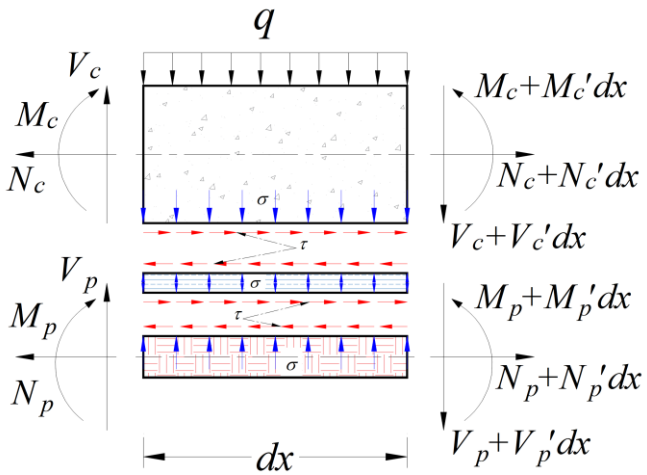

Fig. 4.7 Differential element in concrete beams externally bonded FRP laminates with adhesive

For concrete on the top, the shear direction equilibrium condition of the force acting on the differential element shown in Fig. 4.7 is given by:

$$V_c' dx = -\sigma b_p dx - q dx \tag{51}$$

where σ = interfacial normal stress between concrete and FRP laminates, and V_c' = the first derivative of a given function for transverse shear force acting on the cross section of concrete. The moment acting on the differential element of concrete is expressed as:

$$V_c\,dx = M_c'\,dx + \tau\, b_p\,\frac{d_c}{2}\,dx + \frac{q}{2}(dx)^2 + \frac{\sigma}{2} b_p\,(dx)^2 \tag{52}$$

where M_c' = the first derivative for the resultant bending moment acting on the cross section of the concrete. Eq. (53) is obtained by recognizing that the second order term is negligible compared to the first order term:

$$V_c\,dx = M_c'\,dx + \tau\, b_p\,\frac{d_c}{2}\,dx \tag{53}$$

The governing equations for concrete can be given by combining Eq. (51), Eq. (53), and Eq. (27):

$$E_c\, I_c\,\frac{d^4 v_c}{dx^4} = q + \sigma\, b_p + \tau' b_p\,\frac{d_c}{2} \tag{54}$$

Similarly, the shear direction equilibrium condition of the force acting on the differential element of FRP laminates on the bottom is defined as following:

$$V_p'\,dx = \sigma\, b_p\,dx \tag{55}$$

where V_p' = the first derivative for a given function of transverse shear force acting on the cross section of FRP laminates. The moment that ignores the second order term $-\frac{\sigma}{2} b_p\,(dx)^2$ acting on the differential element of FRP laminates is expressed as:

$$V_p\,dx = M_p'\,dx + \tau\, b_p\,\frac{t_p}{2}\,dx \tag{56}$$

Accordingly,

$$M_p = -E_p I_p v_p'' \tag{57}$$

The governing equations for FRP laminates can be given by combining Eq. (55), Eq. (56), and Eq. (57):

$$E_p I_p \frac{d^4 v_p}{dx^4} = -\sigma b_p + \tau' b_p \frac{t_p}{2} \tag{58}$$

Subtracting Eq. (54) from Eq. (58) yields Eq. (59):

$$\frac{d^4 v_p}{dx^4} - \frac{d^4 v_c}{dx^4} = -\sigma \left(\frac{b_p}{E_c I_c} + \frac{b_p}{E_p I_p} \right) + \tau' b_p \left(\frac{t_p}{2 E_p I_p} - \frac{d_c}{2 E_c I_c} \right) - \frac{q}{E_c I_c} \tag{59}$$

In accordance with the linear elastic constitutive law behavior for the adhesive:

$$\sigma = K_n \left(v_p - v_c \right) \tag{60}$$

$$K_n = \frac{E_a}{t_a} \tag{61}$$

where K_n = the normal stiffness, E_a is the modulus of elasticity of the adhesive, t_a is the thickness of the adhesive. Substituting the fourth derivative of Eq. (60) into Eq. (59), Eq. (62) with regard to the interfacial normal stress is expressed as:

$$\frac{\sigma^{(4)}}{K_n} + \chi_s \sigma = \psi_s \tau' - \frac{q}{E_c I_c} \tag{62}$$

where

$$\chi_s = b_p \left(\frac{E_c I_c + E_p I_p}{E_c I_c E_p I_p} \right) \tag{63}$$

$$\psi_s = b_p \left(\frac{t_p}{2 E_p I_p} - \frac{d_c}{2 E_c I_c} \right) \tag{64}$$

4.3.3.2 Solutions of the governing equations

The cases shown in Fig. 4.4 (c) and Fig. 4.4 (d) are applied to define the interfacial normal stress, whereas the case of Fig. 4.4 (b) has no relative transverse movement between concrete and FRP laminates that result in the interfacial normal stress is zero. For the case shown in Fig. 4.4 (c), the concrete and FRP laminates have the same deflection magnitude but different signs:

$$\upsilon_{cc} = -\upsilon_{cp} \tag{65}$$

where υ_{cc} and υ_{cp} refer to the deflection of the concrete and FRP laminates from the case (c), respectively. In order to determine the deflection of the concrete and FRP laminates, consider that case (c) is relative motion in which the adhesive in the intermediate portion is treated as a spring attached rigid bodies under uniformly distributed load Q_2. The equation representing that motion can be written as follows:

$$b_p \left(L - 2a \right) k_1 \upsilon_{cc} = Q_2 \left(L - 2a \right) \tag{66}$$

where k_1 is defined as the spring coefficient,

$$k_1 = \frac{2 E_a}{t_a} = 2 K_n \tag{67}$$

Therefore,

$$\upsilon_{cc} = -\upsilon_{cp} = \frac{Q_2}{2 K b_p} \tag{68}$$

Substituting $Q_2 = q E_p I_p \big/ \left(E_c I_c + E_p I_p \right)$ into Eq. (68), and becomes:

$$\upsilon_{cc} = -\upsilon_{cp} = \frac{q E_p I_p}{2 K b_p \left(E_c I_c + E_p I_p \right)} \tag{69}$$

In accordance with Eq. (60), the normal stress σ_c from case (c) is expressed as:

$$\sigma_c = K_n \left(\upsilon_{cp} - \upsilon_{cc} \right) = -\frac{q E_p I_p}{b_p \left(E_c I_c + E_p I_p \right)} \tag{70}$$

In the case shown in Fig. 4(d), there is no distributed load acting on the area where concrete is bonded to the FRP laminates, and governing equation Eq. (62) can be rewritten as follows:

$$\frac{\sigma_d^{(4)}}{K_n} + \chi_s \sigma_d = \psi_s \tau_d' \tag{71}$$

where σ_d = the normal stress from the case (d). Considering the homogenous part of Eq. (71):

$$\frac{\sigma_d^{(4)}}{K_n} + \chi_s \sigma_d = 0 \tag{72}$$

And the characteristic equation representation of Eq. (72) is as follows:

$$\frac{\lambda_n^{(4)}}{K_n} + \chi_s \lambda_n = 0 \tag{73}$$

where λ_n = the characteristic roots that are given by the following expressions:

$$\lambda_{n1} = \sqrt[4]{\frac{K_n \chi_s}{4}} + \sqrt[4]{\frac{K_n \chi_s}{4}}\, i \tag{74}$$

$$\lambda_{n2} = -\sqrt[4]{\frac{K_n \chi_s}{4}} + \sqrt[4]{\frac{K_n \chi_s}{4}}\, i \tag{75}$$

$$\lambda_{n3} = \sqrt[4]{\frac{K_n \chi_s}{4}} - \sqrt[4]{\frac{K_n \chi_s}{4}}\, i \tag{76}$$

$$\lambda_{n4} = -\sqrt[4]{\frac{K_n \chi_s}{4}} - \sqrt[4]{\frac{K_n \chi_s}{4}}\, i \tag{77}$$

Consequently, the general solution of the homogeneous equation σ_{d0} is as follows:

$$\sigma_{d0} = exp(\beta x)\left[D_1 cos(\beta x) + D_2 sin(\beta x)\right] + exp(-\beta x)\left[D_3 cos(\beta x) + D_4 sin(\beta x)\right] \tag{78}$$

where D_1, D_2, D_3, D_4 are quantities that can be defined using the boundary conditions as illustrated in a subsequent section, as well as:

$$\beta = \sqrt[4]{\frac{K_n \chi_s}{4}} \tag{79}$$

The particular solution σ_{d1} of nonhomogeneous differential equation Eq. (71) can now be calculated based on the right-hand side portion of the structure,

$$\psi_s \tau_d' = K \psi_s \left[\bar{C}_1 \lambda sinh(\lambda x) + \bar{C}_2 \lambda cosh(\lambda x)\right] \tag{80}$$

Hence, the particular solution σ_{d1} is given in the form:

$$\sigma_{d1} = H\,sinh(\lambda x) + T\,cosh(\lambda x) \tag{81}$$

where

$$H = \frac{\psi_s K K_n \bar{C}_1 \lambda}{\lambda^4 + K_n \chi_s} \tag{82}$$

$$T = \frac{\psi_s K K_n \bar{C}_2 \lambda}{\lambda^4 + K_n \chi_s} \tag{83}$$

Thus, the general solution of the governing equation Eq. (71) is given by:

$$\sigma_d = \sigma_{d0} + \sigma_{d1} \tag{84}$$

$$\begin{aligned}\sigma_d = {} & exp(\beta x)\left[D_1 cos(\beta x) + D_2 sin(\beta x)\right] + exp(-\beta x)\left[D_3 cos(\beta x) + D_4 sin(\beta x)\right] \\ & + H\,sinh(\lambda x) + T\,cosh(\lambda x)\end{aligned} \tag{85}$$

It should be noted that the normal stress σ_d will approach zero with increasing x, which results in $D_1 = D_2 = 0$, and Eq. (85) can be rewritten as:

$$\sigma_d = exp(-\beta x)\left[D_3 cos(\beta x) + D_4 sin(\beta x)\right] + H\,sinh(\lambda x) + T\,cosh(\lambda x) \tag{86}$$

Considering the boundary conditions for obtaining two unknown constants D_3, D_4, $M_p(0) = 0$ and $M_c(0) = \frac{qa}{2}(L-a)$ for case (d), which leads to the second derivate of deflection at the end of FRP laminates $v_b''(0) = 0$ and at the end of concrete $v_c''(0) = -\frac{qa}{2E_c I_c}(L-a)$, respectively. Based on Eq. (60), the following boundary condition when $x = 0$ is given by:

$$\sigma_d''(0) = K_n\left(v_p'' - v_c''\right) = K_n\left[\frac{q\,a}{2\,E_c\,I_c}(L-a)\right] \tag{87}$$

Taking into account the third derivative of Eq. (60) and combining with Eq. (27), Eq. (57) can be rewritten as follows:

$$\sigma_d''' = K_n\left[\frac{1}{E_p\,I_p}\left(-\frac{dM_p}{dx}\right) - \frac{1}{E_c\,I_c}\left(-\frac{dM_c}{dx}\right)\right] \tag{88}$$

Substituting Eq. (53) and Eq. (56) into Eq. (88) results in:

$$\sigma_d''' = K_n\left[-\frac{V_p}{E_p\,I_p} + \frac{\tau_d\,b_p\,t_p}{2\,E_p\,I_p} + \frac{V_c}{E_c\,I_c} - \frac{\tau_d\,b_p\,d_c}{2\,E_c\,I_c}\right] \tag{89}$$

At $x=0$ for the case (d), $V_p(0) = -P_2$, $V_c(0) = q\left(\frac{L}{2}-a\right) - P_1$, as well as $\tau_d(0) = K\bar{C}_1$ based on Eq. (46) and Eq. (49). As a result, another boundary condition when $x=0$ is given by:

$$\sigma_d'''(0) = K_n\left[\frac{q}{E_c\,I_c}\left(\frac{L}{2}-a\right) + K\bar{C}_1\,b_p\left(\frac{t_p}{2\,E_p\,I_p} - \frac{d_c}{2\,E_c\,I_c}\right)\right] \tag{90}$$

Hence, substituting Eq. (87) and Eq. (90) into the second and the third derivatives of Eq. (86), respectively, D_3 and D_4 can be expressed as follows:

$$D_3 = \frac{1}{2\,\beta^3}\left\{K_n\left[\frac{q}{E_c\,I_c}\left(\frac{L}{2}-a\right) + K\bar{C}_1\,b_p\left(\frac{t_p}{2\,E_p\,I_p} - \frac{d_c}{2\,E_c\,I_c}\right)\right] - H\,\lambda^3\right\} - D_4 \tag{91}$$

$$D_4 = -\frac{1}{2\,\beta^2}\left[\frac{K_n\,q\,a}{2\,E_c\,I_c}(L-a) - T\,\lambda^2\right] \tag{92}$$

Therefore, through applying the principle of superposition, the normal stress σ is the sum of the normal stress σ_c from case (c) and the normal stress σ_d from case (d), and can be expressed as follows:

$$\sigma = \sigma_c + \sigma_d \tag{93}$$

$$\sigma = exp(-\beta x)\left[D_3 cos(\beta x) + D_4 sin(\beta x)\right] + H sinh(\lambda x) + T cosh(\lambda x) - \frac{q E_p I_p}{b_p \left(E_c I_c + E_p I_p\right)} \tag{94}$$

4.4 Validation and comparisons

In order to verify the accuracy of the proposed method, comparisons were made to published finite element results [43] and existing models by other investigators [1,2], respectively. Although many experimental studies have focused on the performance of reinforced concrete beams strengthened by externally bonded FRP laminates, it was found that measuring interfacial shear and normal stresses is practically impossible [44,45]. Therefore, additional validation was conducted to compare the present solution with the published FE model [43] as an alternative that cannot be compared with experimental results.

Beam-spring-beam (B-S-B) models [43] were developed for predicting interfacial stresses and debonding failure in structural members strengthened by bonded plates using the FE method in which the beam and the bonded plate were both modeled by beam elements while the adhesive layer was modeled by spring elements. As a result, interfacial stresses are constant through the adhesive thickness, which is consistent with the assumptions of the model developed in this study. Also, it should be noted that the stiffness of the spring element adopted the stiffness of adhesives

layer $K = G_a / t_a$ in B-S-B FE model. Therefore, comparisons are performed for validation of the present method with shear stiffness $K = G_a / t_a$. The example from Zhang and Teng is a simply supported reinforced concrete beam strengthened by FRP laminates under UDL. The beam span is $L = 3000\,mm$, UDL acting on the beam is $q = 30\,N/mm$, and the distance from the support to the FRP laminates cutoff point is $a = 300\,mm$. The geometric and material parameters are listed in Table 4.1.

Table 4.1 Material parameters used for comparison with FE analyses

Part	Modulus of elasticity (MPa)	Width (mm)	Thickness (mm)	Poisson's ratio
Concrete	E_c = 30000	b_c = 150	d_c = 300	v_c = 0.18
Adhesive	E_a = 3000	b_a = 150	t_a = 2	v_a = 0.35
FRP laminates	E_p = 200000	b_p = 150	t_p = 3	v_p = 0.3

As shown in Fig. 4.8 and Fig. 4.9, the predictions of the interfacial stress distribution by the present solution are in very close agreement with the corresponding FE results based on similar assumptions, which demonstrates the accuracy of analytical solution in this study. The predicted interfacial shear stress peak value is 5.1% higher than that from FEM; the predicted interfacial normal stress peak value is 3.8% lower than that from FEM. The reason why the discrepancy only appears at the end of FRP laminates is due to the stress singularity [46].

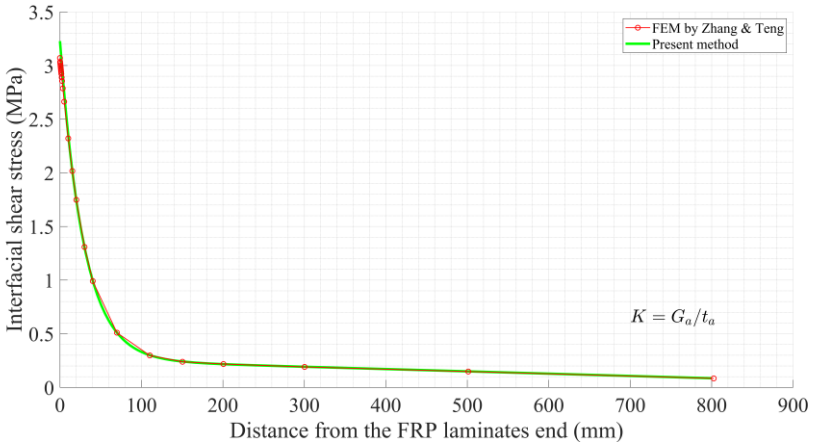

Fig. 4.8 Comparison between FE analysis and present results for the interfacial shear stress

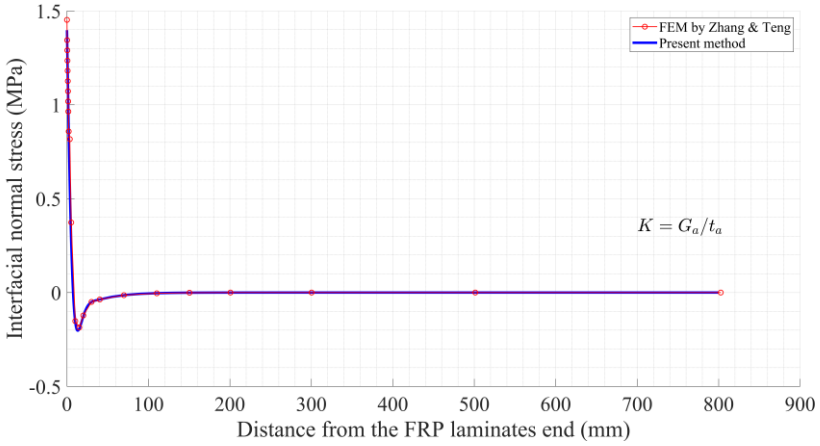

Fig. 4.9 Comparison between FE analysis and present results for the interfacial normal stress

The second validation example is from Smith and Teng [2], which is also the simply supported RC beam with the span of $L = 3000\,mm$, UDL acting on the beam is $q = 50\,N/mm$, and the distance from the support to the FRP laminates cutoff point is $a = 300\,mm$ as shown in Fig. 4.10. The geometric and material parameters are listed in Table 4.2.

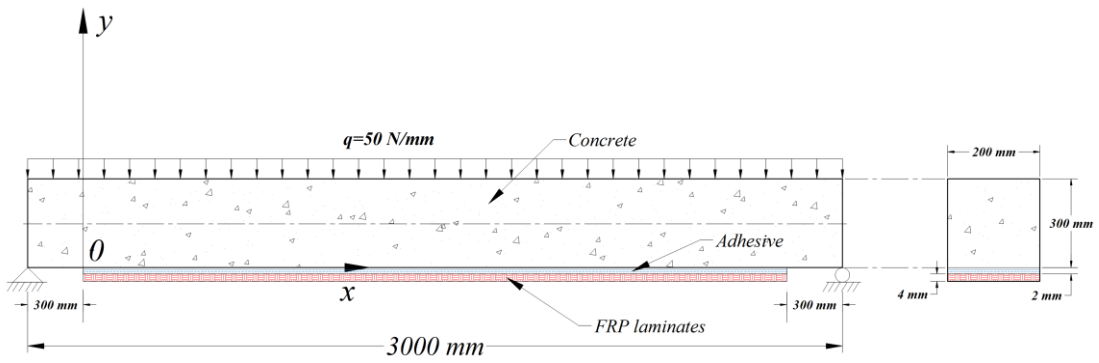

Fig. 4.10 The simply supported concrete beam externally bonded FRP laminates subjected to UDL used for validation

Table 4.2 Material parameters used for comparison analyses

Part	Modulus of elasticity (MPa)	Width (mm)	Thickness (mm)	Poisson's ratio
Concrete	E_c = 30000	b_c = 200	d_c = 300	N/A
Adhesive	E_a = 2000	b_a = 200	t_a = 2	v_a = 0.35
FRP laminates	E_p = 100000	b_p = 200	t_p = 4	N/A

The solution for interfacial shear stress from Eq. (50) based upon $K=\tau_m/s_m$, $K=G_a/t_a$ and $K=383.6\,MPa/mm$ in the present study were compared to the predictions of Malek et al. [1] and Smith et al. [2] and are provided in Figs. 4.11, 4.12, and 4.13, respectively. Specifically, the shear stiffness $K=\tau_m/s_m$ is from the bond-slip model proposed by Ko et al. [30], which is based on a regression analysis of pullout tests of bonded FRP-concrete interfaces. The shear stiffness $K=G_a/t_a$ has been widely applied to previous methods for the analysis of interfacial stress in which the local bond stress-slip relationship between concrete and FRP laminates is not taken into account. The slip modulus $K=383.6\,MPa/mm$ was evaluated by Lorenzis et al. [24]

by means of the shear lag approach together with the determination of the thickness of composite systems using a Scanning Electron Microscope (SEM). As can be seen in Fig. 4.11, the present method with $K = \tau_m / s_m$ and other researchers' methods have a discrepancy in the interfacial shear stress peak values, which gradually vanishes as the distance to the midspan decreases. In contrast, it can be observed from Figs. 4.12 and 4.13 that the results from the present method with $K = G_a / t_a$ and $K = 383.6\ MPa/mm$ show close agreement with Smith et al.'s [2] results, whereas it still has a small discrepancy with the results of Malek et al. [1]. This is because the effect of bending deformation of concrete and FRP laminates on the interfacial shear is not taken into account in Malek et al.'s [1] solution. According to Eq. (24), this might lead to a rise in the value of slip, resulting in the interfacial shear stress predicted by Malek et al.'s [1] method being slightly larger than the values estimated by Smith et al. [2] and the current method.

The predicted results with $K = G_a / t_a$ of the current method are almost identical to those from Smith et al.'s [2] solution with the same shear stiffness illustrated in Fig. 4.12, which demonstrates the accuracy in the interfacial shear stress calculations using composite beam theory of this study. It is worth noting that τ_{max} at the end of the FRP laminates from this study is only 2.5% larger than that of Smith et al.'s [2] solution because the bending resistance provided by the FRP laminates is negligible. This further indicates that the effect of bending deformation of FRP laminates on the interfacial shear stress is negligible compared to that of concrete.

As can be seen in Fig. 4.13, the agreement between predicted results with $K = 383.6\ MPa/mm$ in this study and those from Smith et al.'s [2] solution is good enough to demonstrate the accuracy and efficiency of the present method by considering the shear stiffness K between concrete and bonded FRP laminates. It should be noted that the differences between

the predicted results based on $K=\tau_m/s_m$ with other researchers' are mainly due to the shear stiffness K conducted by Ko et al. [30] is much lower than $K=G_a/t_a$. However, in fact, the definition of the constitutive mechanism of bond-slip for FRP laminate-concrete is a complex problem that is not only governed by properties of the adhesive but also depends on concrete strength, FRP laminates and concrete width ratio and FRP axial stiffness [30,33-35]. Therefore, an accurate assessment of the bond-slip (τ - s) relationship for FRP laminate-concrete is essential to the analysis of the mechanical behavior of concrete beams with externally bonded FRP laminates.

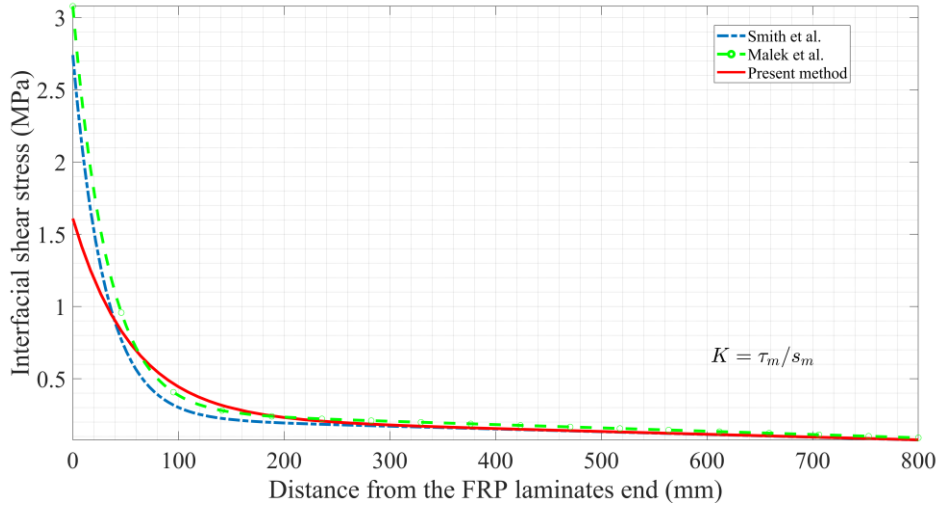

Fig. 4.11 Interfacial shear stress distributions near the end of FRP laminates with $K=\tau_m/s_m$

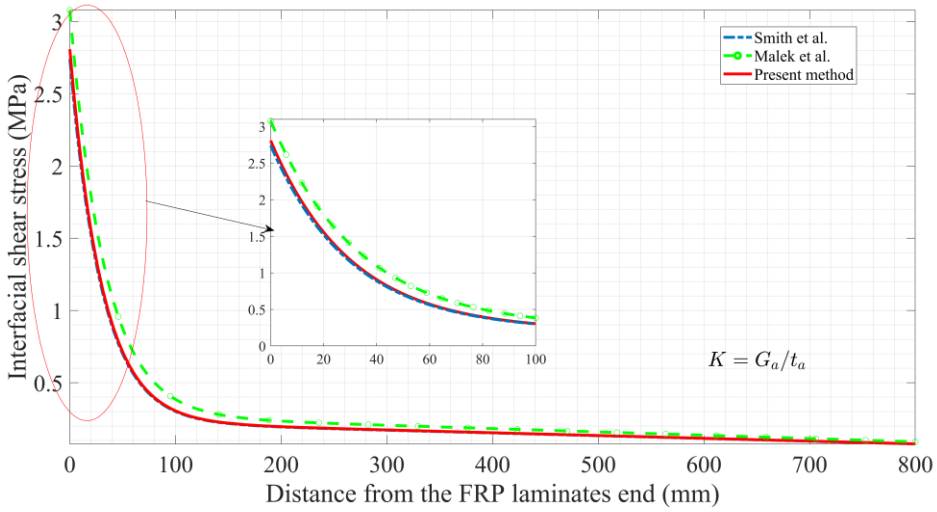

Fig. 4.12 Interfacial shear stress distributions near the end of FRP laminates with

$$K = G_a \,/\, t_a$$

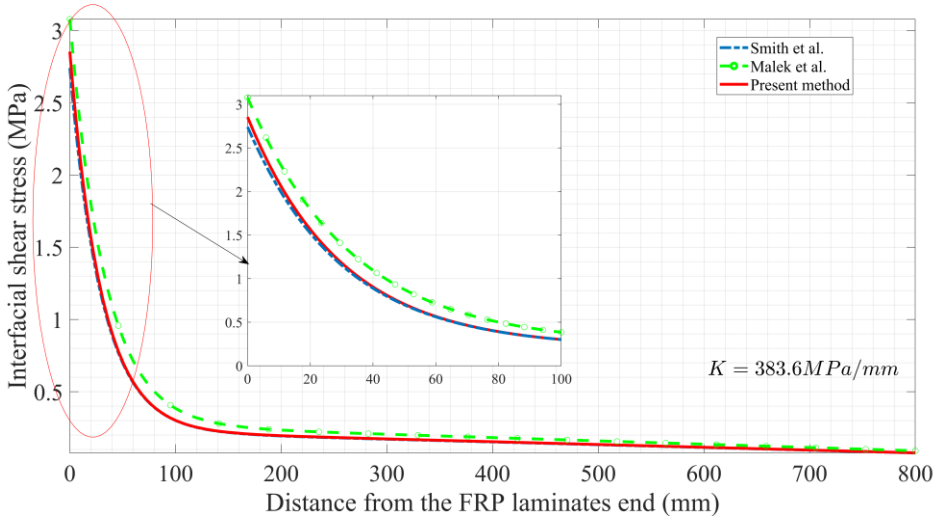

Fig. 4.13 Interfacial shear stress distributions near the end of FRP laminates with

$$K = 383.6\ MPa\ /\ mm$$

From Figs. 4.14, 4.15, and 4.16, the comparison between the predictions of the interfacial normal stress based upon the shear stiffness $K = \tau_m / s_m$, $K = G_a / t_a$ and $K = 383.6\ MPa/mm$ presented in this study and the solutions of Malek et al. [1] and Smith et al. [2] are illustrated, respectively. Fig. 4.14 shows that the present solution with the shear stiffness $K = \tau_m / s_m$ have a discrepancy with results of other researchers near the end of the FRP laminates and the discrepancy gradually vanishes as the distance to the midspan becomes small. The reason is that the determination of interfacial normal stress derived by Eq. (94) takes into account the results of the interfacial shear stress, and interfacial shear stresses based on $K = \tau_m / s_m$ are different from those of other researchers. However, as can be observed from Figs. 4.15 and 4.16, the predicted results with $K = G_a / t_a$ and $K = 383.6\ MPa/mm$ are in close agreement with the solutions of Smith et al. [2]. Also it can be found from Figs. 4.14, 4.15, and 4.16 that there are some discrepancies between the results of Malek et al. [1] and others in the region of negative interfacial normal stress. This is because the tensile stress in FRP laminates was mistaken for the interfacial shear stress in the process of Malek et al.'s [1] solution for interfacial normal stress. Additionally, based on the solution of tensile stress without considering the effects of bending deformation of concrete and FRP laminates, resulting in σ_{max} at the end of FRP laminates of Malek et al. [1] is 24.4% larger than that of Smith et al.'s [2] solution.

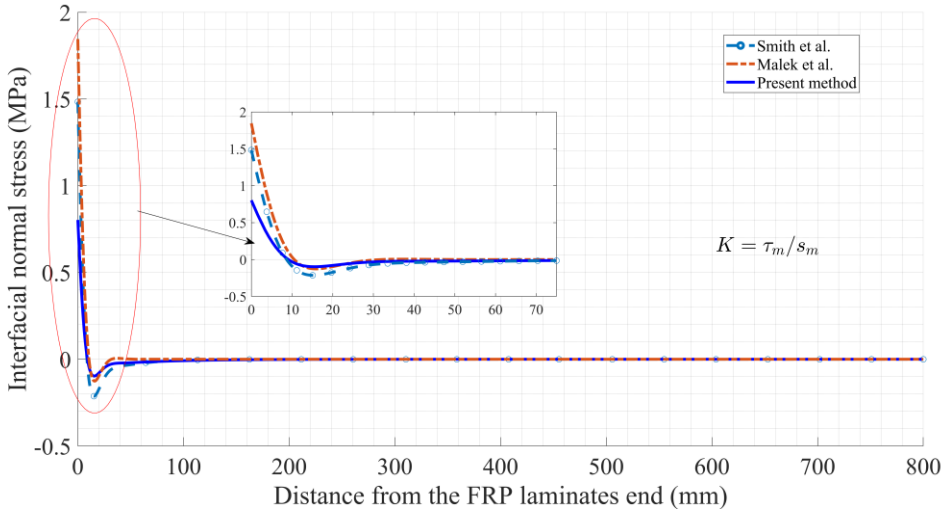

Fig. 4.14 Interfacial normal stress distributions near the end of FRP laminates with

$$K = \tau_m / s_m$$

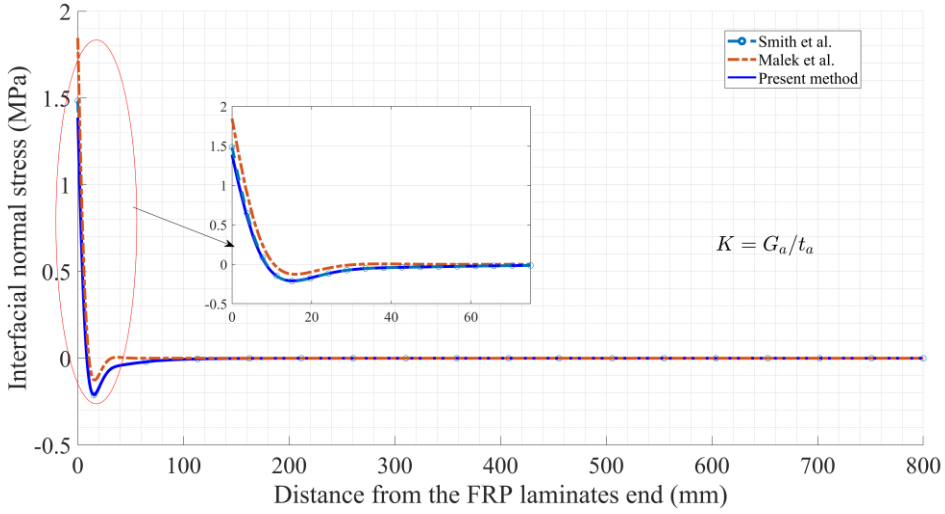

Fig. 4.15 Interfacial normal stress distributions near the end of FRP laminates with

$$K = G_a / t_a$$

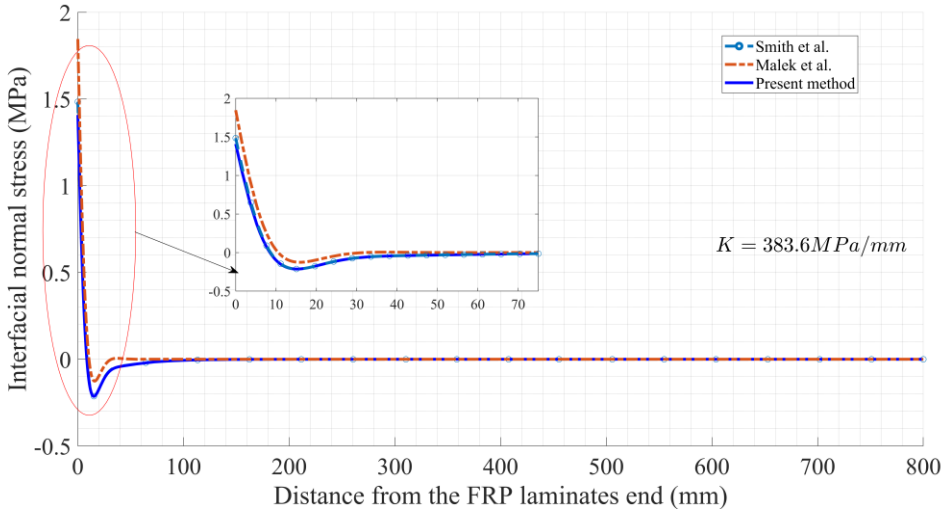

Fig. 4.16 Interfacial normal stress distributions near the end of FRP laminates with

$$K = 383.6\ MPa / mm$$

As the interfacial shear τ and normal stress σ have been determined in Eq. (50) and Eq. (94), respectively, the peak value of interfacial stress at the end of FRP laminates $(x=0)$ can be defined by the following:

$$\tau_{max} = K\left(C_1 + \bar{C}_1 + B\right) \tag{95}$$

$$\sigma_{max} = D_3 + T - \frac{q\,E_p\,I_p}{b_p\left(E_c\,I_c + E_p\,I_p\right)} \tag{96}$$

The results of the maximum value of interfacial stress given by Eq. (95) and Eq. (96) for the example were compared to those of the former [1,2] and are summarized in Table 4.3. Thus, it is evident that τ_{max} and σ_{max} at the end of FRP laminates by the solution with $K = \tau_m / s_m$ in the present study are smaller than that of other solutions because the result depends on the shear stiffness K, whereas the shear stiffness $K = \tau_m / s_m$ from pullout tests for bonded FRP-concrete

interfaces is smaller than the shear stiffness calculated from elastic properties of adhesive, which has been proved in the extensive literature [33-38].

Table 4.3 Comparison of peak values of interfacial stress

Description	Peak value of interfacial shear stress τ_{max} (MPa)	$\frac{\tau_{max}-\tau_{smith}}{\tau_{smith}}$	Peak value of interfacial normal stress σ_{max} (MPa)	$\frac{\sigma_{max}-\sigma_{smith}}{\sigma_{smith}}$
Smith et al. [2]	2.740	0	1.484	0
Malek et al. [1]	3.078	12.3%	1.846	24.4%
Present ($K=\tau_m / s_m$)	1.609	41.3%	0.803	45.9%
Present ($K=G_a / t_a$)	2.808	2.5%	1.387	6.5%
Present ($K=383.6\,MPa/mm$)	2.854	4.2%	1.408	5.1%

4.5 Influence of parameters on the interfacial stress

In order to study the influence of various factors on the peak interfacial shear τ_{max} and normal σ_{max} stress, parameters ranges were selected based on experiment data [25,30] and normalized for better quantification, i.e., the distance from the support to the end of FRP ($a=0\sim400\,mm$), the thickness of FRP laminates ($t_p=0\sim4\,mm$), the width of FRP laminates ($b_p=50\sim200\,mm$), the depth of concrete ($d_c=100\sim400\,mm$), the elastic modulus of concrete ($E_c=20000\sim40000\,MPa$), the elastic modulus of FRP laminates

($E_p = 100000 \sim 300000\,MPa$), the shear stiffness ($K = 30 \sim 3500\,MPa/mm$) and the width of concrete ($b_c = 100 \sim 400\,mm$).

Figs. 4.17 and 4.18 show how various factors affect the peak interfacial shear τ_{max} and normal σ_{max} stress. The maximum interfacial stresses, i.e., τ_{max} and σ_{max}, both are increasing as the distance from the support to the end of FRP laminates becomes larger. Also, as the thickness of FRP laminates increases, the maximum interfacial stresses increase. This is the reason why the application of multiple layers will increase the stress at the end of FRP laminates. In contrast, the results indicate that the effect of FRP laminates width on the peak interfacial stresses are not evident within limits. It is worth noting that the influence of concrete depth and width have some difference: as the depth of concrete becomes larger, the peak value of interfacial stresses decreases significantly, whereas, as the width of concrete becomes larger, the peak value of interfacial stresses decreases relatively less. This is because the larger depth of concrete affects not only the tensile force developed in the concrete, but also the bending moment. In turn, it has a greater impact on the results. It is also found that larger elastic modulus of concrete and FRP laminates results in increasing τ_{max} and σ_{max}. As previously mentioned, Figs. 4.17 and 4.18 further illustrate that the maximum interfacial stresses are closely related to the shear stiffness K, which means that the larger shear stiffness K will remarkably increase the peak value of interfacial stresses.

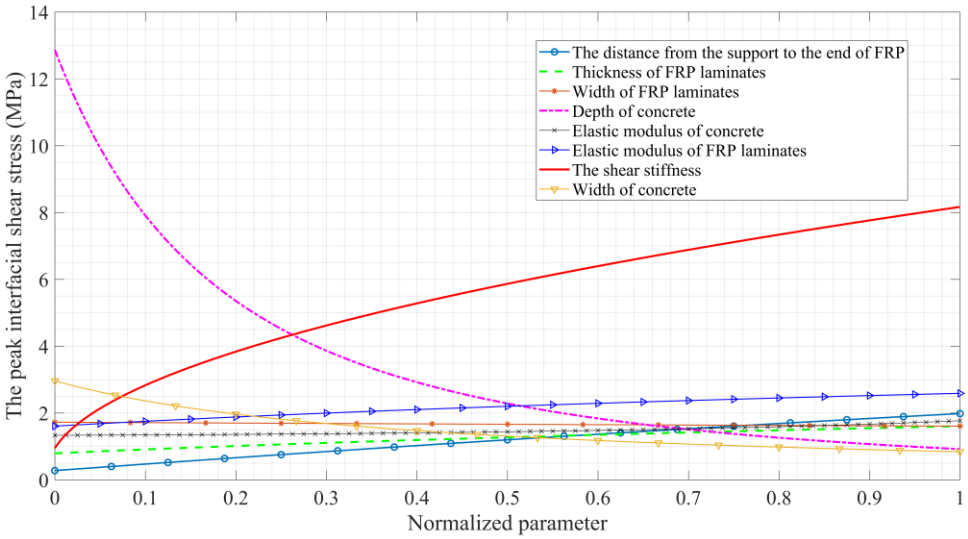

Fig. 4.17 Influence of parameters on the peak interfacial shear stress

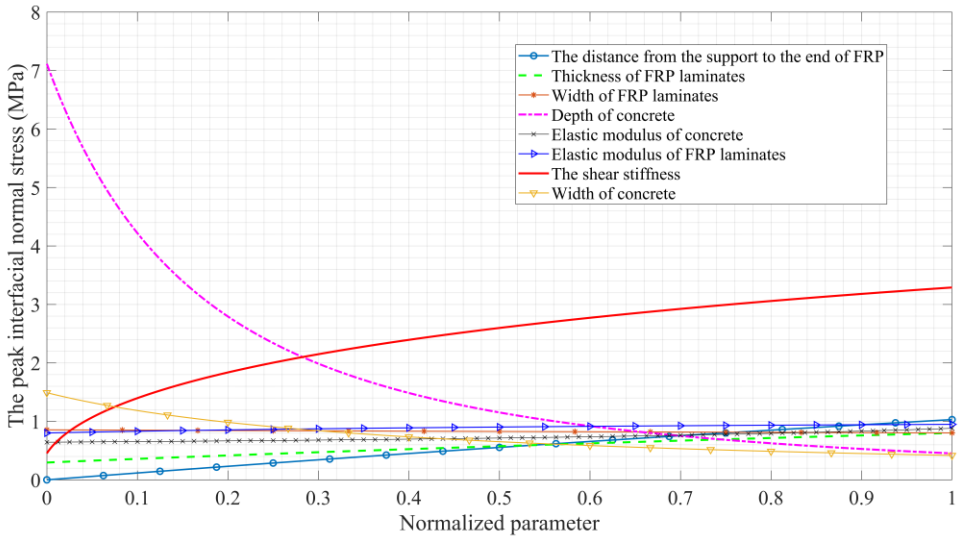

Fig. 4.18 Influence of parameters on the peak interfacial normal stress

In addition, Fig. 4.19 through Fig. 4.26 demonstrate the influence of various factors on the distributions of the interfacial shear τ and normal σ stress determined in Eq. (50) and Eq. (94), respectively. The results from Fig. 4.19 and Fig. 4.25 reveal that the interfacial stress is closely associated with the distance from the support to the end of the FRP and the shear stiffness, and the effect mainly occurs near the end of the FRP laminates. On the other side, the concept of the active bond length of externally bonded FRP systems for strengthening concrete structures [39] also confirms the accuracy of the results. In Fig. 4.21, again for FRP laminates width, the effect on the interfacial stresses are not significant, as mentioned above. Fig. 4.20 shows that FRP laminates thickness has a wide range of influences. As illustrated in Figs. 4.23 and 4.24, the effects of elastic modulus of concrete and FRP laminates are relatively minor, but they work throughout the bond area. By comparing the effect of concrete depth with concrete width on the interfacial stresses' distribution illustrated by Figs 4.22 and 4.26, it is not difficult to recognize that the former is more obvious and the latter is gradually weakening. Furthermore, the similarity between the influence of the concrete depth and width on the interfacial stresses' distribution is that they are both primarily reflected close to the end of FRP laminates.

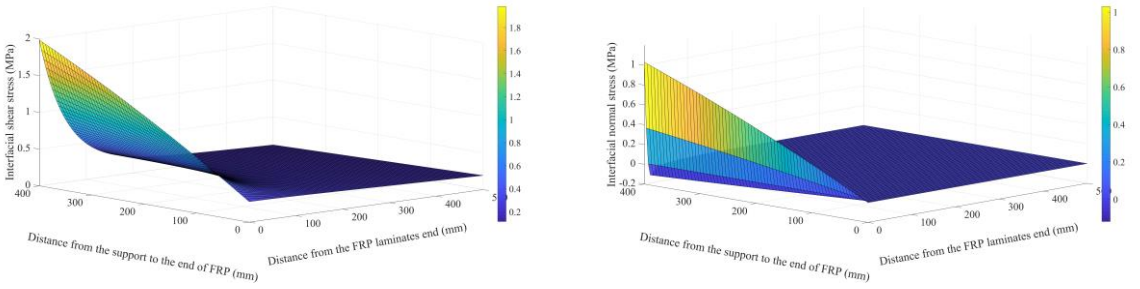

Fig. 4.19 Influence of the distance from the support to the end of FRP on interfacial stress distributions

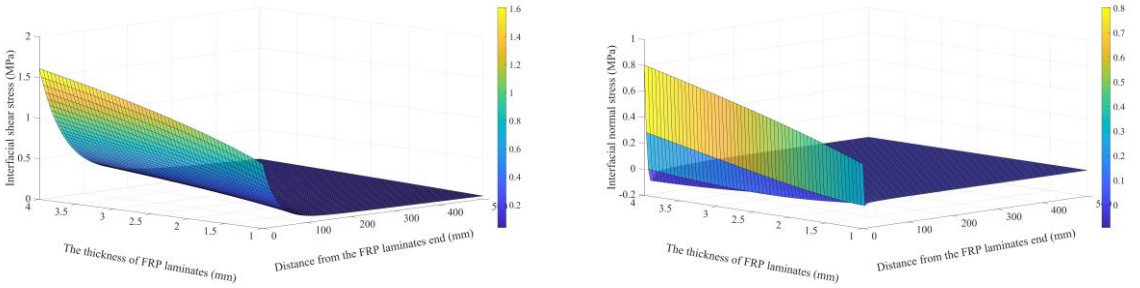

Fig. 4.20 Influence of the thickness of FRP laminates on interfacial stress distributions

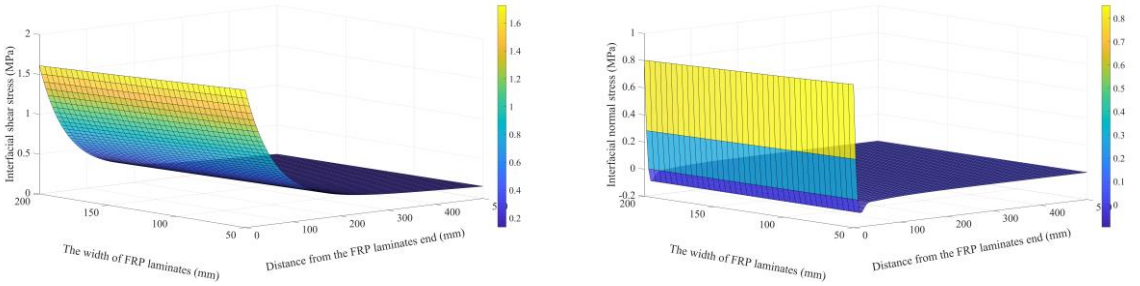

Fig. 4.21 Influence of the width of FRP laminates on interfacial stress distributions

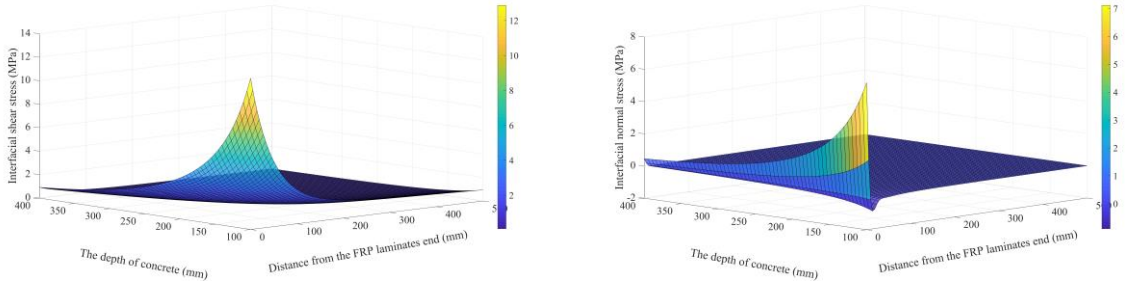

Fig. 4.22 Influence of the depth of concrete on interfacial stress distributions

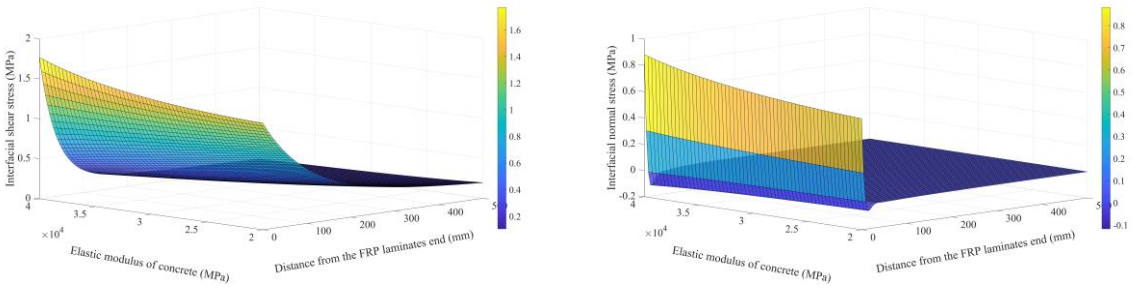

Fig. 4.23 Influence of the elastic modulus of concrete on interfacial stress distributions

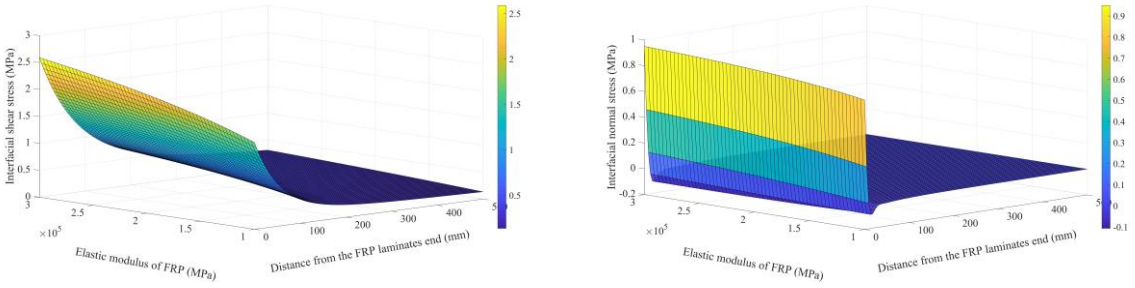

Fig. 4.24 Influence of the elastic modulus of FRP on interfacial stress distributions

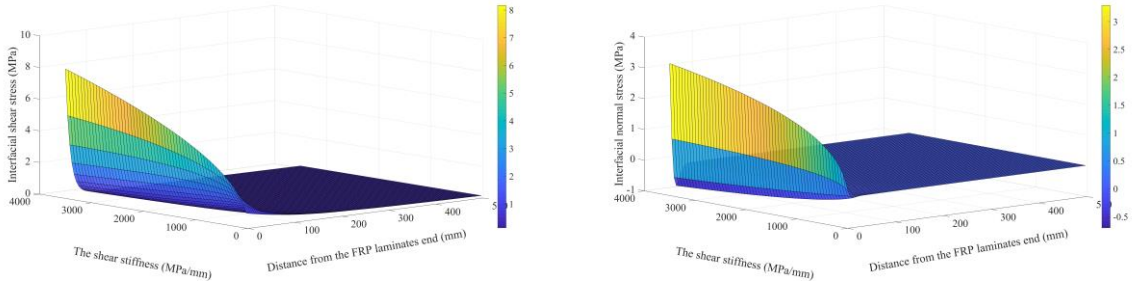

Fig. 4.25 Influence of the shear stiffness on interfacial stress distributions

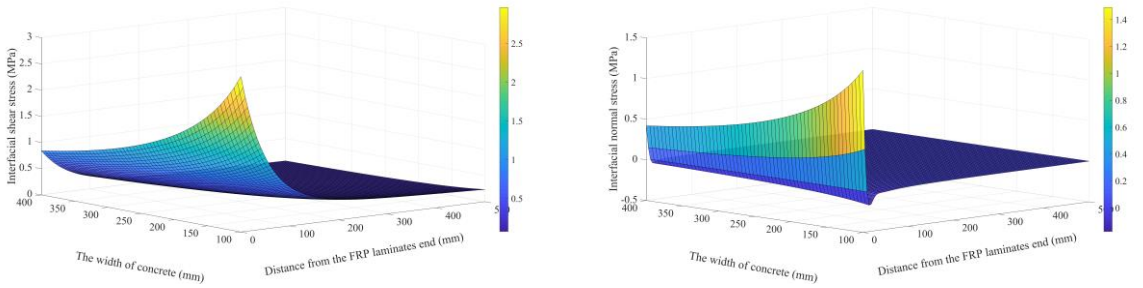

Fig. 4.26 Influence of the width of concrete on interfacial stress distributions

4.6 Conclusions

The interfacial shear τ and normal σ stress in concrete beams strengthened by externally bonded FRP laminates subjected to UDL are analyzed by using composite beam theory in this study. A rigorous analytical approach considering the bond-slip relationship between FRP laminates and concrete is developed for the determination of the mechanics behavior including longitudinal and transverse interactions. Two sets of governing equations are derived for interfacial stresses that include the interfacial shear stress τ and the interfacial normal stress σ. The closed-form solutions are given by means of superposition technique in which UDL is decomposed into three simple subcases. Through comparing the distribution of interfacial stresses evaluated based upon the developed model with those from the published finite element modeling results and existing models by other investigators, the conclusions were drawn as follows:

1. The present approach associated with the shear stiffness $K = G_a / t_a$ shows good agreement with published FE results and analytical solutions by other investigators, and demonstrates the feasibility and effectiveness in the interfacial stresses prediction for concrete

beams strengthened by externally bonded FRP laminates using the composite beam theory developed in this study.

2. Using the model with the shear stiffness based on pullout tests for bonded FRP-concrete interfaces improves the solution accuracy for interfacial stresses.

3. The effect of FRP laminates bending deformation on the determination of interfacial stresses is not obvious, but it is necessary to consider the bending deformation of concrete in order to derive a more rigorous model.

4. It is critical to define the relationship between FRP laminates and concrete for accurately determining the interfacial stress, which further predicts accurately the debonding failure for externally bonded FRP systems for strengthening concrete structures.

5. The advantages of the theoretical development are demonstrated by the parametric study. The influences of various factors on the peak interfacial shear and normal stresses are quantified, and the influence area of different parameters on the distribution of interfacial stress is illustrated through the developed formulation.

Future work will be devoted to the composite beam theory solution for concrete beams strengthened by externally bonded FRP laminates subjected different types of loading. In addition, it will be essential to provide a more accurate assessment of the bond-slip relationship between concrete structures and externally bonded FRP laminates composed of different types of fiber, such as Aramid Fiber Reinforced Polymer (AFRP), Carbon Fiber Reinforced Polymer (CFRP) and Glass Fiber Reinforced Polymer (GFRP).

Notations

p_s	transverse force per length	G_f	interfacial fracture energy
σ	Interfacial normal stress between concrete and FRP laminates	t_a	thickness of the adhesive layer
s_{ult}	the ultimate slip	t_p	thickness of FRP laminates
a	distance from the end of the FRP laminates to the support of the span	G_a	shear modulus of the adhesive
L	span length	P	support reaction
E_c	modulus of elasticity of concrete	q	uniformly distributed load on the beam
E_p	modulus of elasticity of FRP laminates	I_c	moment of inertia of concrete
b_p	width of FRP laminates	I_p	moment of inertia of FRP laminates
q_s	horizontal shear per length	B_D	interfacial material parameter
τ	interfacial shear stress between concrete and FRP laminates	Q_1	$Q_1 = q E_c I_c / \left(E_c I_c + E_p I_p \right)$
s	total slip between concrete and FRP laminates	Q_2	$Q_2 = q E_p I_p / \left(E_c I_c + E_p I_p \right)$
E_b	slip modulus at FRP laminate-concrete interfaces	P_1	$P_1 = 0.5 Q_1 \left(L - 2a \right)$
τ_m	maximum local bond stress	P_2	$P_2 = 0.5 Q_2 \left(L - 2a \right)$
f_c	concrete compressive strength	$N(x)$	resultant axial force in both the concrete beam and the FRP laminates
s_m	slip corresponding to τ_m	A_c	cross section area of the concrete
n	$n = 3$, constant in bond-slip models	A_p	cross section area of FRP laminates
σ_{ac}	concrete stress due to the axial force	ε_c	concrete axial strain
σ_{ap}	FRP laminates stress due to the axial force	ε_p	FRP laminates axial strain
s'_{1c}	the first derivative of concrete displacement due to the axial force	s_1	slip due to axial force
s'_{1p}	the first derivative of FRP laminates displacement due to the axial force	s_2	slip due to bending
h_p	distance from the centroid of FRP laminates to the neutral axis	v_c	deflection of concrete
h_c	distance from the centroid of concrete to the neutral axis	v_p	deflection of FRP laminates
v'_c	slope angle of concrete	M_c	concrete moment due to bending

υ_p'	slope angle of FRP laminates	M_p	FRP laminates moment due to bending
N_c	axial force acting at the centroid of concrete	V_c	transverse shear force acting on the cross section of concrete
N_p	axial force acting at the centroid of FRP laminates	V_p	transverse shear force acting on the cross section of FRP laminates
M_{ex}	external moment	e	$e = h_p + h_c$
ξ	$\xi = \frac{A_c E_c}{b_p\left(1+\frac{A_c E_c}{A_p E_p}\right)} = \frac{A_p E_p}{b_p\left(1+\frac{A_p E_p}{A_c E_c}\right)}$	K	Shear stiffness
υ_b	deflection from the case (b)	N_s^2	$N_s^2 = \frac{e^2 \xi b_p}{Z_s}$
Z_s	$Z_s = e^2 \xi b_p + E_c I_c$	s_b	slip from the case (b)
τ_b	Shear stress from the case (b)	s_d	slip from the case (d)
τ_d	Shear stress from the case (d)	d_c	depth of the concrete beam
K_n	normal stiffness	k_1	$k_1 = \frac{2E_a}{t_a} = 2K_n$
χ_s	$\chi_s = b_p\left(\frac{E_c I_c + E_p I_p}{E_c I_c E_p I_p}\right)$	ψ_s	$\psi_s = b_p\left(\frac{t_p}{2E_p I_p} - \frac{d_c}{2E_c I_c}\right)$
υ_{cc}	deflection of the concrete from the case (c)	σ_c	normal stress from case (c)
υ_{cp}	deflection of FRP laminates from the case (c)	σ_d	normal stress from case (d)
β	$\beta = \sqrt[4]{\frac{K_n \chi_s}{4}}$	λ_n	the characteristic roots
σ_{d0}	general solution of normal stress from case (d)	σ_{d1}	particular solution of normal stress from case (d)
τ_{max}	maximum interfacial shear stress	σ_{max}	maximum interfacial normal stress

References

[1] Malek AM, Saadatmanesh H, Ehsani MR. Prediction of failure load of R/C beams strengthened with FRP plate due to stress concentration at the plate end. ACI Structural Journal. 1998 Mar 1;95:142-52.

[2] Smith ST, Teng JG. Interfacial stresses in plated beams. Engineering Structures. 2001 Jul 1;23(7):857-71.

[3] Ouezdou MB, Belarbi A, Bae SW. Effective bond length of FRP sheets externally bonded to concrete. International Journal of Concrete Structures and Materials. 2009 Dec;3(2):127-31.

[4] Smith ST, Teng JG. FRP-strengthened RC beams. I: review of debonding strength models. Engineering Structures. 2002 Apr 1;24(4):385-95.

[5] Smith ST, Teng JG. FRP-strengthened RC beams. II: assessment of debonding strength models. Engineering Structures. 2002 Apr 1;24(4):397-417.

[6] Lu XZ, Teng JG, Ye LP, Jiang JJ. Bond–slip models for FRP sheets/plates bonded to concrete. Engineering Structures. 2005 May 1;27(6):920-37.

[7] Teng JG, Yuan H, Chen JF. FRP-to-concrete interfaces between two adjacent cracks: Theoretical model for debonding failure. International Journal of Solids and Structures. 2006 Sep 1;43(18-19):5750-78.

[8] Biscaia HC, Chastre C, Silva MA. Linear and nonlinear analysis of bond-slip models for interfaces between FRP composites and concrete. Composites Part B: Engineering. 2013 Feb 1;45(1):1554-68.

[9] Vilnay O. The analysis of reinforced concrete beams strengthened by epoxy bonded steel plates. International Journal of Cement Composites and Lightweight Concrete. 1988 May 1;10(2):73-8.

[10] Zhang L, Teng JG. Simple general solution for interfacial stresses in plated beams. Journal of Composites for Construction. 2010 Feb 3;14(4):434-42.

[11] Roberts TM. Approximate analysis of shear and normal stress concentrates in the adhesive layer of Plated RC Beams. The Structural Engineer. 1989;67:222-33.

[12] Roberts TM, Hajikazemi H. Theoretical study of the behavior of reinforced concrete beams strengthened by externally bonded steel plates. Proceedings of the Institution of Civil Engineers. 1989 Mar;87(1):39-55.

[13] Täljsten B. Strengthening of beams by plate bonding. Journal of Materials in Civil Engineering. 1997 Nov;9(4):206-12.

[14] Arduini M, Nanni A. Parametric study of beams with externally bonded FRP reinforcement. ACI Structural Journal. 1997 Sep 1;94(5):493-501.

[15] Tounsi A, Benyoucef S. Interfacial stresses in externally FRP-plated concrete beams. International Journal of Adhesion and Adhesives. 2007 Apr 1;27(3):207-15.

[16] Sha X, Davidson JS. Analysis of transfer length for prestressed FRP tendons in pretensioned concrete using composite beam theory. Composite Structures. 2019 Jan 15;208:665-77.

[17] Granholm H. On composite beams and columns with particular regard to nailed timber structures. Chalmer Technical University. 1949.

[18] Newmark NM, Siess CP, Viest IM. Test and analysis of composite beams with incomplete interaction. Proceedings of Society for Experimental Stress Analysis. 1951;9(1):75-92.

[19] Girhammar UA, Gopu VK. Composite beam-columns with interlayer slip—exact analysis. Journal of Structural Engineering. 1993 Apr;119(4):1265-82.

[20] Foraboschi P. Analytical solution of two-layer beam taking into account nonlinear interlayer slip. Journal of Engineering Mechanics. 2009 Mar 19;135(10):1129-46.

[21] Bai F, Davidson JS. Analysis of partially composite foam insulated concrete sandwich structures. Engineering Structures. 2015 May 15;91:197-209.

[22] Bai F, Davidson JS. Theory for composite sandwich structures with unsymmetrical wythes and transverse interaction. Engineering Structures. 2016 Jun 1;116:178-91.

[23] Lee YJ, Boothby TE, Bakis CE, Nanni A. Slip modulus of FRP sheets bonded to concrete. Journal of Composites for Construction. 1999 Nov;3(4):161-7.

[24] De Lorenzis L, Miller B, Nanni A. Bond of FRP laminates to concrete. ACI Materials Journal. 2001 May;98(3):256-64.

[25] Nakaba K, Kanakubo T, Furuta T, Yoshizawa H. Bond behavior between fiber-reinforced polymer laminates and concrete. ACI Structural Journal. 2001 May 1;98(3):359-67.

[26] Dai J, Ueda T, Sato Y. Development of the nonlinear bond stress–slip model of fiber reinforced plastics sheet–concrete interfaces with a simple method. Journal of Composites for Construction. 2005 Feb;9(1):52-62.

[27] Lu XZ, Teng JG, Ye LP, Jiang JJ. Bond–slip models for FRP sheets/plates bonded to concrete. Engineering Structures. 2005 May 1;27(6):920-37.

[28] Lu XZ, Ye LP, Teng JG, Jiang JJ. Meso-scale finite element model for FRP sheets/plates bonded to concrete. Engineering Structures. 2005 Mar 1;27(4):564-75.

[29] Guo ZG, Cao SY, Sun WM, Lin XY. Experimental study on bond stress-slip behaviour between FRP sheets and concrete. In: FRP in Construction, Proceedings of the International Symposium on Bond Behaviour of FRP in Structures; 2005 Dec; 77-84.

[30] Ko H, Matthys S, Palmieri A, Sato Y. Development of a simplified bond stress–slip model for bonded FRP–concrete interfaces. Construction and Building Materials. 2014 Oct 15;68:142-57.

[31] Popovics S. A numerical approach to the complete stress-strain curve of concrete. Cement and Concrete Research. 1973 Sep 1;3(5):583-99.

[32] Taerwe L, Matthys S. Fib Model Code for Concrete Structures 2010.

[33] Ferracuti B, Savoia MA, Mazzotti C. Interface law for FRP–concrete delamination. Composite Structures. 2007 Oct 1;80(4):523-31.

[34] Bizindavyi L, Neale KW. Transfer lengths and bond strengths for composites bonded to concrete. Journal of Composites for Construction. 1999 Nov;3(4):153-60.

[35] Bilotta A, Ceroni F, Di Ludovico M, Nigro E, Pecce M, Manfredi G. Bond efficiency of EBR and NSM FRP systems for strengthening concrete members. Journal of Composites for Construction. 2011 Jan 13;15(5):757-72.

[36] Dehghani E, Daneshjoo F, Aghakouchak AA, Khaji N. A new bond-slip model for adhesive in CFRP–steel composite systems. Engineering Structures. 2012 Jan 1;34:447-54.

[37] Yuan H, Teng JG, Seracino R, Wu ZS, Yao J. Full-range behavior of FRP-to-concrete bonded joints. Engineering Structures. 2004 Apr 1;26(5):553-65.

[38] Fawzia S, Zhao XL, Al-Mahaidi R, Rizkalla S. Bond characteristics between CFRP and steel plates in double strap joints. The International Journal of Advanced Steel Construction. 2005;1(2):17-27.

[39] Bakis CE, Ganjehlou A, Kachlakev DI, Schupack M, Balaguru P, Gee DJ, Karbhari VM, Scott DW, Ballinger CA, Gentry TR, Kliger HS. Guide for the Design and Construction of Externally Bonded FRP Systems for Strengthening Concrete Structures. Reported by ACI Committee. 2002;440(2002).

[40] Pellegrino C, Tinazzi D, Modena C. Experimental study on bond behavior between concrete and FRP reinforcement. Journal of Composites for Construction. 2008 Apr;12(2):180-9.

[41] Grant JA, Fisher JW, Slutter RG. Composite beams with formed steel deck. Engineering Journal. 1977 Mar;14(1).

[42] Nie J, Cai CS. Steel–concrete composite beams considering shear slip effects. Journal of Structural Engineering. 2003 Apr;129(4):495-506.

[43] Zhang L, Teng JG. Finite element prediction of interfacial stresses in structural members bonded with a thin plate. Engineering Structures. 2010 Feb 1;32(2):459-71.

[44] Mukhopadhyaya P, Swamy N. Interface shear stress: a new design criterion for plate debonding. Journal of Composites for Construction. 2001 Feb;5(1):35-43.

[45] Yang J, Ye J, Niu Z. Simplified solutions for the stress transfer in concrete beams bonded with FRP plates. Engineering structures. 2008 Feb 1;30(2):533-45.

[46] Hein VL, Erdogan F. Stress singularities in a two-material wedge. International Journal of Fracture Mechanics. 1971 Sep 1;7(3):317-30.

Chapter 5 Verification of Composite Beam Theory with Finite Element Model for Pretensioned Concrete Members with Prestressing FRP Tendons

5.1. Introduction

Along with the strikingly rapid development of composite materials in the field of civil engineering, the applications of fiber reinforced polymers (FRPs) on strengthening concrete structures have attracted more and more attention. The applications of FRPs can be divided into the form of FRP tendons as internal reinforcements or FRPs laminates as externally bonded reinforcements. In the previous decades, extensive analytical and experimental studies have been conducted on the local bond-slip relationship of concrete flexural members reinforced by FRP tendons [1-8] or concrete members strengthened by externally bonded FRPs laminates [10-19]. It was found that a sound understanding of the bond behavior between FRPs reinforcement and the concrete substrate played a major role in the development of design guidelines and performance evaluation of FRPs strengthening concrete members. Therefore, a reliable and rigorous analytical model based on the innovative partial composite action, taking into account the corresponding bond characteristics, is essential to accurately assess the mechanical properties of strengthening or retrofitting concrete structures using FRPs. A previously developed method [23] focused on pretensioned concrete members with prestressing FRP tendons. The transfer length was solved by combining the local bond-slip relationship for FRP tendons in concrete with composite beam

theory. In the presented paper, finite element modeling of pretensioned concrete members with prestressing FRP tendons is proposed in order to provide further verification of the developed analytical methodology.

Composite beam theory proposed by Granholm [20] in 1949 and Newmark et al. [21] in 1951 was initially used to solve for the case of nailed timber structures and T-beams consisting of a rolled steel I-beam and a concrete slab, respectively. In terms of partially composite action, the theoretical analysis was developed for the member consisting of two separate elements connected by discrete connectors. Furthermore, the influence of relative displacement between the two elements, i.e. the effect of slip, was fully considered. From this perspective, therefore, composite beam theory is not limited to the types of structures mentioned above but is instead devoted to a wide range of structures comprised of two or more interconnected elements under reasonable assumptions. For example, Bai and Davidson [25] implemented a rigorous analysis of foam insulated concrete sandwich panels in which structural deflection was divided into two components, shear and flexural. The structural behavior was taken into account as partially composite in terms of composite beam theory. Sha and Davidson [9,23] provided closed form solutions using composite beam theory for determining the transfer length of pretensioned concrete members strengthened by FRP tendons as well as predicting the interfacial stress in concrete beams with externally bonded FRPs laminates. Through the research on the developmental course of composite beam theory [21,23,25], it has been observed that theoretical methods were mainly verified against the existing experimental data from the literature. However, in order to comprehensively evaluate the accuracy and reliability of the developed method, as a supplementary verification, finite element analyses (FEA), is an effective methodology that can be employed to compare with theoretical solutions.

As an important numerical technique, FEA has been widely used to study the behavior of prestressed concrete beams [27-29]. Most research has focused on pretensioned concrete members with prestressing steel strands; only a very limited number of FE models are specifically available for pretensioned concrete with prestressing FRP tendons. The main reason for the lack of in-depth FE research in this field is the challenging nature of the interaction between FRP tendons and concrete matrix. Hence, this paper establishes a three-dimensional FE model that simulates prestressing FRP tendons in which the transfer length is determined. In addition, the different friction coefficients between FRP tendons and the surrounding concrete obtained by experimental studies [30] are fully considered to improve the accuracy of FE modeling approaches.

One of the most compelling advantages of FEA over other analytical solutions is that a simulation associated with fewer assumptions may be closer to the corresponding experimental outcomes. Besides, visualizations of the pre- and post-processing of FEA can help engineers easily find vulnerabilities in the design. Despite some obvious advantages, mesh convergence is a critical issue that must be taken into account in the process of developing FE models. In this work, a comparative study is conducted between numerical simulation with fine and coarse meshes to illustrate the effect of mesh density on convergence. Another noteworthy point is that the concrete model used for numerical simulation is based on the linear elastic assumption. Although the concrete damaged plasticity (CDP) model from Abaqus [22] has often been used to simulate the nonlinear behavior of concrete in other studies, the strains associated with the present paper are assumed to be in a range that essentially has a linear and brittle stress-strain relationship in compression. Furthermore, determining the development length in pretensioned members are designed for zero tension in the concrete under service load conditions through Rabbat et al.'s [26] tests. The main focus of this study is to determine the transfer length at the serviceability state

level in which concrete has not yet cracked, and therefore it is reasonable to assume that the concrete is within the linear-elastic range.

In this paper, the general approach of composite beam theory is summarized specifically for FRPs strengthening concrete members and used to determine the transfer length of prestressing FRP tendons in pretensioned concrete. Taking account of the empirical bond-slip relationship between FRP tendons and concrete matrix, governing differential equations are derived in terms of the equilibrium of axial force acting on each element as well as the balance of the overall bending moment. Using the FEA commercial software Abaqus [22], a comparison of numerical results with those obtained by using composite beam theory is conducted. The present FE model has been established with consideration of the friction coefficient from the experimental study on the FRP tendons and prestressed concrete members. Additionally, different mesh densities are compared for the convergence analysis. As a result, a satisfactory agreement has been reached between the theoretical solutions and FEA responses, which further demonstrates the feasibility and effectiveness of the developed composite beam theory.

5.2 Background of the bond mechanism

Understanding the nature of bond behavior plays a critical role in assessing how the prestress force is transferred from the prestressing FRP tendons to the concrete. A large amount of research [27,29,31,32] indicates that the chemical adhesion, friction, and mechanical interlocking could explain the interaction between prestressing tendons and concrete. Chemical adhesion only affect the bond strength in the minimal slip range. With the increase of slip, friction and mechanical interlocking play a role in the bond strength when the adhesive bond gradually

decreases. For prestressed tendons with rough surface, such as seven-wire strands, ribbed bars, and deformed rebars, the mechanical action of the helical outer wire of a strand bearing against the surrounding concrete matrix is referred to as mechanical interlocking. It should be noted, however, although the contribution of mechanical interlocking to bond strength is important, it is still not the key factor. This is because the rough surface of surrounding concrete that is in contact with prestressing tendons will eventually be sheared off due to the mechanical interlock action if the pretensioned structure has sufficient confinement. However, that does not seem to be occurring [32]. In other words, this would imply that friction known as the "wedge effect" dominates the interaction between prestressed tendons and concrete.

Friction can be defined as a relationship that is responsible for transmitting the shear and normal forces between contacting bodies, i.e., prestressing tendons and the surrounding concrete matrix. According to the commercial FE program Abaqus [22], friction behavior is generally analyzed using the base form of the Coulomb friction model in which the critical shear stress is given by the following expression:

$$\tau_{crit} = \mu\, p \tag{1}$$

where τ_{crit} is the critical shear stress, p is the contact pressure, and μ is the friction coefficient. In the Coulomb friction model shown in Fig. 5.1, shear stresses between two contacting surfaces, $\tau \le \mu\, p$ is the case in which the two contacting bodies are in a state of sticking before sliding occurs and $\tau > \mu\, p$ is when shear stresses exceed a certain magnitude defined as the critical shear stress τ_{crit}, which refers to the transition from sticking to slipping along the interface of contacting bodies. The slope of the function, the friction coefficient μ, is in the range of 0.3 to 0.7 according to most research literature [28,32]. However AASHTO [34] reports that the value of friction

coefficient μ from a modified shear-friction model increases from approximately 0.6 to 1.4, depending on the concrete surface conditions and the shape of the reinforcement. Thus it can be seen that some inconsistencies exist among the specification and literature used to explain the bond behavior between concrete members and the reinforcement, which directly affects the reliability of the analysis results based on the value of friction coefficient.

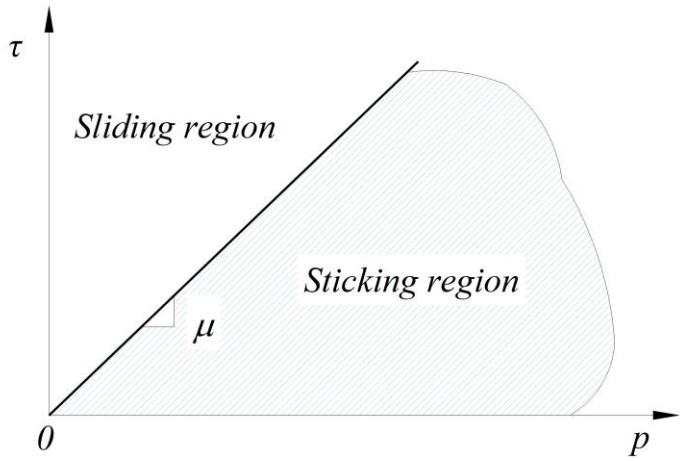

Fig. 5.1 Coulomb friction model [22]

It is worth mentioning that the current work using FEM to estimate the transfer length is based on the friction coefficient specifically for FRP tendons in pretensioned prestressed concrete members. Previous studies on finite element analysis [27-29] of pretensioned concrete members used the value of friction coefficient recommended by the specification to address the bond behavior, which is suitable for steel reinforcement as a prestressed strand. However, when FRP tendons are considered, it is necessary to redefine the friction coefficient through the available experimental data. Khin et al. [30] carried out pull-out tests of Vinylon and Carbon FRP tendons with cement mortar and confined by highly expansive material (HEM). During the test, the bond stress versus confining pressure for specimens was recorded using high precision pressure transducers to determine the friction coefficient of FRP tendons from the slope of curve. These

values from Khin et al. [30] are listed in Table 5.1 and used as the friction coefficient in the presented FE model.

Table 5.1 Friction coefficient used for FRP tendons [30]

FRP tendons	Concrete	Friction coefficient
Vinylon FRP rods	HEM	0.23
Carbon FRP strands	HEM	0.30
Vinylon FRP rods	HEM and mortar	0.20
Carbon FRP strands	HEM and mortar	0.19

For another description of the bond behavior model, the local bond stress-slip relationship $\tau = \tau(s)$ was used in the analytical model [23] developed by using composite beam theory for determining the transfer length for FRP tendons in prestressed concrete. The results of pullout tests [1-4,6,8] show that the local bond stress as a function of slip depends on a variety of factors, including concrete strength, the roughness of reinforcement surface, concrete cover, bar diameter, and epoxy resin properties. Over the years, numerous existing models of the bond stress τ and slip s have been proposed to evaluate the bond performance that is established on the basis of nonlinear local bond stress-slip relationship $\tau = \tau(s)$ between concrete and the reinforcement. Three well-known models have been developed for steel and FRP tendons, namely the Bertero-Eligehausen-Popov (BEP) model [1], the modified Bertero-Eligehausen-Popov (mBEP) model and the Cosenza-Manfredi-Realfonzo (CMR) model [6]. The BEP model is defined by Eq. (2), which is adopted in CEB-FIP Model Code 90 [2]:

$$\tau = \tau_0 \left(\frac{s}{s_0} \right)^{\alpha} \tag{2}$$

where τ_0 is the maximum shear stress, s_0 is the slip corresponding to τ_0, and α is the coefficient of 0.4 that is available for the case of steel [2]. Considering different requirements in the engineering analysis process, the mBEP and CMR expressions were proposed as the bond stress-slip alternative analytical models given by the following Eq. (3) and Eq. (4), respectively.

$$\tau = C\, s^{\alpha}\left(1-\frac{s}{\bar{s}}\right) \tag{3}$$

$$\tau = \tau_m\left[1-\exp\left(-\frac{s}{s_r}\right)\right]^{\beta} \tag{4}$$

For the mBEP model, τ_0 is rewritten by C and assuming $s_0 = 1mm$ from the BEP expression, $\bar{s}$ is the slip related to $\tau = 0$. The expression of CMR, τ_m is the peak bond stress, and unknown parameters s_r, β are determined by the curve fitting of experimental data. More detailed reviews of these analytical models for the curve $\tau - s$ can be found in the literature [1,6,8,23]. In previous work by Sha and Davidson [23], the BEP expression with calibrated parameters of C and α from Focacci et al. [8] was used as the constitutive bond-slip definition between the FRP tendons and concrete, as illustrated in Fig. 5.2. The latter two models, i.e., the mBEP and CMR expressions are equivalent to the BEP expression in the case of structural analyses in which the slip is sufficiently small.

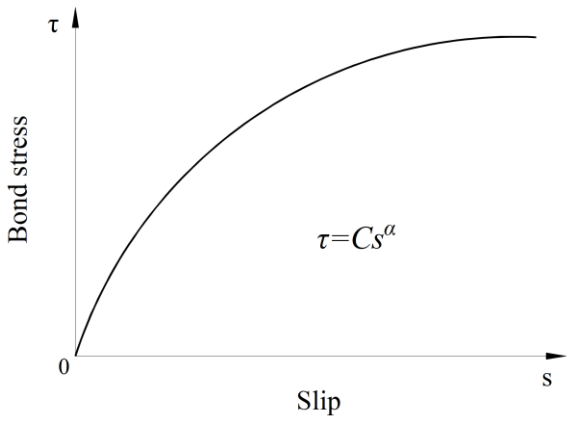

Fig. 5.2 BEP model of bond-slip relationship [8]

Thick-wall cylinder theory [28] depends on the Coulomb friction model to perform the analysis on prestress transfer in pretensioned concrete members. The concrete is conceived as a hollow cylinder in which the inner diameter is equal to that of prestressed tendons and the outer diameter is the distance across the short side (diameter) of the component. Accordingly, the estimation of bond behavior relies on the radial compressive stress as well as deformation compatibility conditions of the interface between prestressed tendons and the surrounding concrete. Based on extensive experimental and analytical investigations [4,6,35], many researchers nevertheless point out that the confinement pressure has a small effect on the bond strength between reinforcement (steel or FRP) and surrounding concrete for the situation in which deformed rebar with spiral shape surface is used as reinforcement. However the bond resistance strongly depends on the confined stress known as radial compressive stress in other cases such as smooth rods. Different from the thick-wall cylinder theory, the nonlinear bond stress-slip relationship is taken into account for deriving the governing differential equations using composite beam theory developed herein for analyzing the behavior of pretensioned concrete members with prestressing FRP tendons. Consequently, in addition to further verifying the previous work of

predicting transfer length for prestressing FRP tendons by means of the developed FE model, the second aim of the current study is to prove the superiority of composite beam theory considering the slip effect through the comparative studies between the analytical and numerical results.

5.3 Analytical solution for FRPs strengthening concrete members

5.3.1 General approach of composite beam theory

The following assumptions and limitations are specifically proposed for FRPs strengthening concrete members using the general approach of composite beam theory:

(1) Linear elastic constitutive behavior and small displacement are applied to each component in the developed analytical models.

(2) FRPs' bending resistance is negligible compared to that provided by the concrete member.

(3) Slender beams are considered and therefore Euler-Bernoulli beam theory can be applied to each component of a composite structure and therefore the shear deformation is neglected through the cross section of the concrete beam and FRP components, respectively.

5.3.1.1 Axial force equilibrium

A differential element of the composite beam is composed of the concrete and FRPs, as illustrated in Figure 5.3; the upper part represents concrete and the lower part is FRPs. Axial forces acting on the cross sections of two separate infinitesimal elements are transmitted as the internal

forces through bond stress τ that is a function of slip. As a result, equilibrium can be established in the Eq. (5):

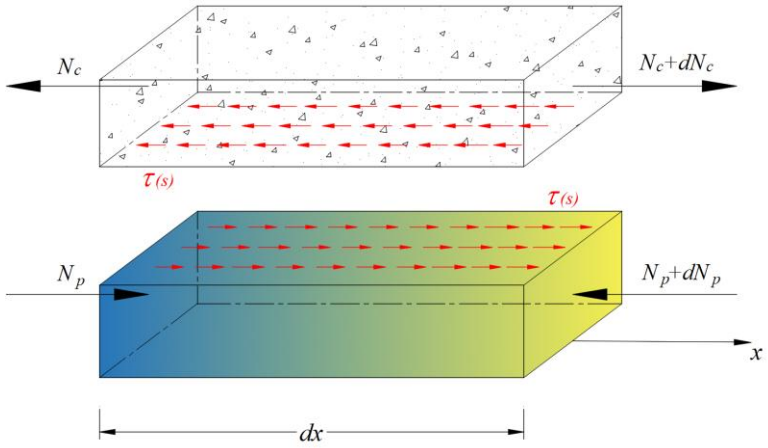

Fig. 5.3 Differential element of the composite beam

$$\tau C\, dx = dN_c = dN_p \tag{5}$$

in which N_c and N_p denote the resultant axial force acting on the cross section of the concrete and FRPs, respectively, and C represents the contact edge distance of the interface between FRPs and the surrounding concrete in the transverse direction. For example, C can be used to refer to the total circumferences of FRP tendons in prestressed concrete members. In the case of a concrete beam strengthened by externally bonded FRP laminates, it is the width of FRP laminates. Substituting $N_c = \sigma_c A_c$ and $N_p = \sigma_p A_p$ into Eq. 5 results in:

$$\tau C = \left(A_c \sigma_c\right)' = \left(A_p \sigma_p\right)' \tag{6}$$

in which A_c is the cross section area of concrete, σ_c is the concrete stress due to axial force, A_p is the cross section area of FRPs, and σ_p is the FRPs stress due to axial force. Accordingly, $\sigma = E\,\varepsilon$ applies to both the concrete and FRPs elements due to the assumption of the linear elastic constitutive behavior. Since the slip is a relative motion, the sign convention of axial force are not considered in the equation. Eq. (6) then becomes:

$$\tau C = A_c\, E_c\, \varepsilon_c' = A_c\, E_c\, s_c'' \tag{7a}$$

$$\tau C = A_p\, E_p\, \varepsilon_p' = A_p\, E_p\, s_p'' \tag{7b}$$

where E_c and E_p refer to the modulus of elasticity of the concrete and FRPs, respectively. Since s_c' is the first derivative of the concrete displacement due to the axial force, the concrete axial strain $\varepsilon_c = s_c'$. Similarly, $\varepsilon_p = s_p'$ corresponds to FRP strains.

As mentioned above, the analysis of the behavior of FRPs strengthening concrete members is based on partial composite action. To some extent this means that relative movement between FRPs and the surrounding concrete, namely slip s, is permitted.

$$s = s_1 + s_2 + s_3 \tag{8}$$

$$s_2 = s_c + s_p \tag{9}$$

Thus, Eq. (8) indicates that the slip s can be divided into three components: the slip s_1 due to bending illustrated later, the relative displacement s_2 between the concrete and FRPs due to the axial force as expressed by Eq. (9), and the slip $s_3 = \int \varepsilon_{is}\, dx$ resulting from prestressing tendon

retraction, where ε_{is} is the strain caused by prestress before transmission. For the case of a concrete beam strengthened by externally bonded FRP laminates, $s_3 = 0$.

In terms of the $\tau = \tau(s)$ relationship obtained by experimental studies on FRPs reinforcement in concrete, combining with Eq. (9), the new equilibriums are established by Eq. (10a) and Eq. (10b):

$$\tau(s) C = A_c E_c \frac{s_2''}{\left(1 + \frac{A_c E_c}{A_p E_p}\right)} \tag{10a}$$

$$\tau(s) C = A_p E_p \frac{s_2''}{\left(1 + \frac{A_p E_p}{A_c E_c}\right)} \tag{10b}$$

As a result, the governing equation relevant to the axial force is generated in the form:

$$\tau(s) = \zeta s_2'' \tag{11}$$

in which $\zeta = \frac{A_c E_c A_p E_p}{C\left(A_c E_c + A_p E_p\right)}$.

5.3.1.2 Bending moment equilibrium

The known external moment M_{ex} is balanced by the internal moment and axial force acting on the cross section of each element, as expressed in the following:

$$M_{ex} = M_c + M_p + N_c h_c + N_p h_p \tag{12}$$

where the internal bending moment $M_c = -E_c I_c \upsilon_c''$ in the concrete beam with the second derivative of the deflection υ_c'' and the moment of inertia I_c. Bending resistance from the FRP component is ignored, $M_p = 0$. Combining Eq. (7a) and Eq. (7b), the internal axial forces in the concrete and FRPs are given by:

$$N_c = N_p = \zeta C s_2' \tag{13}$$

As demonstrated in Fig. 5.4, h_c is the distance from the concrete beam centroid to the neutral axis, and similarly, h_p corresponds to FRPs. Furthermore, it can be observed that the slip s_1 is associated with the neutral axis and the slope angle of each part when the bending moment is occurring. The slip s_1 can be written in the general form:

$$s_1 = h_c \upsilon_c' + h_p \upsilon_p' \tag{14}$$

where υ_c' denotes the slope angle of concrete, υ_p' relevant to that of FRPs. Considering that concrete flexural members reinforced by FRP tendons, the slip s_1, in this case, can be expressed as follows:

$$s_1 = e\upsilon' \tag{15}$$

The reason for this change is that the structural behavior is limited to elastic and small displacement, the constitutive relation is assumed to be linear, and each component of the composite beam has the same deflection $\upsilon_c = \upsilon_p = \upsilon$. In the meantime, it will be readily understood that the eccentricity is equal to the distance from the neutral axis of the concrete beam to the FRPs', i.e. $e = h_c + h_p$.

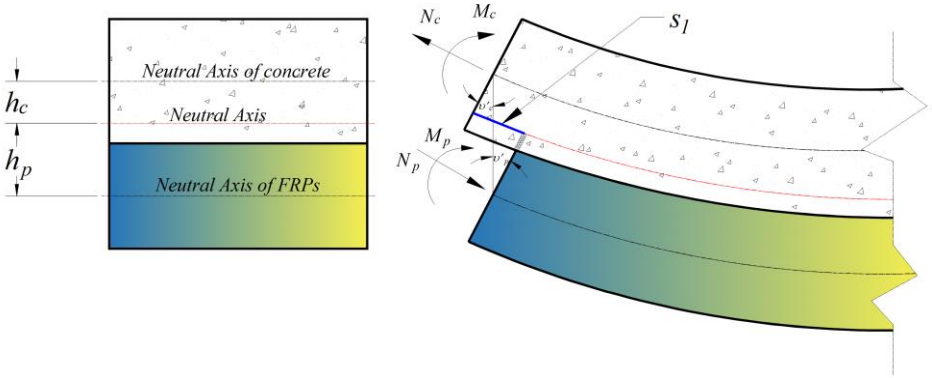

Fig. 5.4 The slip s_1 due to bending moment

Substituting Eq. (13) into Eq. (12), results in the expression for bending moment as follows:

$$M_{ex} = -E_c I_c \upsilon_c'' + \zeta C s_2' \left(h_c + h_p\right) \tag{16}$$

Consequently, plugging $s_2 = s - s_1 - s_3$ into the differential equation Eq. (11) and Eq. (16) and simplifying, the set of governing equations that are specifically developed for FRPs strengthening concrete members using composite beam theory can be given by:

$$\begin{cases} s'' - \dfrac{\tau(s)}{\zeta} = h_c \upsilon_c''' + h_p \upsilon_p''' \\ \dfrac{\upsilon_c''}{\alpha_s} + h_p \upsilon_p'' - s' = -\dfrac{M_{ex}}{D_s} - \varepsilon_{is} \end{cases} \tag{17}$$

in which the new symbols are introduced for simplicity:

$$D_s = \zeta C (h_c + h_p) \tag{18}$$

$$\alpha_s = \frac{D_s}{E_c I_c + D_s h_c} \tag{19}$$

According to the general form of governing equations Eq. (17), it can be observed that the bond-slip relationship $\tau = \tau(s)$ corresponding to various forms FRPs strengthening concrete structures would be taken into account. For the application of prestressed concrete with FRP tendons, the governing equations can be generated by combining the relationship of bond-slip, i.e., $\tau(s) = 8.847\, s^{0.337}$ [8], in metric (SI) units:

$$\begin{cases} s'' - \dfrac{8.847}{\zeta} s^{0.337} = e\upsilon''' \\ \upsilon'' - \dfrac{T_s^{\,2}}{e} s' = -\dfrac{M_{ex}}{K_s} - \dfrac{T_s^{\,2}}{e} \varepsilon_{is} \end{cases} \tag{20}$$

where

$$K_s = E_c\, I_c + e^2\, \zeta\, C \tag{21}$$

$$T_s^2 = \frac{e^2\, \zeta\, C}{K_s} \tag{22}$$

5.3.2 Predictions of transfer length for prestressed FRP tendons application

It is critical to estimate the transfer length of prestressed concrete beams, not only because it affects the bending and shear strength of the structure, but also it is valuable for designers to understand it for structural detailing. The effective prestressing force is transferred from the prestressed tendons to the concrete in the transfer zone, in which the distance is related to the transfer length. The conventional experimental investigation used to measure the transfer length mainly depends on the strain change in the concrete or the prestressed tendons before and after release. The determination of transfer length is implemented in terms of the strain distribution

along the length of the beam using the 95% Average Maximum Strain (AMS) method. For the analytical solution, the proposed model relied upon a novel and theoretically pure composite beam theory developed specifically for pretensioned prestressed concrete members with FRP tendons, the details of which were provided in the previous work [23]. Based on the boundary condition of a simply supported beam without any external loading as shown in Fig. 5.5, correspondingly, the closed form solution with $\alpha = 0.337$ for the governing equation Eq. (20) is given by the following, in metric (SI) units:

$$s(x) = \begin{cases} 0, & 0 \le x \le L/2 - L_t \\ A(x - L/2 + L_t)^B, & otherwise \end{cases} \tag{23}$$

in which

$$L_t = \left[\frac{\varepsilon_{is} (1+\alpha)(0.5\varepsilon_{is})^{-\alpha}}{\psi (1-\alpha)^{1+\alpha}} \right]^{\frac{1}{1+\alpha}} \tag{24}$$

$$A = e^{\frac{\ln \frac{2(1+\alpha)}{\psi(\alpha-1)^2}}{\alpha-1}} \tag{25}$$

$$B = \frac{2}{1-\alpha} \tag{26}$$

$$\psi = \frac{8.847}{\zeta (1 - T_s^2)} \tag{27}$$

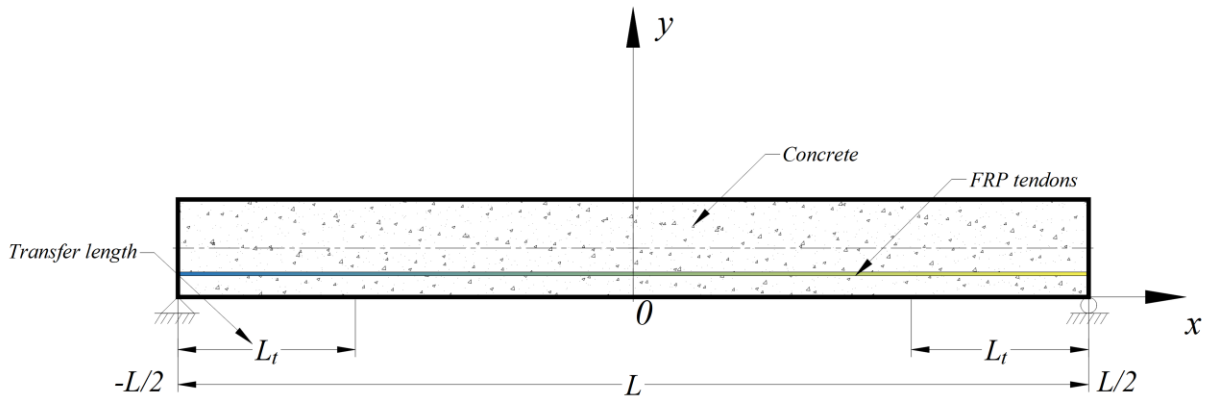

Fig. 5.5 The coordinate system of the pretensioned concrete with prestressed FRP tendons

Transfer length L_t expressed by Eq. (24) is derived by taking advantage of the type of piecewise function for the slip s (Eq. (23)), considering the local bond-slip relationship [8] resulting from the average behavior of FRP tendons with diameters of 6.4 mm, 9.5 mm, 12.7 mm and 15.9 mm. Previously, it has been validated through the comparison between the prediction of strain profile and the available experimental data from literature.

5.4 Numerical implementation with finite element modeling

5.4.1 Finite element modeling of pretensioned RC beams with FRP tendons

Experimental studies on the transmission of prestressing force conducted by Nanni et al. [36] are utilized herein to develop a FE model using the commercial software Abaqus [22]. As a result, the strain profiles are provided for the determination of transfer length and further verified the general approach of composite beam theory. The specimen is a simply supported beam with the span of $4000\,mm$ and the rectangular cross-section of $210\,mm \times 120\,mm$. The pretensioned concrete beam prestressed with a single AFRP tendon is modeled using two levels of 50% and

100% initial prestress force. In order to simulate the prestressing process, the prestress of $698\,MPa$ and $349\,MPa$ are applied to the prestressing tendon in the initial step, respectively. Taking advantage of double-symmetry conditions, a quarter of pretensioned RC beams with FRP tendons modeled in the simulation is given as shown in Fig. 5.6. As explained in the previous section, both concrete and FRP tendons are modeled as linear elastic, isotropic materials with parameters reported in Table 5.2.

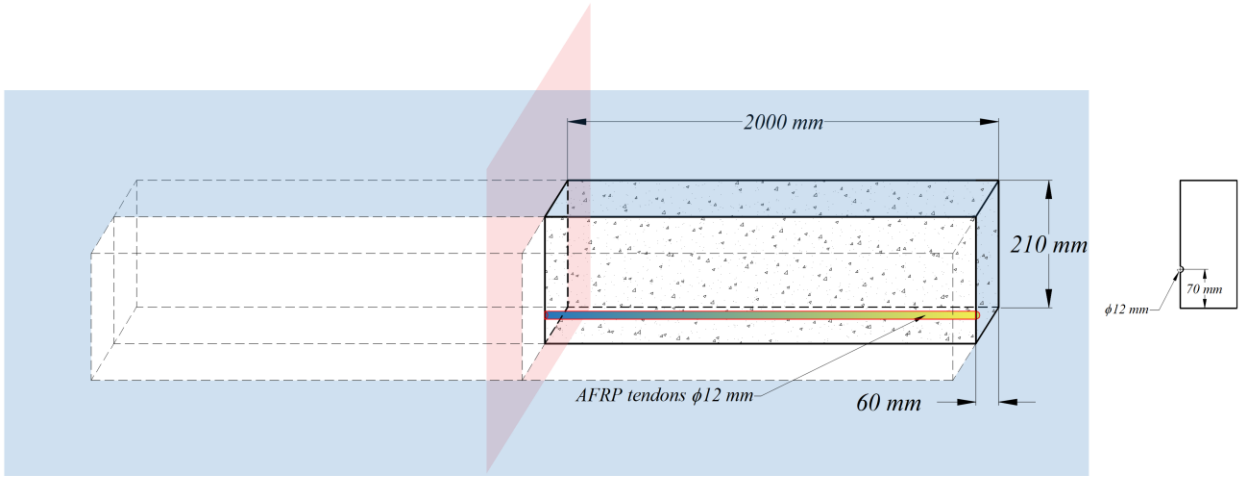

Fig. 5.6 Geometric details of 1/4 of the beam using double-symmetry conditions in Abaqus

Table 5.2 Material parameters [36] used for FE simulation

Part	Modulus of elasticity (MPa)	Poisson's ratio	Density (tonne/mm^3)
Concrete	25000	0.2	2.4e-9
AFRP tendons	67600	0.35	1.4e-9

C3D8R with 8-node linear brick is employed for modeling the concrete in Abaqus, which is a reduced integration element with hourglass control. The C3D6 element, which is a 6-node linear triangular prism, is used for the FRP tendons. The geometry of these two elements are illustrated by Fig. 5.7.

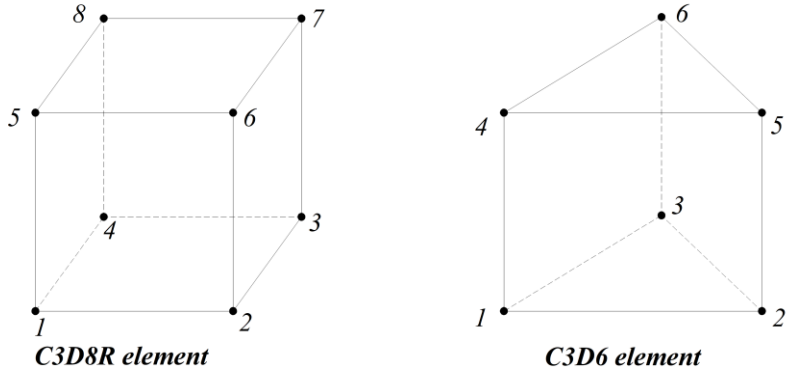

Fig. 5.7 Geometric characteristics of elements used for concrete and FRP tendons

In order to optimize computing time and results precision, the mesh around the FRP tendons is very refined and the mesh density increases as the distance from the midspan increases. The quarter symmetry FE model of pretensioned concrete beam with boundary conditions is represented in Fig. 5.8. As can be seen, the symmetry restraints on the Y-Z and X-Y symmetry planes are U1=UR2=UR3=0 and U3=UR1=UR2=0, respectively. Meanwhile, a support condition of UY = 0 is applied to the end of the beam.

The interaction between the concrete and FRP tendons modeled by FE consists of three parts: tangential behavior, normal behavior, and cohesive behavior. According to the concept of Coulomb friction model as previously described, the tangential behavior between two contacting surfaces is defined in accordance with four different friction coefficients μ listed in Table 1 from Khin et al. [30]. The reason for this is to explain variable bond stress along the beam in the region

of transfer length. Normal behavior is modeled using “hard” contact as the contact pressure-overclosure relationship, which prevents penetration of the concrete into FRP tendons in the FE simulation of bond behavior. Another consideration is to prevent transmission of tensile stress through the interface between the FRP tendons and concrete. Cohesive behavior adopted in the present FEA is due to the slip at the interface. At the same time, by defining initial values of predefined field variables in Abaqus, the initial stress is applied to the FRP tendon as a prestress. Moreover, since the purpose of this research is to predict the transfer length at the serviceability state using FEA and to further verify the previously proposed composite beam theory, creep and shrinkage are not considered.

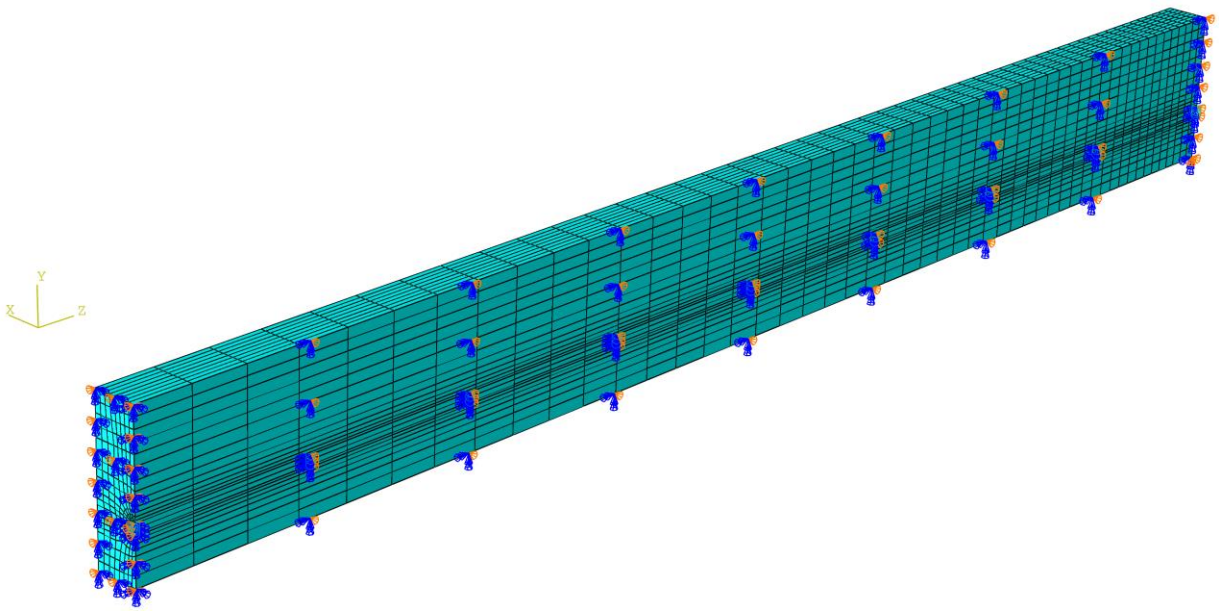

Fig. 5.8 FE model of pretensioned concrete beam with boundary conditions

5.4.2 Convergence analysis and verification of FE model

In order to investigate the dependence of nonlinear solutions obtained from the proposed FE model on the mesh size, two models with different mesh densities are simulated in Abaqus. By means of the solution technique of full Newton and automatic control of the time increment, the mesh convergence study is performed on the three-dimensional FE model of pretensioned concrete beam using coarse mesh and fine mesh, respectively. The cross-sectional and longitudinal views corresponding to both the fine and coarse models are shown in Fig. 5.9. For the coarse mesh shown in Fig. 5.10, the FE model is composed of 10000 hexahedral elements of type C3D8R and 800 wedge elements of type C3D6. A similar meshing method is correspondingly given in the fine model, which is made up of 77500 hexahedral elements for concrete as well as 3200 wedge elements for FRP tendons, as shown in Fig. 5.11. Two models associated with coarse and fine are meshed by defining the number of elements along the selected edges, where the number of elements defined on each edge of the fine model is twice as those applied in the coarse model. As presented in Figs. 5.10 and 5.11, the result has very close agreement with a 1% difference between the maximum von Mises stress that occurs at the midspan of FRP tendons.

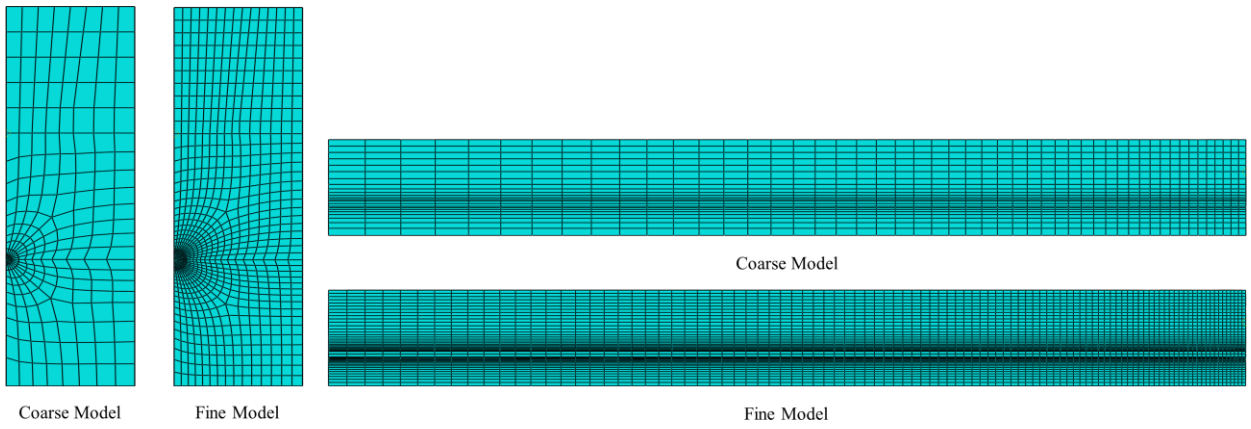

Fig. 5.9 Mesh density for both coarse model and fine model

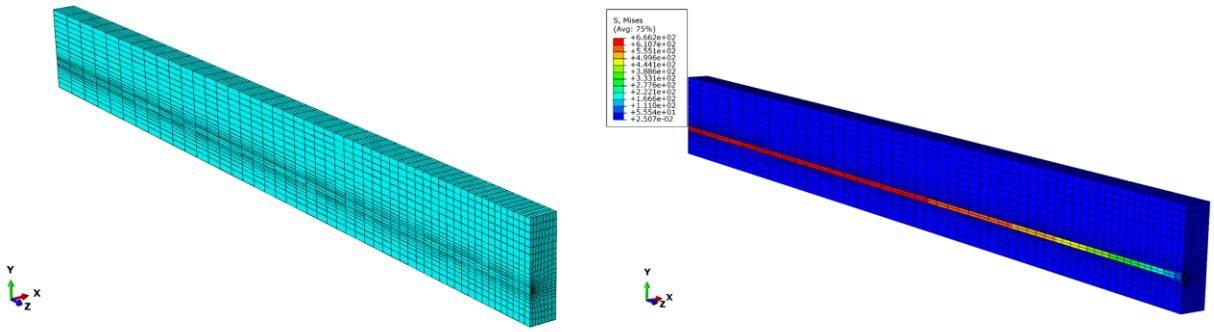

Fig. 5.10 FE model with coarse mesh

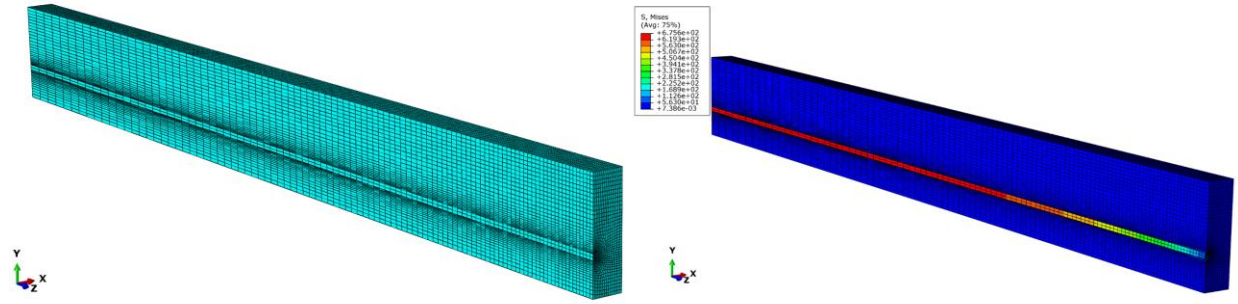

Fig. 5.11 FE model with fine mesh

To further demonstrate the mesh convergency and the feasibility and accuracy of the 3-D FEA solution, a comparison is made between the FE results and the strain profile from the experiment [36]. Fig. 5.12 represents a group of nodes that are located at the position on concrete surface at the level of the FRP tendons within the fine FE model and coarse FE model, which provides the longitudinal strain value along the beam, corresponding to the results recorded in the test. The values predicted by the FE model and experimental results at 100% and 50% of prestress force release are compared in Fig. 5.13 and Fig. 5.14, respectively. As can be seen, there is a reasonable agreement with the strain measurements. Compared to the effective prestress strain of

153 microstrains collected through the test at 100% force release, the fine and coarse FE model approximately overestimate by 4%. Corresponding to the effective prestress strain of 67 microstrains at 50% force release, they are exceeded by approximately 15% to 19%.

Based on 95% AMS method, comparisons of transfer length predicted by the present FE models with measured results [36] are summarized in Table 5.3. It can be clearly observed that the value of transfer length slightly decreases with increase of the friction coefficient in both FE models, especially for the fine mesh model. The difference is due to the stronger bond that will shorten the distance to reach the effective prestress. Moreover, it is shown that the predictions using FE model with fine mesh match experimental results better than those from the coarse mesh model through convergence analysis. The difference between the measured transfer length for high pretension and the fine mesh FE model with friction coefficient $\mu = 0.30$ is 10%. Since the method for determining transfer length during the test is carried out by combining 95% Average Maximum Strain (AMS) method with the measurement of the strain change in the concrete. Inconsistency and preference may exist in evaluation of the strain plateau between different researchers. For another reason, the measured value of transfer length reported in Table 5.3 are the average of multiple test results [36] in which FRP tendons are released at different days. Therefore, though 10% difference between the transfer length predicted by FE model and that from the experiment is not an ideal value, it also can be proved that the feasibility of the present method through reasonable agreements between the measured strain profile with that predicted by FE model. At the same time, it can be noticed that FE model performance are not as good at low pretension level of 50%, the reason will be analyzed and discussed in the later section.

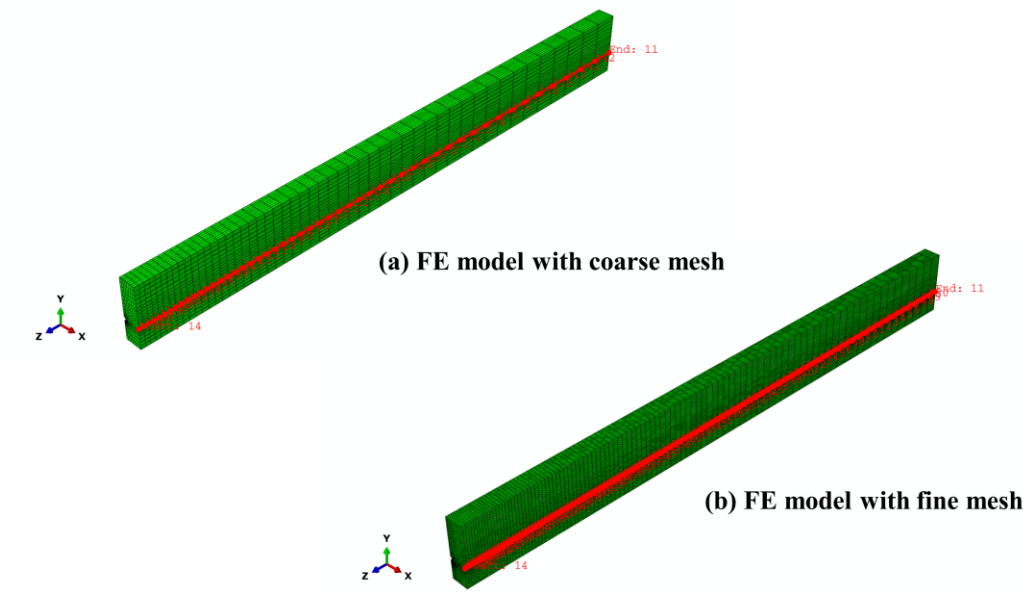

Fig. 5.12 Nodes location on concrete surface at the level of the FRP tendons in the FE models

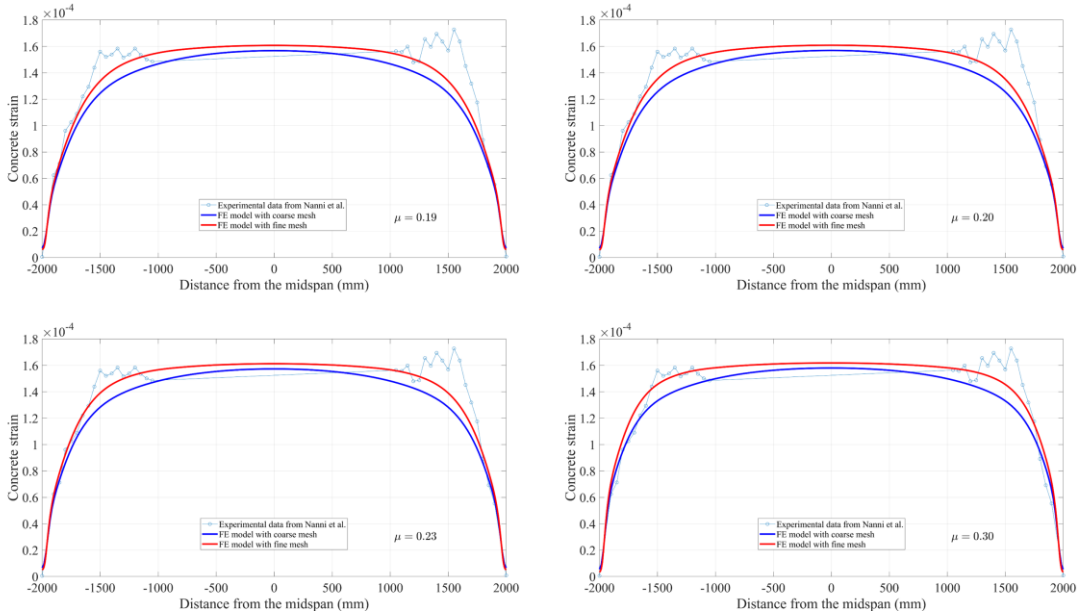

Fig. 5.13 Comparison of the strain profile at 100% release

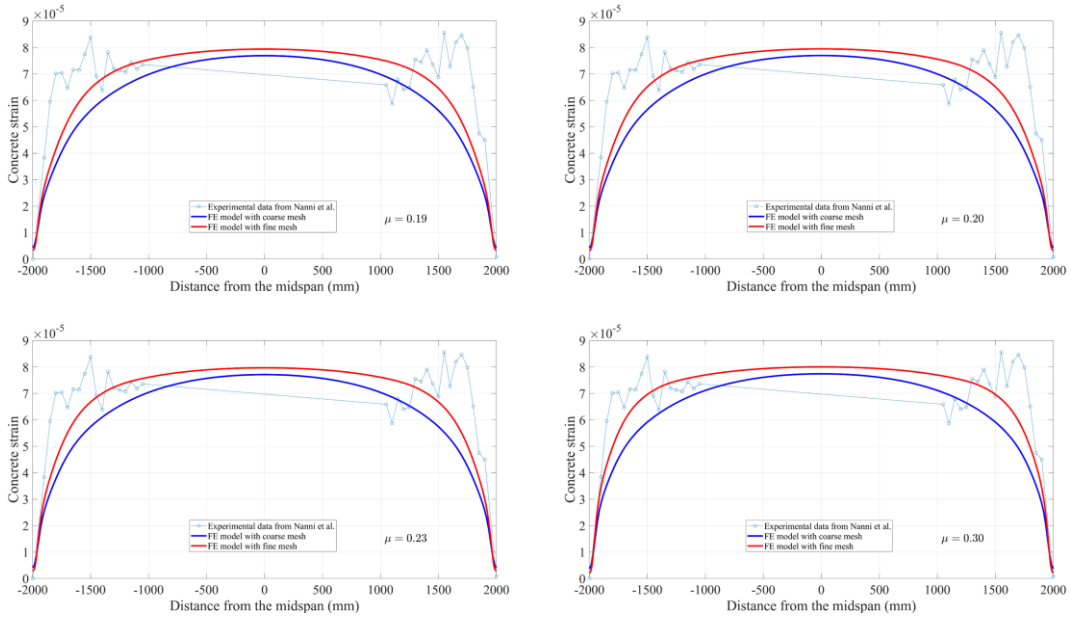

Fig. 5.14 Comparison of the strain profile at 50% release

Table 5.3 Comparison of transfer length between FE simulation and experiment

Beam group	Measured (mm)	Predicted by FE model (mm)				
			$\mu=0.19$	$\mu=0.20$	$\mu=0.23$	$\mu=0.30$
High pretension (100% force release)	450	Fine	670	651	597	496
		Coarse	939	939	893	806
Low pretension (50% force release)	400	Fine	967	943	897	831
		Coarse	1192	1192	1192	1138

5.5 Comparison and discussion

For further proving the performance of the application of composite beam theory on predicting the transfer length for prestressed FRP tendons strengthening pretensioned concrete

members, the present FE model is used to compare with the previously developed analytical solutions. As can be seen from Fig. 5.15, it is worth noting that theoretical results for 50% and 100% release levels are in excellent agreement with those from the experiment compared to the FE model result. In particular, the slope of both curves related to the rate of strain change within transfer zones can be accurately calculated by analytical model using composite beam theory. In the corresponding zones, a small discrepancy exists between FE model for 50% force release and strain profile measurements, in other words, the concrete strain in the transfer zone cannot be accurately calculated by FE model for 50% force release. This is caused by the assumption of the bond mechanism between FRP tendons and concrete in the FE model and meshing sensitivity in the simulation. Although it is common practice to use the Coulomb friction model with friction coefficient to simulate the friction behavior between FRP tendons and concrete, the other two bond components, both of chemical adhesion and mechanical interlocking, are not taken into account. For this reason, a comprehensively understanding and accurate definition of the bond behavior between FRP tendons and concrete is critical to accurately determining the transfer length. This is also the reason why the FE fine model with friction coefficient $\mu = 0.3$ significantly overestimates the values measured in the tests at 50% force release by 107%. In addition, mesh sensitivity as another reason will be discussed in the study of future work.

Since it is impossible to exactly match the values measured from testing, the local bond-slip relationship between FRP tendons and concrete is taken into account to predict the transfer length using closed form solutions from Eq. (24) in the analytical model. This results in error between predictions and test values of 7% and 26% for high pretension (100% force release) and low pretension (50% force release), respectively. In this perspective, the accuracy of the transfer

length obtained from theoretical solution in terms of partially composite action is superior to that of numerical simulation by using Coulomb friction model based on FEA.

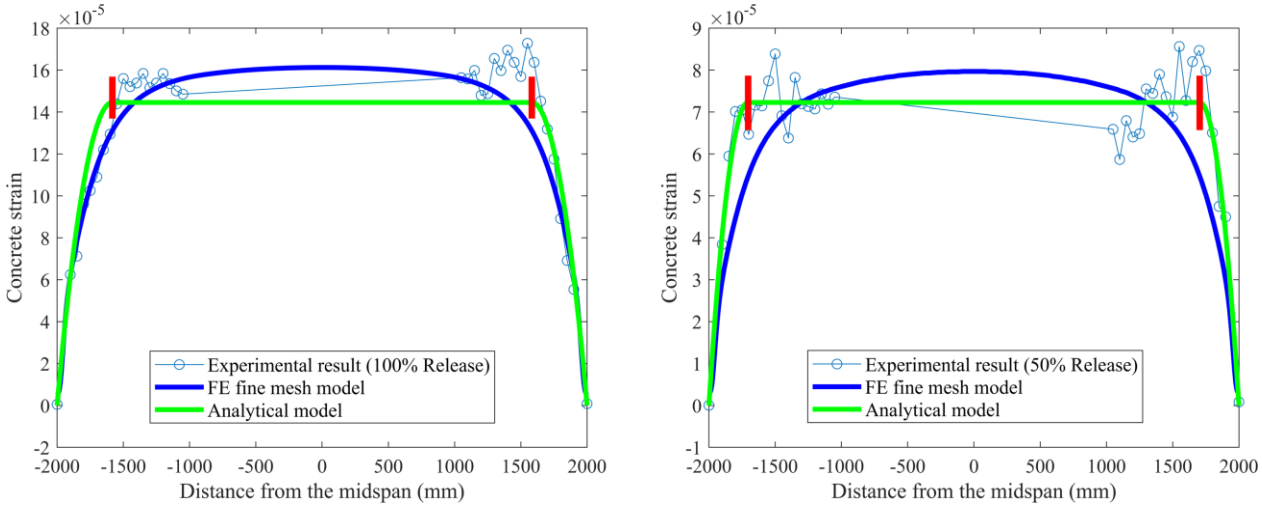

Fig. 5.15 Strain profile predicted by FE model at 100% and 50% release vs. analytical solutions

In addition, extensive studies [25,37] have shown that the influence of interface slip on the mechanical behavior of composite structures cannot be neglected. For this reason, the curves presented in Figs. 5.16 and 5.17 are used to conduct the comparison between the slip predicted by the closed form solution given by Eq. (23) and those from FE models with various friction coefficients. Note that the value predicted by the analytical solution using composite beam theory is smaller than FE model predictions; the main reason is attributed to different bond behavior models that are adopted in theoretical and numerical solutions. The local bond stress-slip relationship $\tau = \tau(s)$ used in the analytical model is based on the experimental investigation from the available literature [8] in which the effects of three factors on bond behavior are comprehensively considered, including chemical adhesion, friction, and mechanical interlocking as mentioned in the previous section. Whereas only friction is modeled as a tangential behavior

associated with the friction coefficient from the pullout test [30] during the process of FE simulation, many studies have confirmed that friction plays a major role in the interaction between FRP tendons and concrete. However, the interface slip can be still reduced by the other two factors, i.e. adhesion and mechanical interlocking. This is also the reason why the prediction values for transfer length from FE models is larger than test results summarized in Table 5.3. To a certain extent, it is further proved that the analytical solution for FRPs strengthening concrete members considering the empirical bond-slip relationship in terms of composite beam theory is reasonable.

On the other hand, it is obvious to see that a remarkable increase in interface slip occurs when the value of friction coefficient decreases as shown in Figs. 5.16 and 5. 17. This is because the bond strength between concrete and FRP tendons is reduced as the decrease of friction coefficient, resulting in the larger slip.

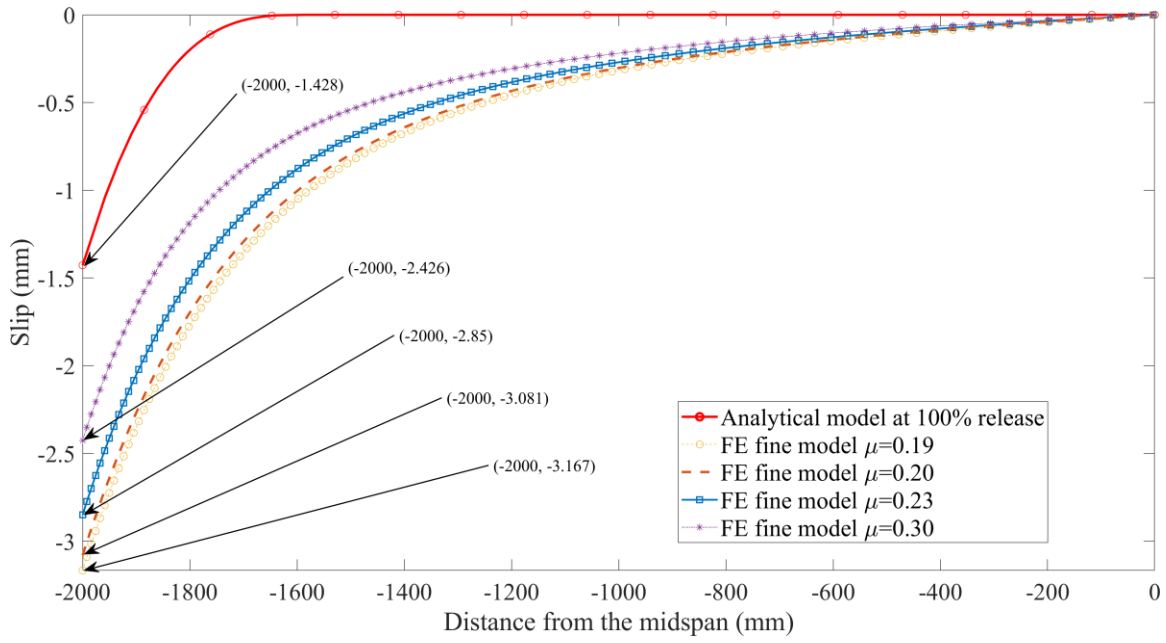

Fig. 5.16 Slip predicted by FE model at 100% release vs. analytical solutions

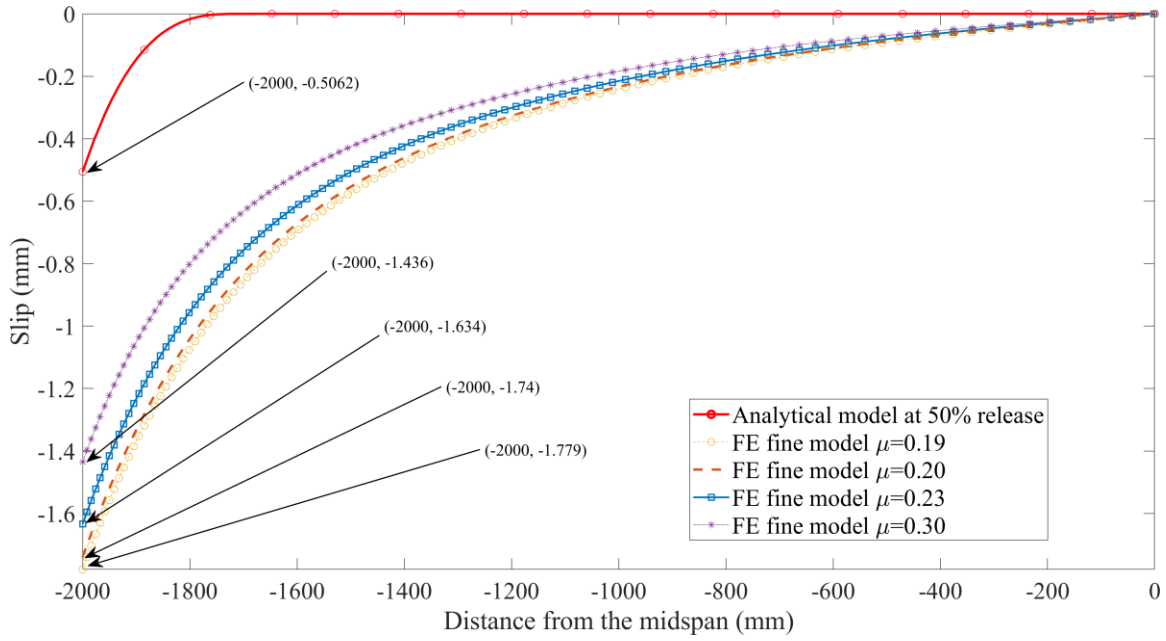

Fig. 5.17 Slip predicted by FE model at 50% release vs. analytical solutions

Through normalizing the parameters, the influence of friction coefficient μ tabulated in Table 5.1 and bond stress coefficient α ($\alpha = 0 \sim 0.6$) given by the expression of $\tau = \tau(s)$ on the transfer length is compared. It has been found from the result as represented in Fig. 5.18 that the transfer length of prestressed FRP tendons in pretensioned concrete members is exponentially proportional to the bond stress coefficient α and inversely proportional to the friction coefficient μ. Furthermore, from the perspective of varying tendencies of the curves, the extent of effect of the bond stress coefficient is more distinctive than the friction coefficient. In essence, different forms of the function that describes the bond behavior are adopted in the theoretical solution and numerical simulation that lead to differing impacts.

In analytical solutions using composite beam theory, the BEP expression is chosen as the bond-slip relationship $\tau = \tau(s)$ to estimate the transfer length of pretensioned concrete members prestressed with FRP tendons. An important difference from the linear equation modeling the

interaction between contact bodies using FEM is that the function form of $\tau = \tau(s)$ is a power function of the slip s in the analytical solution. By understanding the concept of transfer length, the distance that the effective prestressing force is transferred by the bond stress τ from the prestressed tendons to the concrete in which the axial force of concrete increases from 0 to a constant. In other words, there is no interactive shear stress related to the bond between FRP tendons and concrete outside of the transmission zone. This exactly fits the typical characteristics of power functions with $0 < \alpha < 1$, where the slope of the curve gradually becomes flat as the variable increases. With the use of the BEP relationship to explain the bond mechanism, another advantage is that the closed form solution for transfer length by means of Dirichlet and Neumann boundary conditions avoids many approximations and computational effort compared to the 95% AMS method in the numerical simulation.

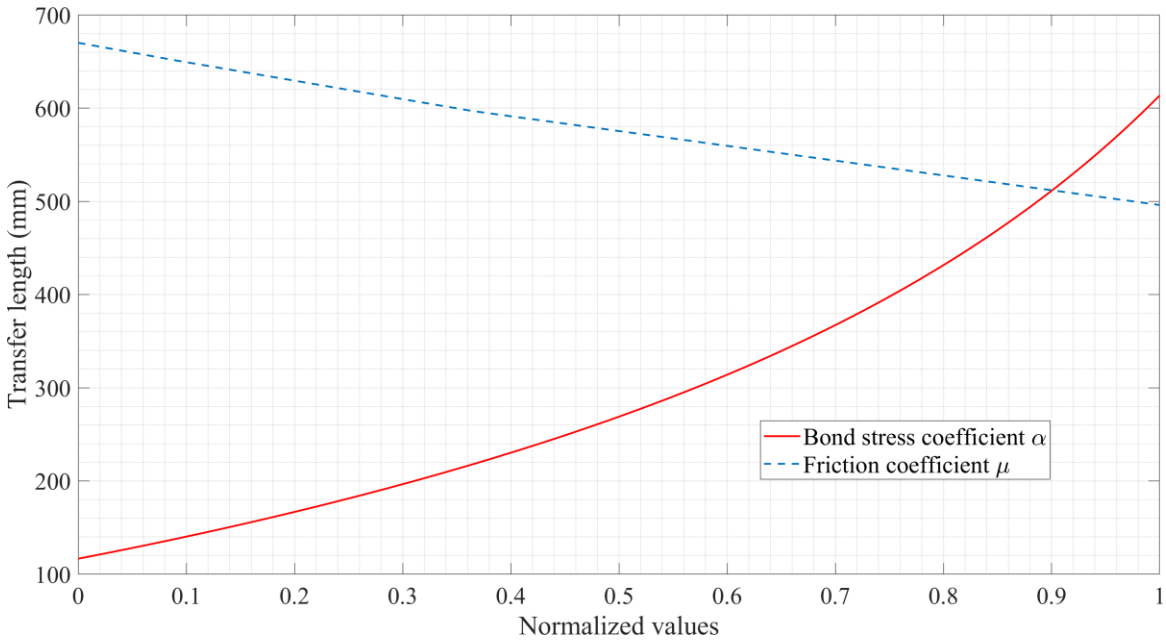

Fig. 5.18 Influence of bond stress coefficient α and friction coefficient μ on transfer length

5.6 Conclusions

Testing is considered to be the best way to predict phenomenon and obtain necessary information. However, large-scale testing is time-consuming, expensive and has many limitations. With this consideration along with the need to further verify the accuracy and feasibility of the previously developed method, a three-dimensional FE model of pretensioned concrete members with prestressing FRP tendons was developed. Based on different friction coefficients of FRP tendons reported from the pullout test, fine and coarse FE models were implemented for convergent analysis. In addition, the general approach of composite beam theory is summarized for providing convenient use in engineering practice, specifically for FRPs strengthening concrete members. Lastly, comparison between the analytical solution and FE simulation is carried out and discussed. The main accomplishments and conclusions are as follows:

1. A general form of the governing equations has been presented specifically for FRPs strengthening concrete members in terms of composite beam theory. Associating with the knowledge of the local bond stress-slip relationship $\tau = \tau(s)$ between FRPs and concrete, the closed form solution can be solved under corresponding boundary conditions.

2. Comparisons with the experimental data demonstrates good agreement, which indicates that the proposed FE model with fine mesh is acceptable. The measured transfer length for high pretension agrees with the prediction from the fine FE model with friction coefficient $\alpha = 0.3$ within a 1% range.

3. Comparisons between the FE model results and previously developed analytical solutions demonstrate that theoretical results using composite beam theory is superior to that of numerical simulation.

4. Although friction plays a key role in the interaction between concrete and prestressed tendons, the slip prediction comparisons show that if the adhesion and mechanical interlocking are ignored, the bond behavior cannot be accurately evaluated.

5. The transfer length prediction is strongly dependent on the adopted function form of the bond-slip relationship $\tau = \tau(s)$ between concrete and FRP tendons in the analytical model using composite beam theory. For the analytical solution of mechanical behavior of concrete members strengthened with FRPs in terms of partially composite action, the most critical issue is to have knowledge of the local bond-slip relationship in the interface region.

Therefore, it is necessary to adopt a new method to describe the bond behavior between concrete and FRP tendons in the future FE simulation. In this process, adhesion, friction, and mechanical interlocking must be fully considered in order to provide more accurate predictions and facilitate engineering applications.

References

[1] Eligehausen R, Popov EP, Bertero VV. Local bond stress-slip relationships of deformed bars under generalized excitations, Report No. UCB/EERC 83-23. University of California, Berkeley. 1983 Oct.

[2] CEB-FIP M. 90. Design of concrete structures. CEB-FIP-Model-Code 1990. Lond Br Stand Inst 1993.

[3] Russo G, Zingone G, Romano F. Analytical solution for bond-slip of reinforcing bars in RC joints. Journal of Structural Engineering. 1990 Feb;116(2):336-55.

[4] Malvar LJ. Bond stress-slip characteristics of FRP rebars. Naval Facilities Engineering Service Center Port Hueneme CA; 1994 Feb.

[5] Nanni A, Tanigaki M, Hasuo K. Bond anchorage of pretensioned FRP tendon at force release. Journal of Structural Engineering. 1992 Oct;118(10):2837-54.

[6] Cosenza E, Manfredi G, Realfonzo R. Behavior and modeling of bond of FRP rebars to concrete. Journal of Composites for Construction. 1997 May;1(2):40-51.

[7] Lees JM, Burgoyne CJ. Transfer bond stresses generated between FRP tendons and concrete. Magazine of Concrete Research. 1999 Aug;51(4):229-39.

[8] Focacci F, Nanni A, Bakis CE. Local bond-slip relationship for FRP reinforcement in concrete. Journal of Composites for Construction. 2000 Feb;4(1):24-31.

[9] Sha X, Davidson JS. Analysis of Interfacial Stresses in Concrete Beams Strengthened by Externally Bonded FRP Laminates Using Composite Beam Theory. Composite Structures. 2020 Mar 19:112235.

[10] Lee YJ, Boothby TE, Bakis CE, Nanni A. Slip modulus of FRP sheets bonded to concrete. Journal of Composites for Construction. 1999 Nov;3(4):161-7.

[11] De Lorenzis L, Miller B, Nanni A. Bond of FRP laminates to concrete. ACI Materials Journal. 2001 May;98(3):256-64.

[12] Nakaba K, Kanakubo T, Furuta T, Yoshizawa H. Bond behavior between fiber-reinforced polymer laminates and concrete. Structural Journal. 2001 May 1;98(3):359-67.

[13] Dai J, Ueda T, Sato Y. Development of the nonlinear bond stress–slip model of fiber reinforced plastics sheet–concrete interfaces with a simple method. Journal of Composites for Construction. 2005 Feb;9(1):52-62.

[14] Lu XZ, Teng JG, Ye LP, Jiang JJ. Bond–slip models for FRP sheets/plates bonded to concrete. Engineering Structures. 2005 May 1;27(6):920-37.

[15] Lu XZ, Ye LP, Teng JG, Jiang JJ. Meso-scale finite element model for FRP sheets/plates bonded to concrete. Engineering Structures. 2005 Mar 1;27(4):564-75.

[16] Guo ZG, Cao SY, Sun WM, Lin XY. Experimental study on bond stress-slip behaviour between FRP sheets and concrete. In FRP in Construction, Proceedings of the International Symposium on Bond Behaviour of FRP in Structures. 2005 Dec;77-84.

[17] Zhou YW, Wu YF, Yun Y. Analytical modeling of the bond–slip relationship at FRP-concrete interfaces for adhesively-bonded joints. Composites Part B: Engineering. 2010 Sep 1;41(6):423-33.

[18] Biscaia HC, Chastre C, Silva MA. Linear and nonlinear analysis of bond-slip models for interfaces between FRP composites and concrete. Composites Part B: Engineering. 2013 Feb 1;45(1):1554-68.

[19] Ko H, Matthys S, Palmieri A, Sato Y. Development of a simplified bond stress–slip model for bonded FRP–concrete interfaces. Construction and Building Materials. 2014 Oct 15;68:142-57.

[20] Granholm H. On composite beams and columns with particular regard to nailed timber structures. Chalmer Technical University. 1949.

[21] Newmark NM, Siess CP, Viest IM. Test and analysis of composite beams with incomplete interaction. Proceedings of Society for Experimental Stress Analysis. 1951;9(1):75-92.

[22] Hibbit K. Sorensen Inc. ABAQUS/Standard User's Manual, Version. 2002;5.

[23] Sha X, Davidson JS. Analysis of transfer length for prestressed FRP tendons in pretensioned concrete using composite beam theory. Composite Structures. 2019 Jan 15;208:665-77.

[24] Zhang L, Teng JG. Finite element prediction of interfacial stresses in structural members bonded with a thin plate. Engineering Structures. 2010 Feb 1;32(2):459-71.

[25] Bai F, Davidson JS. Analysis of partially composite foam insulated concrete sandwich structures. Engineering Structures. 2015 May 15;91:197-209.

[26] Rabbat BG, Kaar PH, Russell HG, Bruce Jr RN. Fatigue tests of prestressed girders with blanketed and draped strands. Transportation Research Record. 1978(665).

[27] Arab AA, Badie SS, Manzari MT. A methodological approach for finite element modeling of pretensioned concrete members at the release of pretensioning. Engineering Structures. 2011 Jun 1;33(6):1918-29.

[28] Abdelatif AO, Owen JS, Hussein MF. Modelling the prestress transfer in pre-tensioned concrete elements. Finite Elements in Analysis and Design. 2015 Feb 1;94:47-63.

[29] Yapar O, Basu PK, Nordendale N. Accurate finite element modeling of pretensioned prestressed concrete beams. Engineering Structures. 2015 Oct 15;101:163-78.

[30] Khin M, Tanaka M, Venkataramana K, Harada T. Experimental Study on Friction Factor for Fiber Reinforced Polymer Tendons in Pretensioned Prestressed Concrete Members. Special Publication. 1999 Aug 1;188:856-64.

[31] Janney JR. Nature of bond in pre-tensioned prestressed concrete. In Journal Proceedings 1954 May 1; Vol. 50, No. 5: 717-736.

[32] du Béton FI. Bond of reinforcement in concrete: state-of-art report. Bulletin. 2000;10:160-7.

[33] Den Uijl JA. Bond modelling of prestressing strand. Special Publication. 1998 Oct 1;180:145-70.

[34] AASHTO LRFD bridge design specifications and commentary. Washington, DC. 2012.

[35] Soroushian P, Choi KB, Park GH, Aslani F. Bond of deformed bars to concrete: effects of confinement and strength of concrete. Materials Journal. 1991 May 1;88(3):227-32.

[36] Nanni A, Utsunomiya T, Yonekura H, Tanigaki M. Transmission of prestressing force to concrete by bonded fiber reinforced plastic tendons. ACI Structural Journal. 1992 May 1;89(3):335-44.

[37] Nie J, Cai CS. Steel–concrete composite beams considering shear slip effects. Journal of Structural Engineering. 2003 Apr;129(4):495-506.

Chapter 6 Summary and Future Work

6.1 Summary

The emphasis of this dissertation is laid to present a novel theory of mechanic-based which is attempted to describe the flexural behavior of FRP reinforced concrete members, with regard to the engineering practice problems, such as transfer length and interfacial stresses.

For prestressed concrete reinforced with FRP tendons, Chapter 3 discusses in detail the derivation of a set of governing equations and a closed-form solution for determining the transfer length, which takes into account the nonlinear relationship between FRP tendons and concrete. Correspondingly, predicted strain profiles by this method are in agreement with the experimental data available in the literature.

For concrete beams strengthened by externally bonded FRP laminates presented in Chapter 4, a rigorous analytical approach considering the bond-slip relationship between FRP laminates and concrete is developed for predicting interfacial stresses. With the superposition technique for boundary conditions and developed composite beam theory, two sets of governing differential equations can be used to explain the coupling mechanical behavior between longitudinal and transverse interactions. It has proved that the present prediction for interfacial stresses is accurate and feasible by comparison with those from existing theoretical and numerical simulation.

A three-dimensional FE model of prestressed concrete members with prestressed FRP tendons was proposed in Chapter 5 with attempting to further verify the validity of the previously developed theoretical method. Furthermore, a general method of composite beam theory are summarized for FRPs strengthening concrete members, so as to provide convenient use in engineering practice. As a result, predictions from the previous analytical solution have been shown to be in reasonable consistent with the FE simulation. With respect to the friction coefficient and bond stress coefficient, the difference between the theoretical and the numerical method is discussed.

6.2 Future work

This research develops an advanced composite beam theory related to the mechanics performance of concrete members strengthened by FRP systems. However, there are still some practical and theoretical issues that needs to be resolved in future work.

For example, experimental and theoretical studies on the local bond stress-slip relationship between concrete and FRP tendons of various materials should be conducted. Besides, an analytical solution can be established for prestressed concrete members with draped FRP tendons in terms of composite beam theory.

Considering the retrofitting techniques with externally bonded FRP laminates, a comprehensive evaluation of the bond behavior at the interface between the concrete substrate and FRP laminates composed of different types of fiber, such as Aramid Fiber Reinforced Polymer (AFRP), Carbon Fiber Reinforced Polymer (CFRP) and Glass Fiber Reinforced Polymer (GFRP), is still an important issue that cannot be ignored.

With the rapid development of computer and visualization technologies, numerical simulation studies are gaining more attention. It is urgent to implement an approach to describe accurately the bond behavior between concrete and FRP tendons in the future FE simulation. At the same time, the influence of adhesion, friction, and mechanical interlocking should be fully taken into account in the analysis process.

6.3 Publications

- Sha Xin, Davidson James. Analysis of transfer length for prestressed FRP tendons in pretensioned concrete using composite beam theory. *Composite Structures*. 2019 Jan 15;208:665-77.

- Sha Xin, Davidson James. Analysis of Interfacial Stresses in Concrete Beams Strengthened by Externally Bonded FRP Laminates Using Composite Beam Theory. *Composite Structures*. 2020 Mar 19:112235.

- Sha Xin, Davidson James. Verification of composite beam theory with finite element model for pretensioned concrete members with prestressing FRP tendons. Submitted to *Composite Structures* in September 2020